

INFORMATION TO USERS

The most advanced technology has been used to photograph and reproduce this manuscript from the microfilm master. UMI films the text directly from the original or copy submitted. Thus, some thesis and dissertation copies are in typewriter face, while others may be from any type of computer printer.

The quality of this reproduction is dependent upon the quality of the copy submitted. Broken or indistinct print, colored or poor quality illustrations and photographs, print bleedthrough, substandard margins, and improper alignment can adversely affect reproduction.

In the unlikely event that the author did not send UMI a complete manuscript and there are missing pages, these will be noted. Also, if unauthorized copyright material had to be removed, a note will indicate the deletion.

Oversize materials (e.g., maps, drawings, charts) are reproduced by sectioning the original, beginning at the upper left-hand corner and continuing from left to right in equal sections with small overlaps. Each original is also photographed in one exposure and is included in reduced form at the back of the book. These are also available as one exposure on a standard 35mm slide or as a 17" x 23" black and white photographic print for an additional charge.

Photographs included in the original manuscript have been reproduced xerographically in this copy. Higher quality 6" x 9" black and white photographic prints are available for any photographs or illustrations appearing in this copy for an additional charge. Contact UMI directly to order.

U·M·I

University Microfilms International
A Bell & Howell Information Company
300 North Zeeb Road, Ann Arbor, MI 48106-1346 USA
313/761-4700 800/521-0600



Order Number 9015358

Phase instabilities in small particles

Ajayan, P. M., Ph.D.

Northwestern University, 1989

U·M·I
300 N. Zeeb Rd.
Ann Arbor, MI 48106

1

2

3

NORTHWESTERN UNIVERSITY

PHASE INSTABILITIES IN SMALL PARTICLES

A DISSERTATION

SUBMITTED TO THE GRADUATE SCHOOL

IN PARTIAL FULFILMENT OF THE REQUIREMENTS

for the degree

DOCTOR OF PHILOSOPHY

Field of Materials Science and Engineering

By

AJAYAN P. M.

EVANSTON, ILLINOIS

December 1989

ABSTRACT

Phase Instabilities in Small Particles

Ajayan P. M

The purpose of this study is to understand the structure, morphology and stability of small particles in the size range of 1-10 nanometers and the nature of their interactions with support materials.

The first part of the study uses a continuum model to calculate the free energy surfaces of a series of related decahedral multiply twinned particle structures; surface energies are evaluated using constrained minimization of the surface energy at constant volumes for particle shapes and the strain energies, using an asymmetric disclination model in the framework of two-dimensional elasticity. Entropy contributions arise from the temperature dependence of the surface anisotropy and stored elastic energy and the dilatation due to disclination. A phase diagram was constructed for small particle structures as a function of particle size and

temperature which showed a region, distinct from the thermodynamic melt, where there is high probability for various small particle morphologies to co-exist.

The second part of the thesis deals with high resolution electron microscopy of small gold particles supported on magnesium oxide support. It is seen that under normal electron flux small particles tend to sink into the substrate material in order to reduce the free energy of the system. Under high flux electron irradiation microscopic pillars grow from MgO underneath the gold particles isolating the gold particles from the substrate. Once the gold particles are isolated from the support, they start changing their structures rapidly. This state, the quasi-molten phase was predicted in the theoretical model, persisted even after the electron beam intensity is turned down to zero and hence appears to be an inherent property of small particles.

This work is dedicated to my parents, Mr. K. M. Panicker and Mrs. Radha Panicker and my sister P. M. Anitha.

" God is an intelligible sphere, whose center is everywhere
and whose circumference is nowhere "

Alain de Lille

(from *Corpus Hermeticum*)

Acknowledgements

I acknowledge the continuous support and encouragements from my advisor, Professor Laurence D. Marks, without whom this work would not have been possible. I also acknowledge his direct contribution in the surface energy evaluation of small particle shapes using the constrained minimization routine (section 2.1.1) and in the problem of the modified Wulff construction for the case of a sinking particle (appendix 4.B)

Professor John Dundurs was responsible for most part of the elasticity calculations including the evaluation of temperature gradients and thermal strains (sections 2.1.2 to 2.2.3). I also thank him for being a member of my Ph.D examination committee. I would also like to acknowledge the other members of the committee, Professors Julia R. Weertman and D. Lynn Johnson for their time and consideration.

My acknowledgements are due to Dr. Boon Teo and Dr. Manfred Kappes for supplying some of the cluster specimens and Dr. Murray Gibson who let me use his microscope facility at the AT & T Bell laboratories in Murray Hill, New Jersey.

Special thanks are due to the past and present

members of my laboratory all of whom have widened my knowledge in scientific as well as other worldly matters. Outside the lab I have had many friends whose help and consideration did make my life in Chicago, a pleasant one.

Last, but not the least, I would like to acknowledge the National Science Foundation for funding this project.

TABLE OF CONTENTS

	Page
ABSTRACT	ii
ACKNOWLEDGEMENTS	vi
TABLE OF CONTENTS	viii
LIST OF TABLES	xii
LIST OF FIGURES	xiii
CHAPTER 1 INTRODUCTION	
1.1 Small Particles : Size Dependent Physical Properties	1
1.2 Atomic Clusters	5
1.3 Small Particles : Statics	9
1.3.1 Structure and Potential Energy	9
1.3.2 MTP's : Growth and Twinning	19
1.4 Small Particles: Structural Dynamics	26
1.5 Electron Microscopy of Small Particles	31
CHAPTER 2 THEORETICAL EVALUATION OF THE POTENTIAL ENERGY SURFACES	
2.1 Potential Energy	39
2.1.1 Surface Energy	43
2.1.2 Elasticity of the Disclination	46
2.1.3 Strain Energy of the Disclination	51
2.1.4 Surface Stress Energy	52
2.2 Temperature Distribution	55
2.2.1 Thermal Stresses	59
2.2.2 Thermal Strain Energy	60

2.2.3 Thermal Stress and Disclination Interaction Energy	62
2.3 Potential Energy Surfaces	64
CHAPTER 3 FREE ENERGY SURFACES AND THE PHASE DIAGRAM	
3.1 Entropy Contribution	70
3.1.1 Dilatation due to the Disclination	74
3.2 Free Energy Surfaces	75
3.3 Quasi-melting in Small Particles	78
3.4 Phase Diagram of Small Particles	83
3.5 Statistical Energy Fluctuations	88
3.6 Discussion	93
CHAPTER 4 EXPERIMENTAL OBSERVATIONS OF SOME NOVEL PARTICLE-SUBSTRATE INTERACTIONS	
4.1 Small Particles and Substrates	99
4.2 Experimental Method	105
4.3 Sinking Small Particles	111
4.3.1 Theoretical Model for Sinking Small Particles	119
4.4 Microscopic Pillar Growth Instabilities	125
4.4.1 Theoretical Model for Microscopic Pillar Growth	139
4.5 Effect of Temperature on Gold-MgO System	151
CHAPTER 5 EXPERIMENTAL EVIDENCE FOR QUASI-MELTING	
5.1 Experimental Search for Quasi-Melting	159
5.1.1 How does Small Particles Absorb Energy from Electron Irradiation	160
5.2 Experimental Evidence for Quasi-Melting	164
5.3 Conclusions	177

CHAPTER 6 ON SOME ASPECTS OF ELECTRON IRRADIATION OF SMALL PARTICLES

6.1	Fluxional Dependence of Structure	181
6.2	On the Structure of Larger Particles under Electron Irradiation	183
6.3	Electron Beam Induced Diffusion Limited Aggregation	191

CHAPTER 7 SUMMARY AND SUGGESTIONS FOR FUTURE WORK

7.1	Summary	197
7.2	Suggestions for Future Work	199

REFERENCES 202

APPENDIX 2.A EQUILIBRIUM PARTICLE SHAPE & THE WULFF CONSTRUCTION

2.A.1	Equilibrium Particle Shapes and the Wulff Construction	220
2.A.2	Modified Wulff Construction for an MTP	224

APPENDIX 2.B DISCLINATION & IT'S AIRY STRESS FUNCTION

2.B.1	Disclinations in Twinned Crystals	229
-------	-----------------------------------	-----

APPENDIX 4.A EXPERIMENTAL DETERMINATION OF INTERFACIAL ENERGY & SURFACE ENERGY ANISOTROPY IN GOLD-MgO SYSTEM

4.A.1	Evaluation of Interfacial Free Energy and Surface Anisotropy from Wulff Construction	235
-------	--	-----

APPENDIX 4.B	EQUILIBRIUM SHAPE OF A SINKING PARTICLE AND THE MODIFIED WULFF CONSTRUCTION	
	4.B.1 Equilibrium Shape of the Sinking Particle	240
	4.B.2 Analysis of the Sinking Problem	241
	4.B.3 Discussion	250
VITA		253

List of Tables

	Page
1.1 Collection of results published in recent years showing the observation of twinned structures with anomalous symmetry in small particles of various materials.	10-11
2.B.1 Table showing the relationship between the biharmonic functions that form part of the Airy stress functions, corresponding stresses, and displacements.	232-233

List of Figures

	Page
1.1 Typical low resolution electron microscope image showing the particle shapes that occur during the early stages of vacuum deposition of Ag onto rock salt.	12
1.2 (a) The basic structures of the two most commonly observed MTPs in different orientation	13
(b) Atomic resolution images of the icosahedral and decahedral MTPs	14
1.3 The mechanism of growth of a twinned particle by successive twinning.	22
1.4 The formation of the twinned crystal by layer by layer growth on an existing icosahedral nucleus.	24
1.5 A typical sequence of a structural transformation during the electron beam irradiation of a small particle of gold, taken from single frames of a real time video recording.	27
1.6 Arbitrary potential energy surface showing the relationship and the phase changes in twinned particle structures.	31
1.7 Schematic showing the geometry of incidence in profile imaging high resolution electron microscopy.	31
2.1 The evolution of particle shapes as an eccentric disclination passes from one to the other end of the crystal.	42
2.2 The general shape of the individual segments used in the calculation of surface energy.	42
2.3 Plot of E_s with b for a 25Å particle for three different values of surface anisotropy ratio.	45

2.4	Double coordinate system used to solve the disclination problem.	48
2.5	Schematic of a particle sitting on a substrate used in the evaluation of temperature distributions in the particle.	48
2.6	Potential energy surfaces (surface and strain energy terms) for a 25Å particle for different surface anisotropy ratios.	65
2.7	Magnitude of the activation energy barriers for various shapes with respect to a single crystal Wulff polyhedron of the same size.	67
2.8	Plot of the maximum activation barrier between all of the shapes that we consider as a function of the particle size.	67
3.1	Free energy surfaces for a 25Å particle for four different values of temperature. Energy units are arbitrary and the scale has been compressed for better comparison.	76
3.2	Boltzmann distributions for different shapes at three different temperatures.	79
3.3	Plot of the variation in the index of quasi-melting as a function of temperature and particle size.	79
3.4	Phase diagram for small particles as a function of particle size and temperature.	84
3.5	Plot of relative energy fluctuations as a function of temperature for different particle sizes.	91
3.6	The plot of a representative configurational space volume at different temperatures.	91
4.1	Shape of a winterbottom construction for a particle on a substrate and the effect of	

	substrate interactions on the shape (a&b).	102
4.2	Distribution of two dimensional rafts and single atoms of gold on the surface steps of MgO.	107
4.3	Distribution of gold clusters on transparent cubes of MgO smoke particles.	108
4.4	A small gold particle sitting on a flat MgO surface sinking into the substrate during low flux electron irradiation.	112
4.5	The atomic resolution images of the gold particle sinking into the substrate material of MgO.	113
4.6	Shows that sinking of particles into substrate takes place much faster at higher electron fluxes.	116
4.7	Schematic of a particle on a substrate, with non-planar (a) interface, two different intermediate configurations during sinking (b) and with a planar interface (c).	120
4.8	Schematic of the energy function as the particle of any arbitrary shape sinks into a substrate.	123
4.9	Formation of microscopic pillars on MgO substrate supporting small gold particles during high flux electron irradiation.	127
4.10	Experimental images showing the time sequence of pillar growth.	128
4.11	Sequence of pillar growth but here the final pillar formed is indented in the center due to a block of mass being drawn up during growth.	129
4.12	An extreme case of pillar growth where two particles supported on a small MgO cube is pushed out by pillars, giving the final image	

	a unique profile.	130
4.13	(a) Image of an MgO surface holding particles of various sizes forming pillars after irradiation, the pillar height being inversely proportional to the size of the particle.	131
	(b) Data from (a) of pillar height as a function of particle size.	132
4.14	Scatter plot of all the data obtained so far showing the relation between pillar height and particle size.	135
4.15	Plot of the square of encapsulation width as function of time, fitted by power law, for three different sequences.	142
4.16	Plot of the cube of the height of encapsulation and pillar formed as a function of time.	143
4.17	Experimental image showing the formation of a bent pillar suggesting change in diffusion direction during growth.	145
4.18	Roughening of the MgO surface at around 300°C and the start of encapsulation of the gold particles by MgO.	152
4.19	Final encapsulated gold particles sitting on MgO surface after the system was heated to 600°C.	153
4.20	The effect of high flux electron irradiation on the encapsulated gold-MgO system.	154
4.21	Rounded surface profile of gold-MgO-hydrocarbon contamination system during heat treatment.	155
5.1	Sequence in which a small particle under electron irradiation sinks into diffusing overlayers of MgO, comes out of the encapsulation and finally becomes	

	structurally unstable.	166
5.2	Another sequence of a small particle gets pushed onto the top of a pillar and becomes structurally unstable.	167
5.3	Sequence of particle shapes during it's structural fluctuations. The images are averages of eight frames each taken from real time video recording.	168
5.4	Schematic of a small particle sitting in a deep potential energy well on the substrate once pushed out floats on a configurational energy surface which is very flat.	170
5.5	Plots showing the relationship between the beam current needed to initiate quasi-melting in small particles for various particle sizes.	173
6.1	sequence of particle structures under electron irradiation for three different current densities.	184
6.2	Images of a large gold particle with two parallel twin boundaries under high flux electron irradiation.	185
6.3	Images of another sequence of a large gold particle undergoing microfaceting and volume shrinkage under the electron beam.	186
6.4	The sequence of images of a large gold particle with one twin boundary undergoing localized twinning (moire fringes) or stacking changes into a distorted 9R type structure.	189
6.5	The image of the fractal structure produced from the growth and coalescence of gold clusters on NaCl during high flux electron irradiation.	192

6.6	Plot of the areas encompassed by the fractal structure formed by coalescence of gold clusters against the size of the circular probe, in a log-log scale.	193
2.A.1	Schematic showing the polar plots for surface free energy and the Curie-Wulff construction giving the equilibrium shape, a polyhedron.	221
2.A.2	Schematic used in the proof of Curie-Wulff construction.	221
2.A.3	A typical $\langle 110 \rangle$ section of the plot as well as the shape of a single crystal tetrahedra for a fcc material and for a strongly faceted model.	225
2.A.4	The shape of a single crystal segment derived from the modified Wulff construction from which the complete Dh particle is constructed.	226
2.B.1	Schematic showing how the operation in forming a wedge disclination is carried out.	231
4.A.1	The experimental images and schematics of Wulff construction shapes of small gold particles on MgO, used to evaluate the interfacial energy of Au-MgO interface and surface anisotropy of gold particles.	236
4.B.1	Schematic showing the geometry of the equilibrium particle shape which is cut along the plane of the interface.	243
4.B.2	Schematic showing the Wulff construction of the top and bottom parts of the equilibrium shape with different scaling.	243
4.B.3	Schematic showing the deformation of the first kind where the top and bottom parts are independently deformed with out changing the substrate cross-section.	247

4.B.4 A deformation which changes the substrate intersection cross-sectional area but does not transfer volume between the top and bottom.	247
4.B.5 Deformation of the third kind which involves volume transport between the top and bottom parts.	248
4.B.6 The image of a partially sunken particle and its tracing to show the position of the Wulff center inside the particle volume.	248

Chapter 1 Introduction

1.1 Small Particles: Size Dependent Physical Properties

The properties of matter are mostly decided by how the atoms are arranged in the structure. In majority of the solids, the atoms are periodically arranged to form crystalline lattices which possess long range order. When one traverses from the bulk of the crystal to the surface, the symmetry is abruptly broken since the atoms lose coordination on one side of the interface. Consequently, the properties of the surface are quite distinct from the bulk. A small particle, consisting of only a few thousand or less atoms, is characterized by a large surface to volume ratio and subsequently a large number of surface atoms compared to the bulk; hence one would expect that the material will behave differently at smaller sizes. This is truly the case. The central question one has to address is, " how does the bulk behavior evolve with increasing particle size starting with the atomic state? "

There are numerous examples of the above mentioned size dependence in physical and electronic properties and these have diverse technical applications of importance to the

scientific world. The lattice vibration spectrum, and hence the heat capacity in small particles has been shown to differ [Dickey and Paskin 1968, Burton 1970, Matsubara et al. 1977, Hasegawa et al. 1980] drastically from that of a bulk material. The finite size of the crystal cuts off the lowest frequencies of the bulk lattice and introduce new low-frequency surface modes. The normal bulk transverse and longitudinal peaks are not visible in the smallest clusters. It was suggested that the two dimensional nature of the phonon spectrum is responsible for the increase in the superconducting transition temperatures [Khluystikov and Buzdin 1987] in many small particle systems, for example lead and tin. Optical properties are sensitive to surface plasmon modes that depend on size, shape as well as the interactions between individual particles and the support, and the magnetic properties depend on the parity of electron number per particle (Halperin 1986).

It was demonstrated [Kubo 1962] that since the spacings of the quantized electronic states become large (compared to kT) in small particles at low temperatures, the electrical and thermal properties exhibited by them differ from the bulk. The electrons in a small particle are unique in that they

deviate from fermi statistics since the number of such electrons is so small. Kubo also pointed out that the detail of the energy spectrum should depend on the precise geometry although particles of the same size would have the same average level spacing. It is also seen that in small particles, the large spacing between the energy levels is reflected in a Poisson distribution of the spectrum.

It has been pointed out that the melting points of materials show a depression as the size is reduced [Takagi 1954, Blackman and Sambles 1970, Couchman and Jesser 1977, Couchman and Ryan 1978, Borel 1981, Ross and Andres 1981, Nimitz et al. 1989]. Recently, many computer simulations on small clusters have revealed the existence of a range of melting with lower and upper critical melting points [Briant and Burton 1975, Eters and Kaelberer 1977, Natanson et al. 1983, Berry et al. 1984, Honeycutt and Anderson 1987, Beck et al. 1988]. Many authors have also found [Gordon et al. 1979, Woltersdorf et al. 1981, Heinemann et al. 1983, Marks et al. 1984, Marks 1985b, Heine et al. 1986, Hayashi 1987] structural modifications in small particles compared to the bulk such as changes in lattice parameter, contraction of the surface layer, surface reconstructions different from the bulk

material and residual stresses.

Because of this deviation in the physical properties of small particles from the corresponding bulk material, the study of the physics involved in the size dependence become both important and interesting. Small noble and transition metal particles, in the size range of a few nanometers, have also been used in many areas; heterogeneous catalysts, fields where surface and interface properties are important such as heat exchangers, magnetic and dielectric devices and superconductors, and hence are industrially important. For example, the efficiency of a catalytic reaction depends on the reactivity of the catalyst particles and this in turn is directly related to their structure and the nature of the surface facets that are exposed during a reaction. Hence an understanding of the surface morphology of small particles is important as well as necessary in catalysis research. In almost all cases the particles are supported by a substrate (usually a metal oxide) and the interaction of the particle with the substrate become crucial in the activity of the catalysts. In catalysis or heat exchangers where a large surface area is preferred small particles form an effective medium. At the same time it is essential in many cases that

with decreasing particle size the bulk character is retained (metallic character in a heat exchanger) over a range of conditions.

Clearly, understanding size effects is important in many cases. In this thesis, only the structure and the nature of interactions of small particles with a support will be considered. Before going into details of the structure and stability of small particles, which will correspond throughout this work to particles in the size range of 1-100 nm, it is quite useful to look briefly at work that has been done on very small atomic clusters (collection of a few ten to a few hundred atoms) using computer simulations and theoretical models.

1.2 Atomic Clusters

Using computer models (Monte Carlo or Molecular Dynamics Programs) and searching for energy minima or using sphere packing studies, pair-potential or quantum mechanical calculations, workers such as Bernal (1960), Mackay (1962), McGinty (1971), Hoare and Pal (1972), Lee, Barker and Abraham (1973), Briant and Burton (1975), Eppers and Kaelberer (1975,1977), Farges, de Feraudy, Raoult and Torchet

(1983,1986), Jellenik, Beck and Berry (1986), Landman, Barnett, Cleveland, Scharf and Jortner (1987), Honeycutt and Anderson (1987) have proposed various novel structures for clusters. In a recent paper, Halicioglu and Bauschlicher (1988) have reviewed the physics and properties of microclusters, outlining the progress as well as the limitations of the present state of research. Most of the above studies indicate that below a few thousand atoms, clusters do not correspond to microcrystallites of fcc or hcp type close packed lattices, but form families of compact structures based upon packing of tetrahedra. Many structural sequences based on potential energy minimum criteria have been proposed for clusters of very small sizes [e.g. Werfelmeier 1937, Fukano and Wayman 1969, Hoare and Pal 1972]. However it should be noted that depending on the programs involved and the nature of the ensemble chosen (canonical or microcanonical) different results have been obtained for the stability of various structures. Many authors have observed that whenever the clusters contain certain 'magic number' of atoms [Mackay 1962, Hoare and Pal 1972], they form almost spherical shapes with nearly close packed surfaces which have exceptional stability. Such magic number clusters based on

sphere packing arrangements have been observed experimentally by Kimota and Nishida (1977), Echt, Sattler and Recknagel (1981) and others. These are generally structures with icosahedral symmetry which at larger sizes have been shown to relax to their conjugate structures, the dodecahedrons, or to fcc type close packed lattices. The packing density in an icosahedral cluster is 0.688 compared to 0.724 for a dodecahedron and 0.741 for a close packed structure. Historically the Greeks were aware of the regular polygons; the icosahedron has the largest volume to surface area ratio (the tetrahedron has the lowest) and the dodecahedron is the reciprocal of the icosahedron since the number of vertices and faces in both are interchanged and the number of edges are the same (12 vertices, 30 edges and 20 faces for an icosahedra). The literature on the subject of structures with icosahedral symmetry is rather overwhelming since the discovery by Shechtman, Blech, Gratias and Cahn (1984) of five fold symmetry in real bulk systems. The importance of this quasi-periodic symmetry (since the symmetry by itself cannot fill three dimensional space) has been reviewed in one of the many recent articles by Mort la Brecque (1988).

There have been extensive studies in recent years of the

electronic structure of atomic clusters using ab-initio approaches, see for example Kubo (1962), Messmer (1981), Rao, Khanna and Jena (1986), Landman et al. (1987). There has also been considerable effort trying to establish a shell structure for metallic clusters, which resembles the well established shell theories of atoms and nuclei used in quantum mechanical calculations, for a review of this field see De Heer, Knight, Chou and Cohen (1987). Clusters with magic number of atoms (magic number here corresponds to the shell structure and not sphere packing) have been observed experimentally by Ding and Hesslich (1983), Stephens and King (1983), Knight, Clemenger, de Heer, Saunders, Chou and Cohen (1984). In all this work the point should be stressed that the structures found are only local minima on a configurational energy surface and one can only consider the relative probabilities of the occurrence of a particular morphology. One can consider a solid-like structure, which represents an apparent global minimum, and a liquid-like regime where more than one structure coexist. Similar ideas have been expressed by Berry et al. (1984) and Stillinger and Weber (1982) who consider the vibrational energy levels in clusters, with a deep narrow potential well with a sparse energy spectrum solid-like and a broad shallow

minima with a high density of states liquid-like. We shall return to the question of the morphological potential energy surfaces for small particles in chapter 2.

1.3.1 Small Particles : Structure and Potential Energy

The first observation of anomalous structures having five-fold rotational symmetry axes in material systems was by Melmed and Hayward (1959) during the vapor growth of metal whiskers for field emitter tips and by Ogburn, Paretzkin and Peiser (1964) during the electro-deposition of copper dendrites. This was followed by detailed electron microscopic analyses during the late sixties by Ino (1966), Ogawa, Ino, Kato and Ota (1966), Ino and Ogawa (1967) and Allpress and Sanders (1967). These authors observed that during the vacuum deposition of fcc materials on non-metallic substrates the small particles formed were often non-crystallographic. These poly-tetrahedral structures were called multiply twinned particles or MTP's. A plethora of results obtained since have confirmed that the preferred structure of ultrafine particles of a variety of materials are tetrahedral, icosahedral, cuboctahedral, pentagonal and their complex poly-forms, many of them containing a multiplicity of internal twins. Table.1.1

Authors (year)	Material	Substrate (if evaporated)	Size (Å)	Structure
Melmed & Hayward (1959)	Ni	W, Fe, Pt	Whiskers	5-fold symmetry (pentagonal twins)
Ogburn et al. (1964)	Cu	Electro-deposition	Microns	Pseudo pentagonal twins
Schwoebel (1966)	Au	Au	<1000	5-fold symmetric twins
Mihama & Yasuda (1966)	Au	NaCl	<100	Twinned Particles
Allpress & Sanders (1967)	Au, Pd, Ni	Mica	50-200	Dh, Ic, SC, LTP
Ino & Ogawa (1967)	Au	NaCl, KCl	10-100	Dh, Ic
Kimoto & Nishida (1967)	Ag, Pd, Ni, Co	Evaporation in Ar gas	<1200	Dh, Ic
Komoda (1968)	Au	NaCl, KCl	<150	Dh, Ic
Ogawa et al. (1969)	Au	NaCl, KCl	20-100	Dh, Ic
Yagi et al. (1975)	Ag, Au	MgO, MoS ₂	20-500	Dh, Ic, SC
Gillet (1977)	Au	NaCl	30-250	Dh, Ic
Saito et al. (1978)	Ge	Evaporation in Ar gas	1000-5000	Dh, Twinned polyhedra
Heinemann et al. (1979)	Au	LiF, NaCl	50-200	Dh, Ic, SC
Marks & Smith (1981, 1983)	Au, Ag	KCl	100-1000	Dh, Ic, CTP, LTP
Matsumoto & Matsui (1983)	Diamond	Si	100-2micron	Dh, Ic twinned CCP
Hofmeister (1984)	Au	AgBr	100-1000	Dh, Ic, CTP

Table 1.1 Some experimental results of the observation of MTP structures in small particles of various materials under different conditions. Here Dh, Ic, SC, CTP, LTP and CCP stands for Decahedral MTP, Icosahedral MTP, Single crystal, Complex twinned particle and Cubic close packed structure respectively.

Authors (year)	Material	Substrate (if evaporated)	Size (Å)	Structure
Marks (1985b, 1985c)	Au, Ag	NaCl	100-500	Dh, Ic
Matsui (1984)	Cubic Boron Nitride	Electron beam reduction	100-1000	Dh
Dhere et al. (1985)	Au	Colloidal	150-300	Twinned polyhedras
Dahmen & Westmacott (1986)	Ge precipitate	Al matrix	needles	Dh, CTP
Long et al. (1986)	Pt	Colloidal	5-30	Twinned Polyhedra
Wallenberg et al. (1986)	Pt	Colloidal	<50	Structural instability
Wallenberg (1987)	Zn, Cd Rh, Pt	Various Techniques	10-100	Dh, Ic SC, Rafts
Curtis et al. (1987)	Cu	Colloidal	30-300	Dh, Ic, LTP
Iijima & Ichihashi (1987)	Au	Si/SiO ₂	<50	Structural instability
Iijima (1987a)	Graphitized C clusters	Amorphous C	30-70	Truncated Ic
Iijima (1987b, 1987c)	Si, SiC	Gas evaporation	200-2000	Dh, CTP
Badzian et al. (1988)	Diamond	Si, Graphite	<10 micron	Dh, SC, Ic Cuboids
Giorgio & Urban (1988)	Ag	Inert gas evaporation	30-100	Dh, 3-fold symmetry twins
Malm et al. (1988)	Ru	Micro-emulsion	10-50	Structural instability

Table 1.1 Some experimental results of the observation of MTP structures in small particles of various materials under different conditions. (Continued from last page)

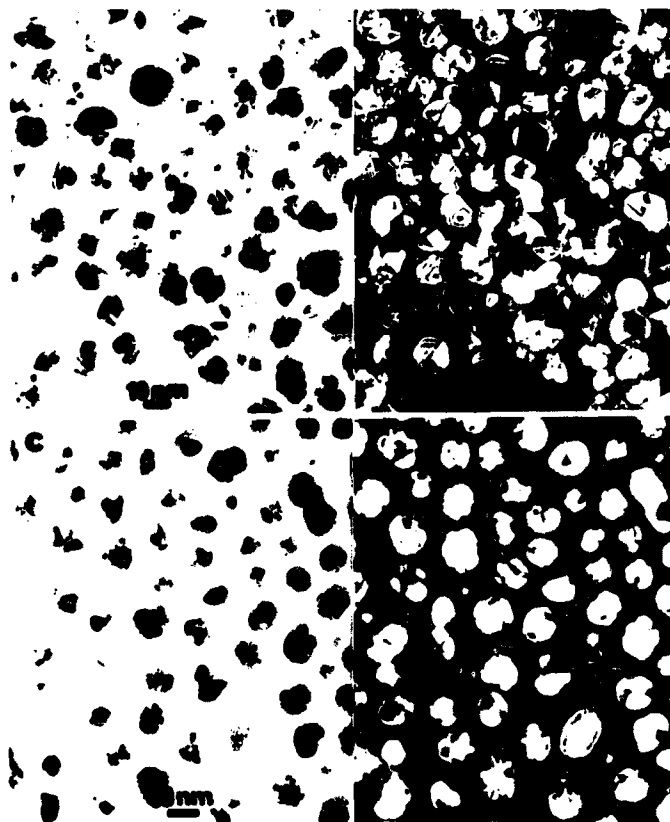


Fig.1.1 A typical ensemble of small particle structures found during the early stages of evaporation of Ag on to NaCl substrate. (a & b) show axial bright field-dark field pair and (c & d) the bright field-hollow cone dark field pair. (from Marks, 1980).

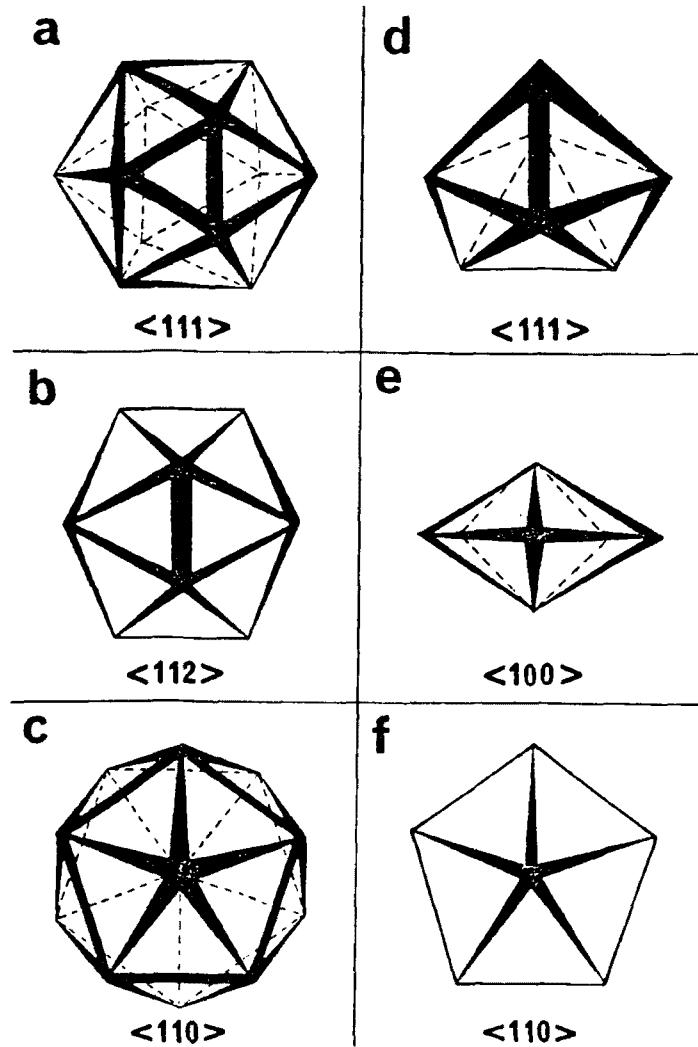


Fig.1.2a (a-c) show the schematic of the structures of the icosahedral MTP in three major orientation. (d-f) similarly show the structures of the Decahedral MTP (from Marks, 1980).

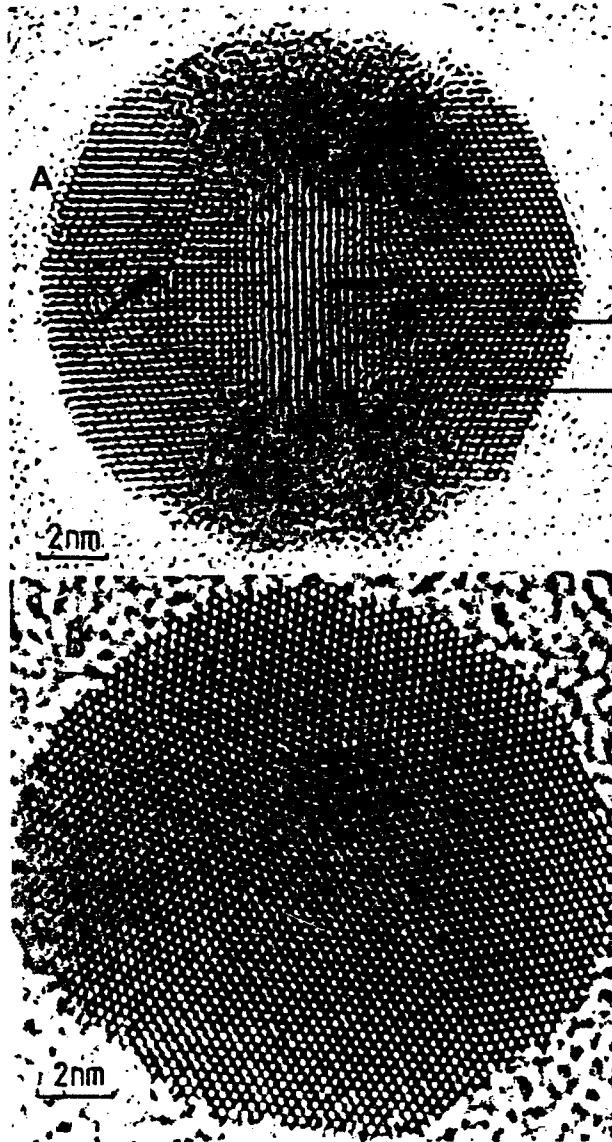


Fig.1.2b High resolution electron microscopy images of Icosahedral (A) and Decahedral (B) MTPs in the $\langle 110 \rangle$ orientation (from Marks, 1980). Arrows indicate partial dislocations in the structure.

shows a collection of some of the results published over the last twenty years on the anomalous structures of various materials prepared by different techniques.

Figure 1.1 shows a typical low resolution electron microscope image showing the particle shapes that occur during the early stages of vacuum deposition of Ag onto rock salt. The basic structures of the two most commonly observed MTP's are shown in Fig.1.2 (a&b) together with atomic resolution electron microscopy images. MTP's are non-crystallographic structures which to a first approximation are a collection of single crystal tetrahedra twin related on their adjoining (111) faces. Five such units pack together with a D_{5h} point group symmetry to form a decahedral particle, and twenty units with an I_c symmetry form an icosahedron. Although these particles assume forms similar (in symmetry and packing) to those found in atomic clusters they are highly distorted and defective [see Marks and Smith, 1983]. It should be noted that when formed from perfect single crystal units, the particle contains spatial discontinuities which introduce inhomogeneous strains. Various defects other than twin boundaries, for instance partial dislocations, stacking faults, grain boundaries, notches at the twin boundary edges, re-entrant

surfaces etc. also have been observed in MTP particles [see Smith and Marks 1981, Marks 1985c; Iijima and Ichihashi 1987]. The additional strain and twin energy associated with the formation of MTP's is balanced by a reduction of surface free energy. There has been conclusive experimental evidence for the presence of inhomogeneous strains in these particles [Marks 1985b]. Various theoretical models, including homogeneous elasticity calculations by Ino (1969), structural modifications by Yang (1979), a Jahn-Teller or Pierls distortion by Bagley (1965), a dislocation model by Saito, Yatsuya, Mihama and Uyeda (1978), a disclination model by de Wit (1972), Howie and Marks (1985), Dundurs, Marks and Ajayan (1988), have been proposed.

Fukano and Wayman (1969) and Hoare and Pal (1972) while considering the stability of clusters found MTP's to be among the more stable morphologies. The equilibrium surface morphologies of cluster size particles and their corresponding free energies have been analyzed in terms of semi-continuum approaches such as three-body interactions, packing corrections and capillary considerations by Griffin and Anders (1979), Martins, Car and Buttet (1981), Halicioglu and White (1981), Wang, Falicov and Searcy (1984), Marks (1985a) and

many others. Gordon, Cyrot-Lackmann and Desjonqueres (1979) calculated the cohesive energies of various size clusters with icosahedral and fcc type cuboctahedral geometries and found that for the same size but different geometries, the cohesive energy difference between clusters is quite small (of the order of 500 cal/mole) and co-existence of such structures is possible. The first real attempt to calculate the energetics of small particles and multiply twinned structures using continuum theories and macroscopic surface free energies was undertaken by Ino in 1969. He evaluated the free energies of various structures by including the cohesive energy, surface energy and adhesive energy associated with the particle-substrate bonding, elastic strain energy and the twin boundary energy associated with the multiple twins. He assumed the shapes of the single crystals and icosahedrons to be those given by the Curie-Wulff construction [see Herring 1951; Linford 1968; Rottman and Wortis 1984] and pentagonal bi-pyramids to approximate the decahedrons. By evaluating the above energy balance he was able to show that for small sizes the icosahedral MTP was the most stable structure but the decahedrons were only quasi-stable with respect to a single crystal.

Later Marks (1984c) and Howie and Marks (1984) worked out semi-quantitative results for the stability of various structures which showed that both MTP's were stable compared to normal close packed structures. In their model the equilibrium shapes of the MTP's were modified forms of the Curie-Wulff polyhedrons, incorporating extra point values for the twin boundaries in the construction. The surface energy was evaluated using a dimensionless energy parameter depending only on the shape and not on the volume of the particle, found by minimizing the surface energy integral with the constraint that volume remains a constant and the different segments match along the adjoining twin boundaries. The surface energies were assumed to be anisotropic and a strong faceting model, with only the low index (100) and (111) facets decorating the surface of the Wulff polyhedron, was used in comparison to a liquid-like isotropic model. This assumption was justified by experimental observations that high index facets are absent in small particles, since the high index faces act as nucleation sites and are eliminated in an atom-by-atom growth process. Experimental values for the surface anisotropies of small particles can be found in the work of Heyraud and Metois (1980), Menon and Martin (1986) and Flueli

and Borel (1988) etc. but results are far from conclusive and information at low temperatures is almost non-existent. The spatial misfit formed when the tetrahedral segments are put together was included in the above model by introducing a $7^{\circ}20'$ wedge disclination and the strain energies were calculated using inhomogeneous two-dimensional elasticity. Disclinations are defects which are readily observed in frustrated configurations such as amorphous materials and in configurations involving interactions between spatially incompatible structures at the molecular scale, see for a discussion, Kleman (1983). They are usually related to symmetries of rotation, similar to dislocations which are related to symmetries of translation in a crystalline lattice, and like dislocations are sources of internal strains [de Wit 1971, Harris and Scriven 1971]. A detailed analysis of the disclination model will be given in chapter 2 and Appendix B.

1.3.2 MTP's - Growth and Twinning

A point that should be raised here is whether MTP's are thermodynamic forms or kinetic shapes, forming and disappearing as growth artifacts. Attempts were made right from the early sixties to explain the formation of micro-twins

in evaporated fcc metal films, see Matthews and Allinson (1963). They proposed that in the event of a thickness gradient in the evaporated film, the nuclei that were formed at the thin end of the deposit were misaligned with respect to each other. As a result of this, in the early stages of growth, it was more probable for neighboring nuclei to have lattices which are nearer to a twin relationship than a parallel alignment. If these nuclei coalesce, one of them could easily rotate and become a twin of the other. As the probability of misalignment increased with decrease in nuclei size, it was seen that the amount of twinning also decreased. It was proposed that after coalescence of many nuclei, the twins could spread over the (111) facet of the larger nuclei as a step would move over a growing crystal.

The problem still was to explain the twin formation in individual nuclei or a small particle before coalescence took place. A model for the growth and twinning in MTP's during crystal growth was proposed by Allpress and Sanders in 1967. They considered that the most stable arrangement of three atoms on a substrate is a triangular array lying fixed on the substrate. Depending on the relative bonding energies between the metal-substrate atoms and metal-metal atoms, a fourth atom

can either form a planar or tetrahedral configuration. In the former case, where the substrate surface is in a high energy configuration (kinked and rough) continued growth could produce planar layers of atoms (forming raft-like or lamellar structures). But in most practical cases, especially during epitaxial vapor depositions where the substrates are smooth, discrete tetrahedras are formed as nuclei. These could further grow into 3-dimensional clusters and by packing considerations expose the low-index faces (where atoms are in high coordination positions) on the surface. Renucleation of a layer of atoms on such surfaces is then accompanied by a large probability of faulting. Thus primary twins could be introduced on to these faces, and could be followed by formation of successive secondary and tertiary twins, finally resulting in pentagonal and icosahedral particles with multiple twins. If the metal-metal interaction is very strong, highly faulted crystallites could result at early stages of growth, but could undergo rearrangements into low energy and ideal tetrahedral structures which then grow into MTP's by the same mechanism. This mechanism of growth by successive twinning is illustrated in Fig.1.3. The authors also suggested that larger crystals could be formed by particle coalescence,

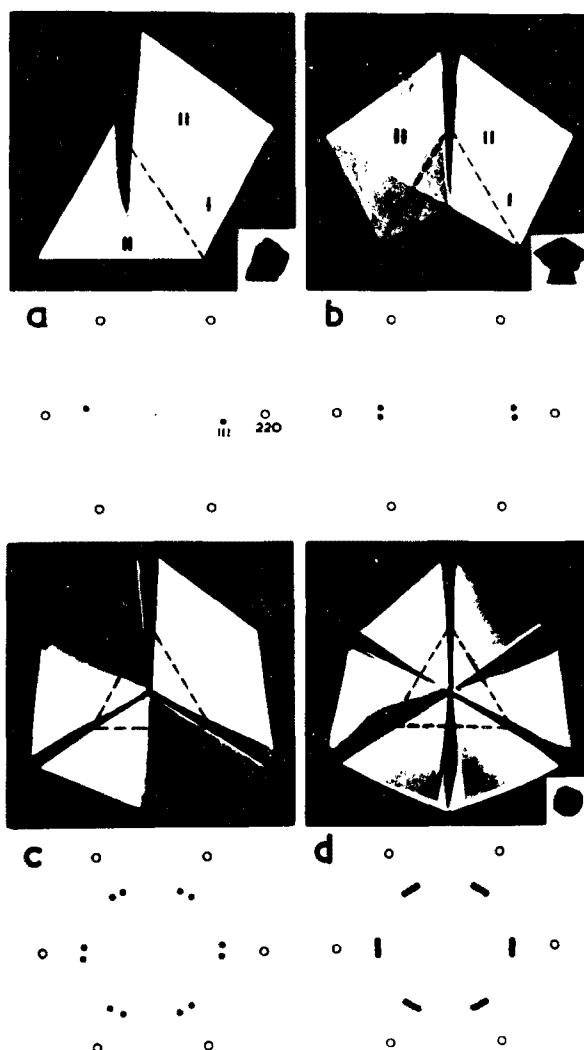


Fig.1.3 Photographs of the model of growth in multiply twinned crystals, with corresponding diffraction patterns from crystals displayed below. a) Twin I grows on the face N of a crystal sitting on the substrate. b) Secondary twin II grows on one face of I and the crystal appears pentagonal when viewed from above. c) Shows another possibility of twinning on an other face of original crystal. d) Tertiary twins are formed on the uppermost faces of the crystal shown in (c). (from Allpress and Sanders, 1967)

either retaining their original structures or, due to high atom mobility and liquid-like coalescence of clusters, reforming into new and rather perfect structures after coalescence.

Gillet in 1979 proposed another model for the formation of MTP's. He suggested that the decahedral and icosahedral particles are characterized by pentagonal crowns of atoms around their five-fold axes. Growth then involves a layer-by-layer process around the existing nuclei, leading to pentagonal symmetry. It can be said simply that the pseudopentagonal symmetry arises from the fact that the angle between two (111) type faces in an fcc material is $70^{\circ} 32'$ or nearly $360^{\circ}/5$ [Ogburn et al. 1964]. Farges, de Feraudy, Raoult and Torchet (1983, 1984) in a similar model proposed two growth mechanisms for the growth of a multilayer icosahedra. They suggested that the growth of an extra layer of atoms on an existing collection of twenty tetrahedra which constitutes an icosahedra nuclei could proceed either by the formation of an extra fcc layer by the adatoms taking up the normal fcc positions, or by the formation of an extra layer corresponding to a twin. The sequence of the two growth mechanisms is given in Fig.1.4. Depending on the potential energy criteria the

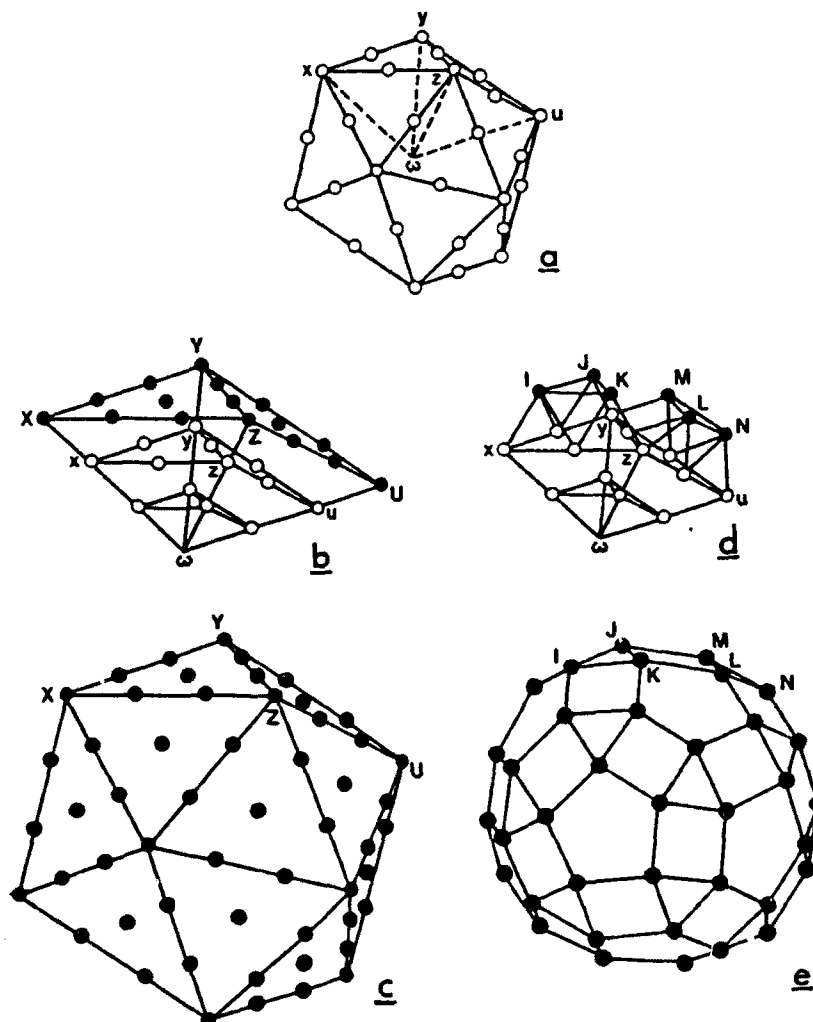


Fig.1.4 Growth mechanism producing a multilayer icosahedron (MTP). a) An icosahedral nuclei having two complete layers (55 atoms). b) The external face of one of the tetrahedrons is covered with a third layer of regular fcc layer. c) 3-layer icosahedron corresponding to (b) when completely covered. d) Same tetrahedra covered with a third layer, but in twin fault position. e) Complete rhombicuboctahedron when a full layer is formed on the structure shown in (d). (from Farges et al., 1984).

authors conclude that the latter arrangement becomes unstable with respect to the former for icosahedra having more than three layers. In a different structural model, Bagley (1965), Yang (1979) etc. proposed that the icosahedrons and decahedrons, rather than being collections of discrete twinned crystallites, are actually structures with a distorted body-centered orthorhombic and rhombohedral point group symmetries respectively. Although they were able to show this from a purely geometric point of view, no analysis was given of the energetics and kinetics of growth and transformation. Recently Iijima (1987c) put forward an argument, similar to the Gillet model, for the growth of decahedral MTP's in fine particles of Si, by considering crystallization from liquid droplets. He assumed that a liquid droplet is formed first and an embryo of the decahedral MTP is nucleated on the surface of the droplet, which subsequently grows along the pentagonal symmetry axes into a compact decahedral MTP. A question of importance is whether the structures are crystallographically inter-related and suggestions by Mackay (1962) and Marks (1980) implies that thermal vibrational modes can induce structural transformations between various existing single crystals and MTP's, although experimental observations to

support this has not yet been presented.

A classic paper is the one by Yagi, Takayanagi, Kobayashi and Honjo (1975) which demonstrates most of the above models experimentally. This was the first proof of the different growth mechanisms that were proposed by various authors, thus clarifying many of the existing controversies regarding the way structures evolve during the atom-by-atom growth phenomena. They observed in-situ inside the electron microscope, the ab-initio nucleation and growth of Au and Ag MTP's, coalescence and reformation into compound MTP's and their formation from successive twinning starting from epitaxial single crystal particles. These experiments prove that MTP's must have at least the thermodynamic stability of a local minima on a morphological energy surface. Apart from ideal pentagonal and icosahedral MTP structures, compound and asymmetric structures [Matsui 1984, Marks 1985c] are also found in most systems which are quite stable up to large particle sizes.

1.4 Small Particles: Structural Dynamics

So far we have been concentrating on the static structure of small particles. But is such a simple static analysis

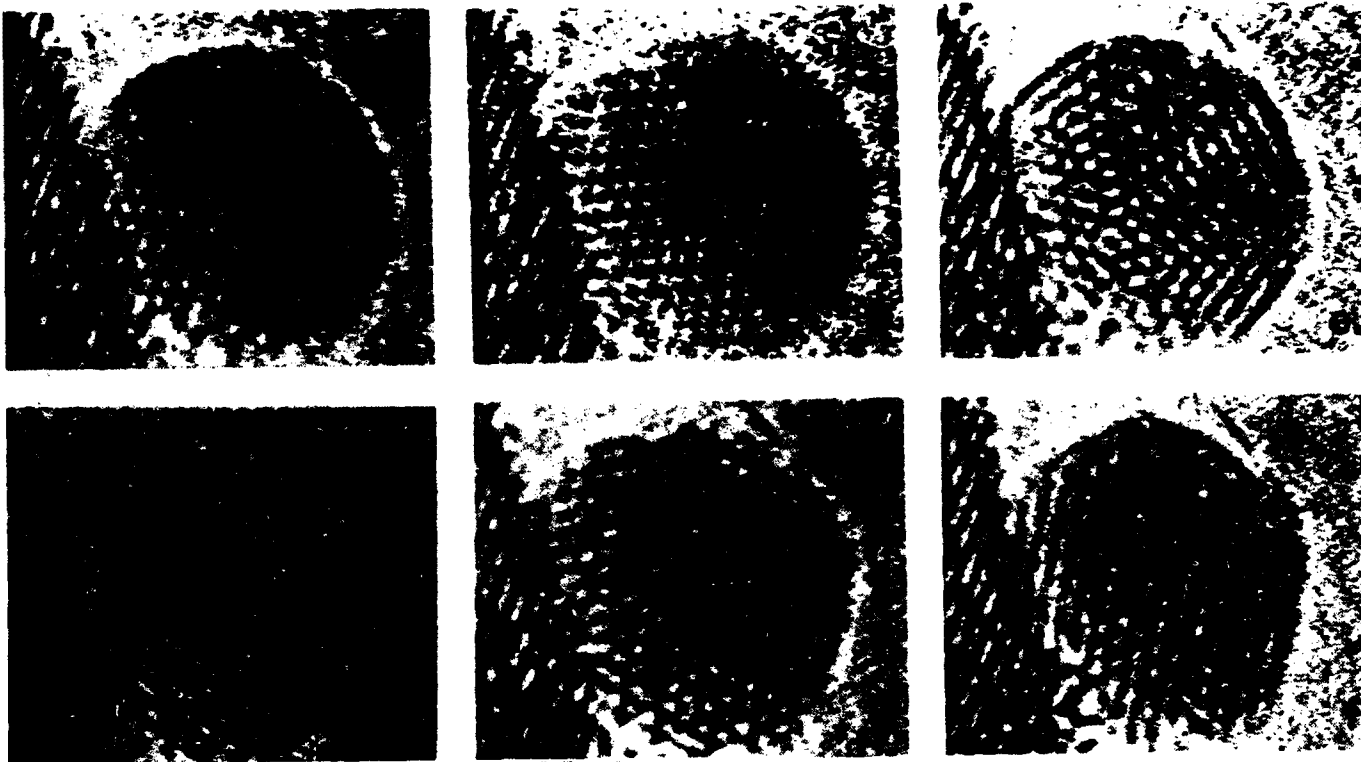


Fig.1.5 Shows the structural changes observed in a 3.5 nm gold crystal supported on amorphous silicon, as seen in single frame exposures from a real time video recording. The shapes change as follows:
 a) Icosahedral b) Single crystal; 1.8 sec. c) Icosahedral; 4.2 sec. d) Stacking fault; 6.0 sec. e) Twin plane; 6.2 sec. f) Single crystal; 9.6 sec. g) Stacking fault (arrowed) & a twin plane; 20 sec. (from Smith et al., 1986).

adequate? High resolution electron microscopy observations using real time video recordings by Iijima and Ichihashi (1986), Smith, Petford-Long, Wallenberg and Bovin (1986) and Wallenberg, Smith, Petford-Long and Smith (1986) have indicated that particles smaller than 50 Å in size, in an intense electron beam, exhibit structural instability and fluctuate between various MTP and single crystal shapes with frequencies greater than 50 Hz. It has also been observed by Malm, Bovin, Petford-Long, Smith, Schmid and Klein (1988) that in material systems that do not readily form MTP structures, for example ruthenium, the fluctuations take place between close packed structures of hcp, ccp and bcc with similar frequencies. A similar type of phase transition between ordered crystalline lattice and a chaotic cloud of ions have been observed recently by Blumel, Chen, Peik, Quint, Schleich, Shen and Walther (1988) in a trapped ion source of laser cooled ions. A typical sequence of a structural transformation during electron beam irradiation of a small particle of gold, taken from single frames of a real time video recording, is shown in Fig.1.5. These observations are consistent with the configurational instabilities of clusters predicted by Hoare and Pal and others except that the phenomena is now extended

to larger systems. It should be noted that the particles are quite stable under low electron beam fluxes which means that there exists a critical activation energy barrier between the stable structure and the instability region. Systematic experiments monitoring the exact evolution of shapes have yet to be done to understand the nature of such transformations. The effect of the substrate interaction could be vital in deciding the value of this activation barrier, as discussed by Blaisten-Barojas, Garzon and Avalos-Borja (1987) in the wetting transitions and morphologies of clusters as a function of the substrate strength, by Ino (1969) in the values of adhesive energies chosen in the calculation of the energies of MTP's, and in the experimental results on quasi-melting which are discussed in chapter 5.

So far the theories had only given information about the structure of individual particles, based on the potential energy arising from the bonding of atoms and electronic contributions. Even this was limited to the idealized structures involved and the size ranges that could be treated by ab-initio theories. The theoretical models of growth and kinetics were treated qualitatively in order to match experimental results. Although the approximate stability of

MTP's with respect to a single crystal particle was demonstrated in the models described in the previous section it should be obvious that in order to understand the nature of phase equilibria between the various asymmetric shapes and the structural fluctuations, one needs to compute the free energy surfaces and the activation energy barriers existing between the different local minima. Marks (1984a) proposed that a modified form of the Wulff construction could be applied to the general problem of surface morphologies in twinned particles. By considering an anisotropic surface energy for a small particle and using a two variable approach, the volume fractions of the different segments that formed the twinned particle for arbitrary values of the partition fraction of the twin boundaries between the adjacent segments, a hypothetical potential energy surface was constructed for the twinned particle. The basic procedure to find such an energy surface would involve a constrained minimization of the surface and twin boundary energy at constant volume. Such a potential energy surface is shown in Fig.1.6. The various allowed solutions of the partition fraction represented the various local minima on the potential energy surface. At higher temperatures when the surface of the particle becomes

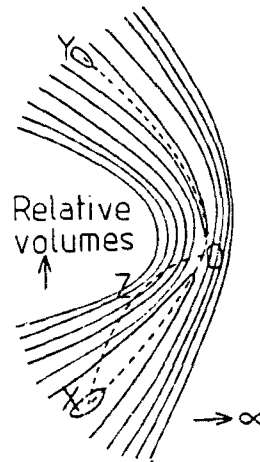


Fig.1.6 Hypothetical potential energy surface for a twinned particle. Energy contours are for non-equilibrium values of relative volumes of tetrahedras and the fractions of twin boundary energy (α) shared by two adjacent segments. X & Y represent single crystals and O is a constrained minima, a Wulff construction for a twinned particle. OX & OY are low energy paths but motion of th particle is constrained by the twin boundary and hence to path OZX. (from Marks, 1984a).

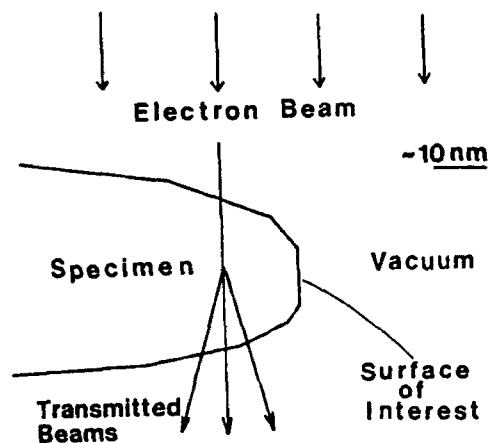


Fig.1.7 Diagram to illustrate the geometry of the profile imaging technique.

more isotropic, the restraint action of the twin boundaries will be lifted and the minima will be converted to saddle points suggestive of a 'phase change' in twinning. But the discussion was qualitative and lacked quantitative figures for energy values as functions of temperature, anisotropy and particle shape.

The next two chapters will be devoted to a theoretical evaluation of the free energy surfaces for small particles and the construction of a phase diagram which will introduce a new phase for the fluctuating small particle structures, which will be called the 'quasi-molten' phase. The chapters that follow will then give experimental results, using atomic resolution electron microscopy, on the structure of small particles, the nature of the interactions with the substrate and experimental verification of our model which predicts the existence of the quasi-molten phase in small particles.

1.5 Electron Microscopy of Small Particles

The amount of literature dealing with electron microscopy of small particles, particularly those consisting of supported metal particles, is enormous. The earlier attempts, using conventional bright field and dark field TEM, SEM and X-ray

techniques, focussed on the characterization of particle sizes and size distributions and these were analyzed statistically to provide meaningful information. But as the capabilities of the instruments improved the focus was shifted to a more important question, namely, what is the atomic nature or the structure of individual particles. High resolution electron (HREM) microscopy has contributed a great deal to the understanding of the atomic structure of small particles (Table 1.1 gives recent references in this field).

Atomic imaging of materials using the electron beam has become possible essentially due to the development of HREM in the past twenty years or so (the details of this technique is the subject matter of numerous books; see for example, Reimer 1984, Spence 1981). The essential difference between this technique and conventional electron microscopy is that in the former one uses the idea of phase contrast between the transmitted and different diffracted beams as a beam of swift electrons pass through the specimen whereas in the latter the amplitude contrast information contained in each of the beams is utilized separately. So in HREM the beams are recombined to produce an interference pattern that resembles the atomic structure of the specimen. The electromagnetic lenses that

combine the beams as well as magnify the image (of the order of a million times) introduce aberrations and hence the transfer of information gets modified. The aberrations modify the phase shift as well as act as a soft aperture cutting off some of the spatial frequencies and the image one obtains at the image plane is the true wavefunction from the exit plane of the specimen modified by a transfer function of the microscope (a phase shift term due to the defocus and spherical aberration and an envelope or soft aperture due to coherent and incoherent effects like energy spread of the beam and convergence; see for reference, Spence (1984)). So, in effect, the microscope acts like a spatial frequency filter transferring the information contained in the scattered beams from the specimen, after weighting the frequencies with a transfer function in a non-linear fashion. Usually one works with a range of conditions which keeps the magnitude as well as the sign of the contrast transfer function of the microscope almost a constant so that all the spatial frequencies are passed to the image in a similar way.

The above suggests that the image obtained from a high resolution microscope is quite sensitive to the instrument parameters one chooses to use and one has to be careful in

interpreting the right image. The possibilities of artifacts which can mislead the unwary is one of the complications of the technique and extensive image simulations have to be done synergistic with experiments to check the correctness of results. One has to usually use conditions in the microscope where one obtains a 'localized' image of the specimen area [Marks 1985d] giving a one to one correspondence with the atomic structure of the object and the image. Another important limitation of the technique is that it uses very thin specimens (of the order of 10 nm) so that the inelastic scattering from thicker specimens does not decrease the resolution and make impossible numerical simulations due to the combined effects of elastic and inelastic scattering; but the latter is not a problem for small particles. For small particles seen in profile or edge on, extensive image simulations are also not essential since the entire particle is usually in the field of view, but it is important that images to be compared are taken under the same microscope conditions.

The basic idea in imaging small particles or surfaces is to utilize this high resolution technique and look at the surfaces in profile [Marks 1986b]. The technique employs a

beam of swift electrons grazing the surface of interest (see Fig. 1.7). The high resolution images then show both the bulk structure and of the surface in profile.

Most of the experimental techniques involve the use of amorphous support materials (amorphous carbon, silica or alumina) so that the white noise contrast from the background can be used to correct axial astigmatism in the microscope; but on the other hand this superimposes background noise and spurious contrast features in the image that can create difficulties in direct interpretation of the results. As indicated by Heinemann and Soria (1986) the high resolution bright field image of an amorphous specimen contains, even if it is planar and featureless, a multitude of contrast features that depend on the microscope operating parameters. So when particles are in the same size ranges as the granular features in the image from the support film, identification of true images become an uphill task. A delineation can be done by choosing conditions that suppress these disturbances and emphasize the true object. Since the atomic scattering factors of metal atoms are higher compared to those of most supports, amplitude contrast can to some extent be utilized in looking at very small particles. One can use a large illumination

aperture angle so that over a larger spatial frequency range reduction of phase contrast occurs at the same focus. Also one can use the defocus value which gives the weakest phase contrast or the 'phase contrast minimum region' near to the Gaussian focus. One can also increase contrast by using lower beam energies but this will result in a decreased resolution. A higher beam intensity is essential for better contrast and will increase the signal to noise ratio but can enhance electron beam induced particle / substrate interactions.

The use of TV image pickup systems and framestores have become routine in electron microscopy of small particles. It should be noted that since tilting of small particles to desired zones is an impossible task one usually relies on a statistical search to find a suitably oriented particle in an ensemble of orientations. The approach of taking pictures of randomly oriented particles and picking out the ones that are good is prohibitively time consuming. An image pickup system allows good quality images to be displayed on a TV monitor which can be inspected leisurely for correct orientations. The shot noise that accompanies the images can be removed using the framestore through integrating over number of frames, taking running averages and filtering the images. Also the

dynamic events that one observes (rapid structural fluctuations in a small particle) can be video taped in real time and analyzed at length. The HITACHI-9000 that was used for the work presented in this thesis was equipped with both video pickup and an image processor (ITEX), driven by an Apollo computer, which can grab images frame by frame and display on the monitor; these features undoubtedly made this work both efficient and convenient.

Chapter 2 Theoretical Evaluation of the Potential Energy Surfaces

2.1 Potential Energy

As mentioned in the last chapter, the focus of the earlier theoretical models dealing with the structure of small particles was calculating singular values of the energy for various structures and particle shapes. These approaches, although provided valuable information regarding the energetics of isolated particle structures, were not useful in predicting the thermodynamic evolution of morphologies and changes in structure that one finds so very often in small particles. The basic impetus for the theoretical model presented in this and the next chapter is to calculate the energies of a series of related Decahedral (Dh) MTP structures (and hence plot the potential energy surface and not singular energy values for static particle shapes), so that one can predict the way the particles will morphologically evolve in any given thermodynamic environment.

The approach to calculating the potential energies for various shapes is essentially the same as that followed by

previous authors [Ino 1966, Howie and Marks 1984]; using Wulff construction (modified to include point values for the twin boundaries in the construction) as the unique energy minimizing surface and classical two-dimensional inhomogeneous elasticity calculations for the strains (due to a disclination, inside the particle). In the earlier works [Howie and Marks 1984, Marks 1984] on the energetics of MTPs, only symmetric MTPs with all the lengths on the basic tetrahedral unit being equal were considered. This was a drawback since asymmetric and compound MTP structures were experimentally observed [Marks 1983]. This earlier model is extended by including asymmetric shapes for MTPs by considering eccentric positions for the disclination inside the particle. The potential energy is then evaluated using a continuum model in two parts; the surface energy of the particle and the elastic strain energy due to the disclination and temperature gradients.

In order to understand how a small particle populates the infinitum number of structural states, a slice is considered, i.e. one line along the n-dimensional configurational energy surface. The energetics of a single crystal, a symmetrical D_h , a series of asymmetric D_h

structures and a crystal with one twin boundary (bi-crystal) was worked out using only the (100) and (111) surface facets (strong faceting model). A three dimensional analysis of the energetics with all possible facets is an intractable problem, but published results [Ino 1969, Marks 1984] indicate that a good approximation is obtained by considering only the above facets. This model is quite realistic since the high index or the high energy faces act as growth planes and get eliminated in the process of growth and particles at smaller sizes are found to be strongly faceted. Changes in the surface facets and the motion of the $7^{\circ}20'$ wedge disclination to the center of the particle corresponds to a change in structure from a single crystal to a Dh, and the motion to the opposite side gives a change in structure from a Dh to a bi-crystal (as illustrated in Fig.2.1). Making use of the mirror plane symmetry inherent in each of the segments and common to all five segments, one can say that segments two and five are identical, as are segments three and four. The general shape of a segment with different surface facets is shown in Fig.2.2 and is similar to the shape of the single crystal except that a (100) face which would appear along a $\langle 110 \rangle$ axis of the decahedral particle is missing. The derivation of the basic

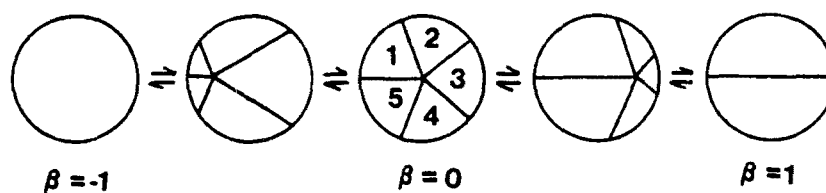


Fig.2.1 Schematic diagram showing the evolution of particle shapes characterized by β , as the disclination passes through the particle.

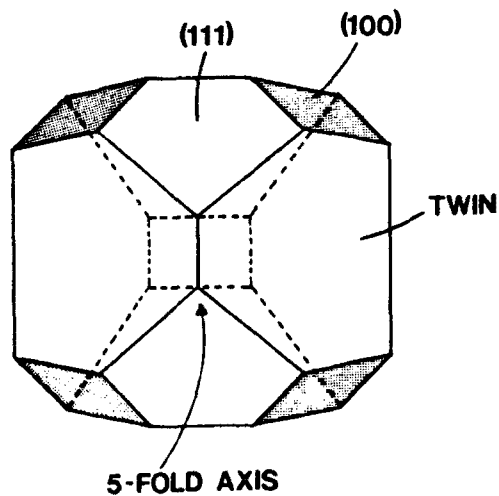


Fig.2.2 The basic tetrahedron unit showing the $\langle 111 \rangle$ and $\langle 100 \rangle$ surface facets used in the surface energy calculation.

single crystal shapes using a modified Wulff construction is given by Marks (1980). All lengths of the segments are made variables, and the constraint is applied that the segments have to match at the boundaries. This restricts the geometric invariance to a certain degree and simplifies the problem to a great extent.

2.1.1 Surface Energy

The problem is to find the surface energy of the particle for a specified volume fraction of each of the five segments. The surface area and volume of each of the segments was worked out for each geometry of shapes and a minimization problem done on the VAX780 computer using the MPNOS command sequence from MINIPACK software package. This was done by minimizing the dimensionless energy parameter E_w where;

$$E_w = (\gamma_{111})^{-1} \left(\int \gamma dS \right) \left(\int dV \right)^{-2/3} \quad (2.1)$$

Here V is the volume of the particle and γ_{111} is the surface energy per unit area of a (111) facet. The net surface energy can then be written in terms of E_w as $E_s = E_w \gamma_{111} V^{2/3}$. During the minimization procedure, the constraint is applied that the

twin facets common to the adjoining segments are identical. This ensures that the adjoining segments match at the boundaries and the five units fit into a complete structure. The volume fractions of one of the segments (V_3) is fixed and E_v is evaluated as a function of this variable, which in turn is expressed in terms of β , the fractional distance of the disclination from the center. The value of $\beta=-1$ corresponds to a single crystal, $\beta=0$ to a symmetric decahedral particle and $\beta=1$ to a bi-crystal. The volume fractions of segments 1 & 4 are kept equal and so are that of 2 & 5. The value of the twin boundary energy is set at $\gamma_t = 0.01 \gamma_{111}$, a reasonable value for fcc metals (perhaps with the exception of Pt and Al). The above calculation is repeated for three different values of the surface anisotropy ratio α or the ratio of the surface specific energy of a (100) surface to that of a (111) surface. Figure 2.3 shows the variation of E_v for a 25 Å⁰ particle as a function of the particle shape parameter, for three different values of the surface anisotropy ratio ($\gamma_{100}/\gamma_{111}$). The plot shows that there is an apparent global minimum for the symmetric decahedral MTP and local minima for the assymmetric ones. The energy variations decrease as the surface anisotropy is decreased. Thus the stability of the

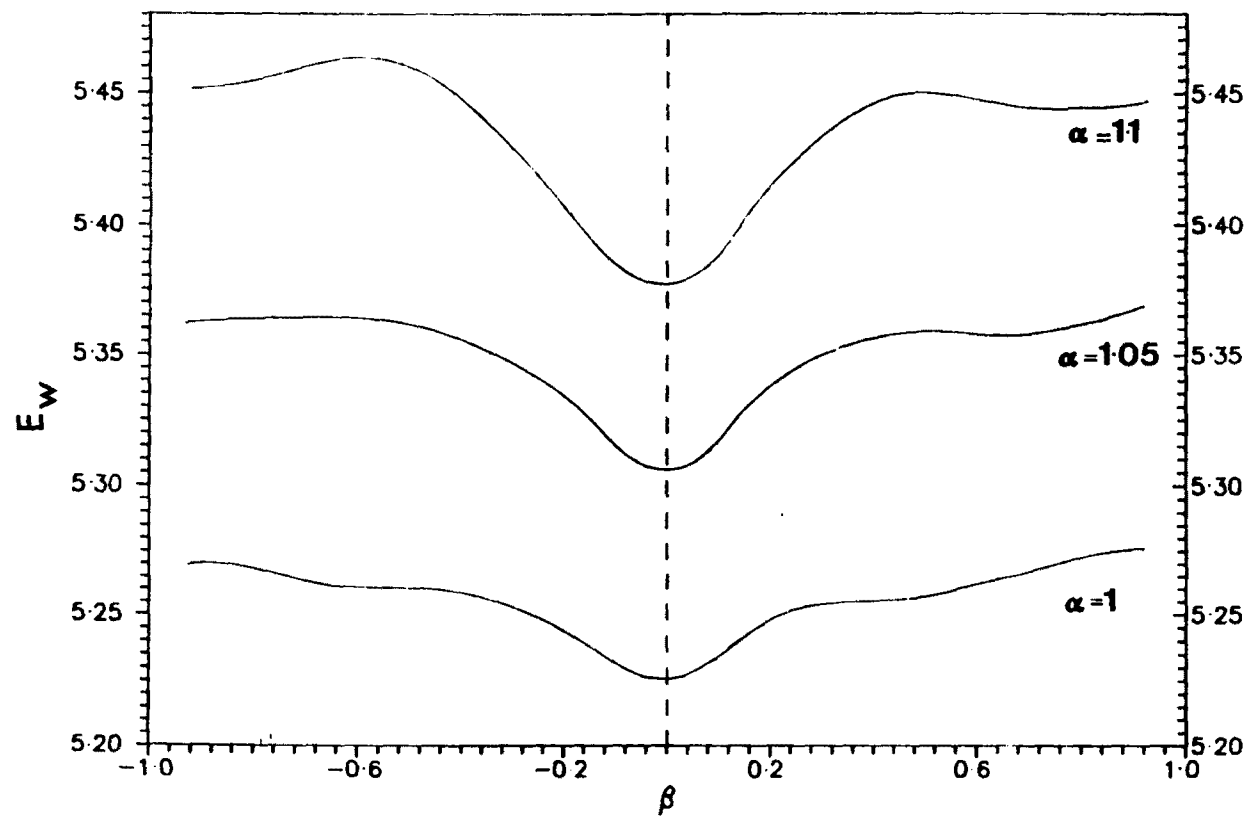


Fig.2.3 Plot showing the variation of the dimensionless surface energy parameter as a function of the particle shape for a 25Å particle, for 3 different values of the surface anisotropy ratio (α).

particle is dependent on the surface anisotropy. Even before introducing the temperature dependence of the system one can predict that the energy variations, and hence the thermodynamic stability, decrease as the surface energy becomes more isotropic. The energy variations should completely disappear as the energy becomes completely isotropic as in the case of a molten droplet giving a spherical shape to the droplet.

2.1.2 Elasticity of the Disclination

We use an isotropic inhomogeneous two-dimensional elasticity model to determine the strain energies. Experimental results from small particles suggest that the strain patterns are highly inhomogeneous and previous homogeneous elasticity calculations [Ino 1969] have been found ineffective [Howie & Marks 1984]. The elastic fields of an off-centric wedge disclination in the circular region can be obtained by using the so called slab analogy [Mindlin and Salvadori 1950]. The slab analogy exploits the fact that the differential equations for the Airy stress function in plane elasticity and the transverse deflection of a thin plate loaded in bending are the same. The slab analogy also relates

the boundary conditions in the two problems: a free boundary in elasticity corresponds to a clamped edge in bending. Next, noting that the singular part of the Airy stress function for the wedge disclination is of the type $[\Omega\mu/\pi(\kappa+1)]r^2\log r$ [Dundurs 1969; a discussion of the disclination and its Airy stress function is given in Appendix.2.B], and $(P/8\pi D)r^2\log r$ (where D is the flexural rigidity) for a plate loaded by transverse concentrated force, it follows that the disclination problem can be solved by translating the well known Michell (1902) result for a clamped circular plate that is loaded by an eccentric force. The Airy stress function for the eccentric disclination can therefore be evaluated as follows (also see Fig.2.4, which gives the double coordinate system employed in solving this problem): using the Michell solution which relates the deflection of the plate w to the load P applied we get;

$$w = P/8\pi D \left\{ r_1^2 \log r_1 / \beta r_2 + 0.5 (\beta^2 r_2^2 - r_1^2) \right\} \quad (2.2)$$

where

$$r_2^2 = r^2 + a^2/\beta^2 - 2ar \cos\theta/\beta \quad \text{and}$$

$$r_1^2 = r^2 + \beta^2 a^2 - 2\beta ar \cos\theta$$

from which one can get

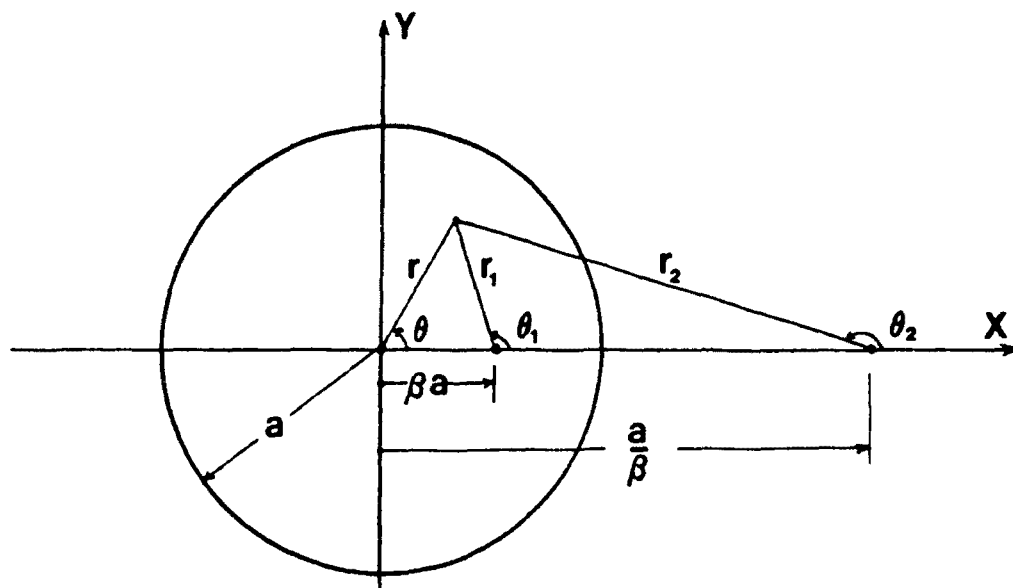


Fig.2.4 The Coordinate system used for the disclination

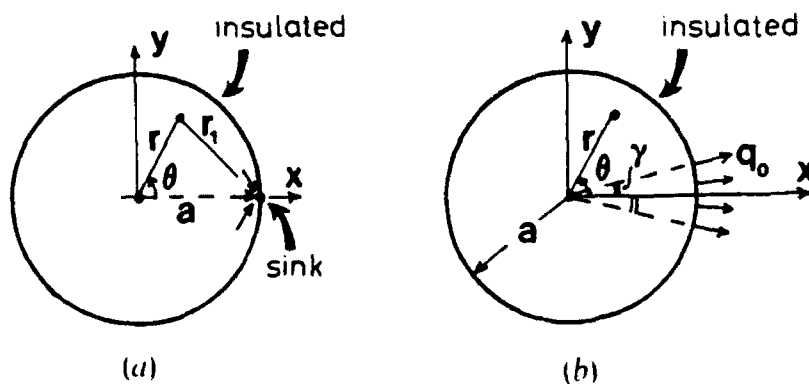


Fig.2.5 Schematic diagram of the particle sitting on the substrate, used in the calculation of the temperature distribution inside the particle.

$$w = P/8\pi D \left\{ r_1^2 \log r_1 / \beta r_2 + 0.5(1-\beta^2)(a^2-r^2) \right\} \quad (2.3)$$

now since

$$r_1^2 = r_2^2 + 2(1-\beta^2)a/\beta r_2 \cos \theta_2 + (1-\beta^2)a^2/\beta^2,$$

$$w = P/8\pi D \left\{ r_1^2 \log r_1 - r_1^2 \log \beta + 0.5(1-\beta^2)(a^2-r^2) - r_2^2 \log r_2 - 2(1-\beta^2)a/\beta r_2 \log r_2 \cos \theta_2 - (1-\beta^2)a^2/\beta^2 \log r_2 \right\} \quad (2.4)$$

Hence the Airy stress function for the disclination is:

$$\begin{aligned} \phi = K \left\{ r_1^2 \log r_1 - r_2^2 \log r_2 \right. \\ - 2(1-\beta^2)a/\beta r_2 \log r_2 \cos \theta_2 \\ - (1-\beta^2)a^2/\beta^2 \log r_2 \\ \left. - [\log \beta + 0.5(1-\beta^2)]r^2 \right\} \quad (2.5) \end{aligned}$$

K is related to Ω , the angle of the wedge that is cut out of the material (positive Ω corresponds to cutting out the material and closing the gap; negative Ω corresponds to cutting the material and inserting a wedge of extra material), by the relation:

$$1/2\mu K(\kappa+1)r 2\pi = r\Omega, \text{ or} \quad (2.6)$$

$$K = \mu\Omega/\pi(\kappa+1), \text{ where}$$

$\kappa = (3 - \nu)/(1 + \nu)$ for plane stress & $\kappa = 3 - 4\nu$ for plane strain. ν is the poisson's ratio for the material. The Airy

stress function ϕ consists of five simple biharmonic functions. Displacement and stress components corresponding to this Airy stress function are:

$$\begin{aligned}
 u_x = & [\Omega/2\pi(\kappa+1)] \{ -(\kappa+1)y(\theta_1-\theta_2) \\
 & + (\kappa-1) [x \log(r_1/\beta r_2) \\
 & - \beta a \log(r_1/r_2) - 0.5(1-\beta^2)x] \\
 & + [(1-\beta^2)a(x-a/\beta)/\beta r_2^2] \\
 & [2(x-a/\beta) + (1-\beta^2)a] \} \quad (2.7)
 \end{aligned}$$

$$\begin{aligned}
 u_y = & [\Omega/2\pi(\kappa+1)] \{ (\kappa+1)(x-\beta a)(\theta_1-\theta_2) \\
 & + (\kappa-1)y[\log(r_1/\beta r_2) \\
 & - 0.5(1-\beta^2)] + (1-\beta^2)ay/\beta r_2^2 [2(x-a/\beta) \\
 & + (1-\beta^2)a] \} \quad (2.8)
 \end{aligned}$$

$$\begin{aligned}
 \sigma_{xx} = & [\Omega\mu/\pi(\kappa+1)] 2y \{ 2\log(r_1/\beta r_2) - (1-\beta^2) \\
 & + 2y^2(1/r_1^2 - 1/r_2^2) - [(1-\beta^2)a/\beta r_2^2] \\
 & (2x-a/\beta - \beta a)(1-2y^2/r_2^2) \} \quad (2.9)
 \end{aligned}$$

$$\begin{aligned}
 \sigma_{xy} = & [\Omega\mu/\pi(\kappa+1)] 2y \{ -(x-\beta a)/r_1^2 + (x-a/\beta)/r_2^2 \\
 & - [(1-\beta^2)ay/\beta r_2^2] [1-2y^2/r_2^2] \\
 & - [(1-\beta^2)a/\beta r_2^2] (x-a/\beta) \} \quad (2.10)
 \end{aligned}$$

$$\begin{aligned}
\sigma_{yy} = & [\Omega\mu/\pi(\kappa+1)] \{ 2\log(r_1/\beta r_2) \\
& - (1-\beta^2) - 2y^2(1/r_1^2 - 1/r_2^2) \\
& - [(1-\beta^2)a/\beta r_2^2] [2(x-a/\beta)(1+2y^2/r_2^2) \\
& - [(1-\beta^2)a/\beta](1-2y^2/r_2^2)] \} \quad (2.11)
\end{aligned}$$

Noting that, on $r=a$, $r_2=r_1/\beta$, it is easy to confirm using the given stress components that the boundary of the circular cylinder is free of tractions. Moreover, using the branch cut $0<\theta_1$, $\theta_2<2\pi$, in (Eq.2.7) and (Eq.2.8) puts the displacement discontinuity on the x axis to the right of the disclination, and from (Eq.2.8)

$$u_y(x, 0^+) - u_y(x, 0^-) = -\Omega(x-\beta a), \quad \beta a < x < a \quad (2.12)$$

2.1.3 Strain Energy of the Disclination

It is convenient to compute the strain energy of the disclination as the work done by the tractions acting on the displacement discontinuity given by (Eq.2.12)

$$W^D = (h/2) \int_{\beta a}^a \Omega(x-\beta a) \sigma_{yy}(x, 0) dx, \quad (2.13)$$

where h is the dimension in the z direction. The details of the calculation involves tedious algebra but, when evaluated, (Eq.2.13) yields the surprisingly simple expression

$$\begin{aligned}
 W^D &= [\Omega^2 \mu a^2 h / 4\pi(\kappa+1)] (1-\beta^2)^2 \\
 &= [e_D^2 \mu V / (\kappa+1)] (1-\beta^2)^2
 \end{aligned}
 \tag{2.14}$$

with V denoting the volume and $e_D = \Omega/2\pi$. Thus,

$$W^D = W_{Dh} (1-\beta^2)^2, \tag{2.15}$$

where W_{Dh} is the strain energy of a symmetrical Dh, given as

$$W_{Dh} = [e_D^2 \mu V / 4(1-\nu)] \tag{2.16}$$

by Howie and Marks (1984) for plane strain with $e_D = 0.0205$. It might be thought that the strain energy per unit volume for the three dimensional case is between those for a long cylinder (plane strain) and a thin circular disc (plane stress). However, the ratio of the plane strain energy to the plane stress energy is $1/(1-\nu^2)$ which ranges from 1 to 4/3.

2.1.4 Surface Stress Energy

To obtain a realistic value of the energy balance between single crystal particles and the many MTP structures considered, we have to include a further energy term--the energy required to strain the surface. The strain energy due to this term is obtained using the approach of Howie and Marks (1984). This can be considered as a correction term to the surface energy term in section 2.1.1 where the surface

energies of unstrained surfaces were used. Although this term can be considered to be quite small compared to the surface energy term, it is of the order of the difference in energies between a single crystal and MTP. This correction term can be expressed by expanding in Taylor series the surface free energy per unit area as

$$\gamma = \gamma_0 + \sum_{ij} e_{ij} \, d\gamma/de_{ij} + \dots, \quad (2.17)$$

where the strain variation is described by the surface stress tensor $g_{ij}(\theta, \vartheta)$ of the material

$$g_{ij}(\theta, \vartheta) = d\gamma(\theta, \vartheta)/de_{ij} \quad (2.18)$$

where i, j are in the surface plane. The correction in the energy term is

$$W^* = \sum_{ij} \int e_{ij} \, g_{ij} \, dS \quad (2.19)$$

Using a simplifying approximation

$$g_{ij}(\theta, \vartheta) = g \, \delta_{ij} \, \gamma_0(\theta, \vartheta) \quad (2.20)$$

where g is a constant, the value of which will be taken as unity here although its value could depend on surface impurities, surface relaxation, lattice imperfections and long and short range atomic interactions etc. For a discussion of the value of g_{ij} and its dependence on various experimental conditions the reader is referred to Linford (1973). The

integral in (Eq.2.19) can be reduced (approximated) to:

$$\begin{aligned}
 w^* &= \sum_{i,j} \int e_{i,j} g_{i,j}(\theta, \vartheta) dS = g \sum_i \int e_{ii} \gamma_i(\theta, \vartheta) dS \\
 &= g e_{00} \int \gamma_*(\theta, \vartheta) dS \\
 &= g e_{00} \gamma_{111} E_w V^{2/3} \quad (2.21)
 \end{aligned}$$

where E_w is the dimensionless energy parameter previously described and e_{00} is the mean strain on the surface.

We begin by computing the hoop strain e_{00} at the boundary for the eccentric disclination. It follows from (Eq.2.9) to (Eq.2.11) that, on $r=a$, we have

$$\sigma_{xx} = [4\pi e_b \mu (1-\beta^2)^2 a^2 \sin^2 \theta] / \pi(\kappa+1) r_1^2, \quad (2.22)$$

$$\sigma_{xy} = -[4\pi e_b \mu (1-\beta^2)^2 a^2 \cos \theta \sin \theta] / \pi(\kappa+1) r_1^2 \quad (2.23)$$

$$\sigma_{yy} = [4\pi e_b \mu (1-\beta^2)^2 \cos^2 \theta] / \pi(\kappa+1) r_1^2 \quad (2.24)$$

where now

$$r_1^2 = a^2 (1 + \beta^2 - 2\beta \cos \theta) \quad (2.25)$$

From the stress transformation formula

$$\sigma_{00} = \sigma_{xx} \sin^2 \theta - 2\sigma_{xy} \cos \theta \sin \theta + \sigma_{yy} \cos^2 \theta \quad (2.26)$$

we get

$$\sigma_{00} = [4\pi e_b \mu (1-\beta^2)^2 / \pi(\kappa+1)] (a/r_1)^2 \quad (2.27)$$

Hooke's law for plane elasticity gives

$$2\mu e_{00} = \sigma_{00} - 0.25(3-\kappa)(\sigma_{xx} + \sigma_{00}) \quad (2.28)$$

and, since σ_{xx} vanishes on $r=a$,

$$e_{00} = \frac{1}{2} e_p (1-\beta^2)^2 (a/r_1)^2 \quad (2.29)$$

The average of the hoop strain on the boundary is

$$e_{00} = (1/2\pi) \int_0^{2\pi} e_{00} d\theta \quad (2.30)$$

Substituting (Eq.2.25) and (Eq.2.29), the result is

$$e_{00} = \frac{1}{2} e_p (1-\beta^2) \quad (2.31)$$

The additional energy term due to the surface stresses can be written using the expression (Eq.2.21) as:

$$\begin{aligned} W^s &= e_{00} g \gamma_{111} E_w V^{2/3} \\ &= \frac{1}{2} e_p g \gamma_{111} E_w V^{2/3} (1-\beta^2) \end{aligned} \quad (2.32)$$

Apart from the surface cost of distortion that we have just calculated, there are other terms in the strain energy such as those due to the effective compressive or expansive loads the surface stresses will exert under which a small particle could relax further and these should depend on the shape of the external surface of the particle. But these extra terms have been evaluated by Howie and Marks and found to be negligible in comparison to that due to the work done from surface distortions in order to balance the tractions on the surface.

2.2 Temperature Distribution

It has always been a curious question, at what

temperature does the small particle sit relative to the substrate in any given thermal surrounding. The temperature gradients inside the particle would also set up thermal gradients which would have a positive contribution to the total strain energy. So it was necessary to understand the nature of the temperature distribution inside the particle.

We assume that the electron beam deposits heat throughout the volume of the particle, that heat is lost only to the substrate and that a steady state has been reached. The temperature T then satisfies the differential equation for two dimensional steady state heat flow:

$$\partial^2 T / \partial x^2 + \partial^2 T / \partial y^2 = -s(x,y)/q \quad (2.33)$$

where $s(x,y)$ is the source density (energy deposited by the electron beam per unit volume and unit time) and q denotes the thermal conductivity. The particular solution for (Eq.2.33) for a constant source density $s(x,y) = s_0$ is

$$T = -(s_0/4q)(x^2+y^2) = -(s_0/4q)r^2 \quad (2.34)$$

It is possible to give a simple closed solution which corresponds to an insulated boundary of the particle, with the heat removed by a sink of strength $\pi a^2 s_0$ per unit thickness and placed at $x=a, y=0$ (Fig.2.5.a):

$$T = T_0 - (s_0 a^2 / q) [r^2 / 4a^2 - \log(r_1/a)] \quad (2.35)$$

where T_0 is the temperature at the center. This solution suffers from the drawback that it is not possible to evaluate the general temperature level because T tends to $-\infty$ at the sink.

Hence a solution must be constructed for heat being removed on a small finite interval of the boundary (Fig.2.5.b). The temperature distribution can be written as

$$T(r, \theta) = -s_0/4q r^2 + A_0 + \sum_{n=1}^{\infty} A_n r^n \cos n\theta \quad (2.36)$$

which satisfies (Eq.2.33). The radial component of the heat flux gives $Q_r = -q \partial T / \partial r$, and from (Eq.2.36)

$$Q_r(a, \theta) = \frac{1}{2} s_0 a - q \sum_{n=1}^{\infty} A_n n a^{n-1} \cos n\theta \quad (2.37)$$

That part of the boundary corresponding to $\gamma < \theta < 2\pi - \gamma$ is taken as insulated ($Q_r=0$). There are two options for the boundary conditions on the interval $-\gamma < \theta < \gamma$ where heat is removed. One can specify a temperature distribution, say $T=0$, on the distribution of the radial heat flux. The first choice leads to a mixed boundary value problem; the solution is complicated because of the singularities at $\theta = \pm \gamma$. Hence the heat flux is specified on $-\gamma < \theta < \gamma$ and for simplicity Q_r is taken as Q_0 , a

constant. Expanding these boundary conditions in a cosine Fourier series on $-\pi < \theta < \pi$, and using the side condition $2\gamma a Q_0 = \pi a^2 s_0$, from the heat balance, we obtain

$$Q_r(a, \theta) = s_0 a \left\{ \frac{1}{2} + \sum_{n=1}^{\infty} (\sin n\gamma / n\gamma) \cos n\theta \right\} \quad (2.38)$$

Matching the coefficients in (Eq.2.37) and (Eq.2.38) yields

$$A_n = -(s_0 \sin n\gamma) / q \gamma n^2 a^{n-2}, \quad n=1, 2, \dots \quad (2.39)$$

To find the constant A_0 in (Eq.2.36) we set $T(a, 0) = 0$ or $\int_{-\gamma}^{\gamma} T(a, \theta) d\theta = 0$. The first choice gives a much simpler result, and hence using it, the final result is:

$$T(r, \theta) = (s_0 / 4q) (a^2 - r^2) + (s_0 a^2 / q\gamma) \sum_{n=1}^{\infty} [1 - (r/a)^n \cos n\theta] \quad (2.40)$$

Taking $\gamma = 1/16$ corresponding to about 3.6° , the temperature at the center of the particle is obtained from the series as

$$T_0 \approx 4.0 s_0 a^2 / q \quad (2.41)$$

The temperature averaged over the volume of the particle is $T_0/2$. The maximum temperature in the particle for this value of γ is

$$T(a, +/\pi) \approx 4.5 s_0 a^2 / q \quad (2.42)$$

When the approximate values of s_0 and k for a 25\AA gold particle sitting on a Si/SiO₂ support for moderate beam fluxes

are put into (Eq.2.41) and (Eq.2.42) the difference between the minimum and maximum temperatures is found to be of the order of 10^{-4} - 10^{-6} °C and hence negligible. For high flux electron irradiation this could be 2-3 orders of magnitude higher, still negligible. This suggests that the temperature gradients in the particle are extremely small and the particle essentially sits canonical with the substrate. This observation suggests the non-feasibility of a thermal origin for the structural instability of small particles under high flux electron beam irradiation observed recently [Iijima and Ichihashi 1986, Smith et al. 1987]. The calculation of the thermal stresses and strain energies, in the forthcoming sections, confirms these results. Our experimental observations in Chapter 5 along with calculation of time scales for temperature drop for small particles are also in accordance with these results.

2.2.1 Thermal Stresses

Toward the computation of the thermal stresses, it is first noted that, except for the single term $-(s_0/4q)r^2$ in (Eq.2.36), the rest of the temperature distribution is a harmonic function (satisfies Laplace's equation $\nabla^2 T=0$). It is

known, however, that a harmonic temperature distribution gives the stresses

$$\sigma_{xx} = \sigma_{xy} = \sigma_{yy} = 0, \quad \sigma_{zz} = -E\alpha T \quad (2.43)$$

in a simply connected cylinder with a free surface but constrained to be in plane strain [Timoshenko & Goodier 1970] Therefore the stress components of interest can be computed easily using the formulas for a radially symmetric temperature distribution:

$$\begin{aligned} \sigma_{rr} &= \alpha E / (1-\nu) \left\{ (1/a^2) \int_0^a T r dr - (1/r^2) \int_0^r T r dr \right\} \\ &= -s_0 \alpha E (a^2 - r^2) / 16q(1-\nu) \end{aligned} \quad (2.44)$$

$$\begin{aligned} \sigma_{\theta\theta} &= \alpha E / (1-\nu) \left\{ (1/a^2) \int_0^a T r dr + (1/r^2) \int_0^r T r dr - T \right\} \\ &= -s_0 \alpha E (a^2 - 3r^2) / 16q(1-\nu) \end{aligned} \quad (2.45)$$

where E denotes the Young's modulus. The expression for σ_{zz} is more complicated because the harmonic part of the temperature distribution enters the expression.

2.2.2 Thermal Strain Energy

The thermal strain energy can be computed from the thermal stresses by

$$W^T = \frac{1}{2} \int_V \sigma_{ij} (e_{ij} - \alpha T \delta_{ij}) dV, \quad i, j = 1, 2, 3 \quad (2.46)$$

where e_{ij} denotes the total strain, so that the quantity inside the parentheses in (Eq.2.46) is the elastic strain. Since

$$e_{ij} = \frac{1}{2} (\partial_i u_j + \partial_j u_i) \text{ and } \sigma_{ij} = \sigma_{ji},$$

$$W^T = \frac{1}{2} \int_V \sigma_{ij} (\partial_i u_j - \alpha T \delta_{ij}) dV \quad (2.47)$$

and using the equilibrium condition $\partial_i \sigma_{ij} = 0$,

$$W^T = \frac{1}{2} \int_V \partial_i (\sigma_{ij} u_j) dV - \frac{1}{2} \alpha \int_V T \sigma_{ii} dV \quad (2.48)$$

next transforming the first integral to a surface integral by Gauss's theorem

$$W^T = \frac{1}{2} \int_S n_i \sigma_{ij} u_j dS - \frac{1}{2} \alpha \int_V T \sigma_{ii} dV \quad (2.49)$$

However, the surface integral vanishes: The side surface of the cylinder is free of tractions and $n_i \sigma_{ij} = 0$. On the ends of the cylinder $\sigma_{31} = \sigma_{32} = 0$ and $u_3 = 0$. Therefore

$$W^T = -\frac{1}{2} \alpha \int_V T (\sigma_{rr} + \sigma_{\theta\theta} + \sigma_{zz}) dV \quad (2.50)$$

This result can be simplified further because, for plane strain [Timoshenko and Goodier 1970],

$$\sigma_{rr} = \nu (\sigma_{rr} + \sigma_{\theta\theta}) - E\alpha T \quad (2.51)$$

Thus finally it is given as

$$\begin{aligned} W^T = & -\frac{1}{2} \alpha (1+\nu) \int_V T (\sigma_{rr}^T + \sigma_{\theta\theta}^T) dV \\ & + \frac{1}{2} E \alpha^2 \int_V T^2 dV \end{aligned} \quad (2.52)$$

where the superscripts T on the stress components are added to emphasize that they are thermal stresses. Substituting into (Eq.2.52) the temperature from (Eq.2.36) and the stresses from (Eq.2.44) and (Eq.2.45), the strain energy of the thermal stresses per thickness is

$$\begin{aligned}
 W^T = & (\pi s_0^2 \alpha^2 E a^6 / 8 q^2) \{ (9-7\nu) / 96(1-\nu) \\
 & + (1/\gamma) \sum_{n=1 \rightarrow \infty} (\sin n\gamma / n^2) \\
 & + (2/\gamma^2) \sum_{n=1 \rightarrow \infty} (\sin^2 n\gamma / n^4) \\
 & + (4/\gamma^2) \sum_{m=1 \rightarrow \infty} \sum_{n=1 \rightarrow \infty} (\sin m\gamma \sin n\gamma / m^2 n^2) \} \quad (2.53)
 \end{aligned}$$

2.2.3 Thermal Stress and Disclination Interaction Energy

Next think of cutting the cylinder and introducing the disclination. This operation is done with the thermal stresses present. The cut is made on $\beta a < x < a$, $y=0$, and the disclination is induced by applying statically to the sides of the cut the tractions that correspond to the disclination stress field. The work done on the body per unit thickness during this operation is

$$\begin{aligned}
 & -\frac{1}{2}h \int_{\beta a}^a \sigma_{yy}^D(x, 0) [u_y^D(x, 0^+) - u_y^D(x, 0^-)] dx \\
 & -h \int_{\beta a}^a \sigma_{yy}^T(x, 0) [u_y^D(x, 0^+) - u_y^D(x, 0^-)] dx \quad (2.54)
 \end{aligned}$$

where the superscripts D and T are used to distinguish the disclination and thermal deformation fields, and the displacement discontinuity in the square brackets is given by (Eq.2.12). The first part of the equation has already been evaluated and the resulting strain energy of the disclination was obtained in (Eq.2.15). The second term is recognized as the interaction energy of the two fields

$$W^I = \Omega h \int_{\beta a}^a (x - \beta a) \sigma_{yy}^T(x, 0) dx \quad (2.55)$$

This can be evaluated by substituting the corresponding expression for σ_{yy}^T and performing the integration. The result obtained is surprisingly simple; since

$$\sigma_{yy}^T(x, 0) = s_0 \alpha E (3x^2 - a^2) / 16q(1-\nu) \quad (2.56)$$

and consequently the interaction energy is

$$W^I = \Omega h s_0 \alpha E a^4 (1 - \beta^2)^2 / 4q(1 - \nu) \quad (2.57)$$

The total strain energy can then be written as:

$$E_{\beta a} = W^D + W^T + W^I \quad (2.58)$$

where W^D given by (Eq.2.15) is the strain energy of the disclination stresses, W^T that of the thermal stresses and W^I the interaction energy of the two fields given by (Eq.2.53) and (Eq.2.57). The most notable feature of the three terms in W is their dependence on size: $W^D \approx a^2 h \approx V$, $W^T \approx a^4 h \approx a^2 V$, $W^I \approx a^6 h \approx a^4 V$. Since the particles have diameter in the range 10-1000Å, the

last two terms in (Eq.2.58) are negligible in comparison with the first, and hence W^D is the only numerically important term in the result.

2.3 Potential Energy Surfaces

The surface energy parameter E_s was plotted against β for three different values of the surface anisotropy ratio α in Fig.2.3. For all values of α , there are strong minima for $\beta=0$ [experimentally consistent result; see Marks 1983], or the case of symmetrical Dh, whereas there are shallow local minima for $\beta=\pm 0.5$, indicating local stability for asymmetric shapes. As the value of α drops, the variation in E_s softens which supports the fact that MTP's are more stable for larger surface energy anisotropies [Howie and Marks 1984]. A rise in temperature decreases the surface anisotropy and the chances of more asymmetric morphologies appearing in an ensemble of particle shapes increase. In other words the configurational space of the ensemble should increase with temperature, an obvious result.

The total energy of the particle, the sum of the surface energy term E_s and $E_{\beta s}$, is plotted in fig.2.6. Although the strong minimum for the symmetric Dh still persists, the

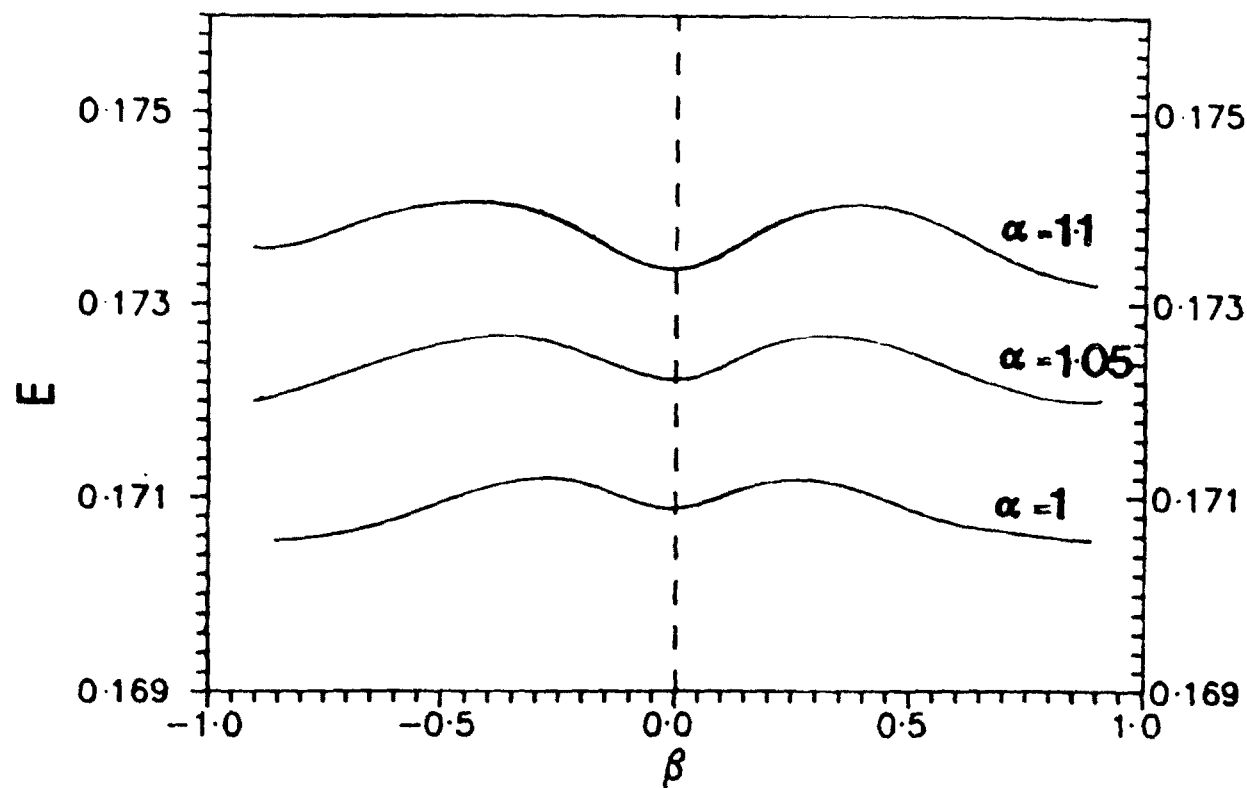


Fig.2.6 The dependence of the total potential energy (arbitrary units) on the particle shape, for a 25Å particle after the strain energy terms are added, for three different surface anisotropy ratios.

magnitude of the energy variations between $\beta=-1$ to $\beta=1$ drops considerably. This indicates that as a more realistic model is used, including all the strain energy terms, the potential energy surface becomes shallow and the minimum for the symmetric Dh structure loses its significance to some extent. The local minimum is far larger than the energy differences between a Dh and a single crystal, for example, and it is far more important to consider the potential energy surface than the simple energy values and the differences. Also the difference in variations in E_c with α becomes less distinct as the strain energy terms are added. It should be noted that, among the strain energy terms, only the internal strain energy due to the disclination field and the surface stresses are important, and other terms are negligible when numerical values are evaluated with appropriate values of constants.

The total energy of the particle can be written in terms of an equivalent radius of the particle, which is the radius of the spherical particle having the same volume. The difference in energies between a single crystal Wulff polyhedron, as the energy of the single crystal is given by Marks (1984) as

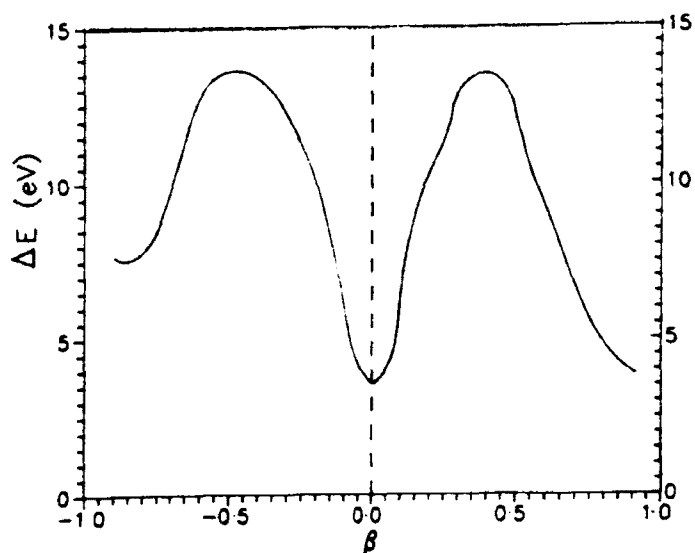


Fig.2.7 The activation energy barriers existing between a single crystal and different particle morphologies plotted against particle shape ($R=25\text{\AA}$, $\alpha=1.1$).

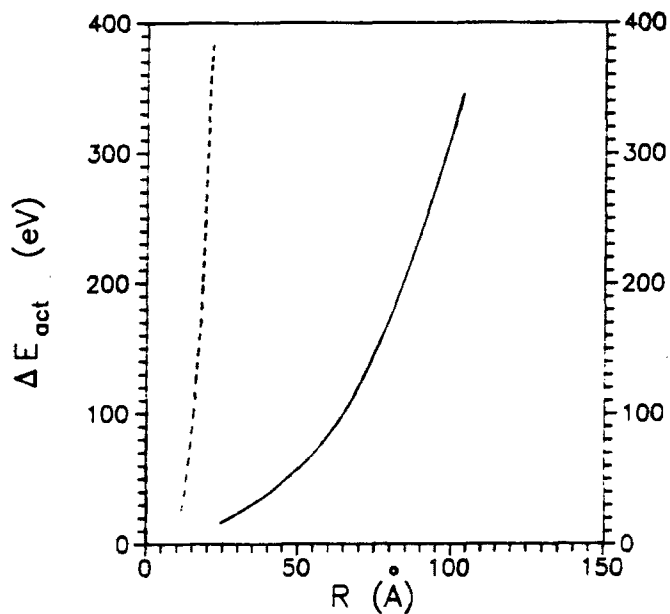


Fig.2.8 Plot of the activation energy barrier against the particle radius with the energy of melting shown by the broken curve.

$$E_{\alpha} = [108\sqrt{3} (1-3\Gamma^3)]^{1/3} \quad (2.59)$$

(where $\Gamma = 1 - \gamma_{100} / \sqrt{3} \gamma_{111}$), and the various shapes characterized by β is plotted against β for a 25Å particle and for $\alpha=1.1$ in Fig.2.7. Note that the magnitude of the maximum activation energy barrier between the different shapes considered is small and of the order of a few electron volts. The activation energy needed for transformation from a single crystal to any of the symmetric or asymmetric shapes is plotted against the particle radius in Fig.2.8. It shows that, as the particle size increases, the activation barrier grows rapidly. In the same plot the classical energy for melting of a small particle is shown (only the enthalpy of melting is considered; the entropy of melting should be of the order of $R \ln 2$ per mole of the substance but for a small particle it will be very small), corrected for melting temperatures at smaller sizes [Couchman and Ryan 1978], which is seen to be orders of magnitude larger. The values of the energies should depend on various experimental factors, such as the nature of the substrate, the gases adsorbed on the surface of the particle and the kinetics of growth, but in any case the result supports the experimental observation that, for large particle sizes, the fluctuations in shapes are much slower and not observable in

realistic time scales, so that the idea of a simple static-particle structure starts to reappear again.

The next chapter will deal with the conversion of potential energy surfaces into free energy surfaces by adding the entropy contributions at different temperatures. A phase diagram for small particles will be constructed from the energy values, showing the stability regimes for various phases that occur in small particle structures including a phase, that will characterize the structural fluctuations, which will be termed as the 'quasi-molten' phase of small particles.

Chapter 3 Free Energy Surfaces and the Phase Diagram

3.1 Entropy Contribution

In the last chapter, only the potential energy surfaces of a small particle were considered, which are static in temperature and time. Free energy surfaces would be much more useful since they would predict the thermodynamic behavior of the system as a function of temperature. This conversion from potential energy to Gibb's free energy is possible if one includes the entropy terms, since the expression $G = E - TS$ would give free energy, G , as a function of temperature T . Similar to the evaluation of the potential energies, the major entropic contributions arise from the surface and strains in a small particle, and the entropy will be a function of β , the particle shape parameter. The degeneracies in the arrangement of different segments are similar in the various shapes considered and hence the entropy of mixing will not be considered (although atomistically these would differ since the volumes of different segments considered vary).

The idea is to consider the entropy contributions from the surface and that due to the disclination as a function of

β . The first term is from the anisotropic and temperature dependent surface free energy and will dominate the entropy terms as for the potential energies. This term can be written as:

$$S_1 = E_s \gamma_s V^{2/3}, \quad \gamma_s = d\gamma/dT \quad (3.1)$$

where E_s is the dimensionless surface energy parameter, dependent on surface anisotropy and shape, and γ_s gives the change in surface energy with temperature. Since the (111) faces dominate the surface of a small particle γ_s is approximately taken as $d\gamma_{111}/dT$ and its value is assumed to be ~ 1.2 ergs/cm². K is a value given by Kirchner and Chadwick (1970) for the change in surface energy with temperature.

The entropy due to the disclination was evaluated, following the analysis given by Huntington, Shirn and Wajda (1955). Their approach to find the entropy due to lattice defects centers around the idea that the crystal and its defects can be treated as harmonic oscillators, and the problem of determining the entropy of a particular lattice defect reduces to evaluating the change in the elastic spectrum that results from the introduction of the defect. But to evaluate the complete lattice vibration spectrum before and after the introduction of the defects is a formidable task.

The task is simplified by dividing the perturbation due to the defect into three distinct regions and approximating that the three contributions to the entropy as:

- a) that resulting from the effect of the large distortions in a region surrounding the defect, the region being a few nearest neighbor distances around the defect.
- b) that resulting from the temperature dependence of the stored elastic energy in the material outside the above region.
- c) that resulting from the effect of the image elastic field on the normal mode frequencies.

The contribution from (a) can be obtained from the ratio of spring constants of the atoms in the perfect crystal and that in the distorted crystal from the region considered in (a). Since the core of the disclination is not as strained as a dislocation core [Hirth and Loathe 1982] and since the particle is small the strains are spread over the entire particle (although non-uniformly) it will be assumed that this contribution is due to the change in spring constants of atoms in the distorted region of the crystal and is negligible. Correspondingly the contribution from (b) will be assumed to be from the entire crystallite. The only variation with

temperature of the stored elastic energy, W^p (Eq.2.15), is assumed to result from the temperature dependence of the elastic constants (at constant pressure):

$$\begin{aligned} S_2 &= -(dW^p/dT) \\ &= - (dW^p/d\mu) (d\mu/dT) \end{aligned} \quad (3.2)$$

Substituting the value of W^p from (Eq.2.15) it is shown that

$$S_2 = -e_b^2 V (1-\beta^2)^2 (d\mu/dT) / 4(1-\nu) \quad (3.3)$$

The value for the change in elastic modulus with temperature, $d\mu/dT$, was taken as equal to 0.38×10^9 dynes/cm².K, a value given by Huntington et al. (1955), for copper.

The contribution from (c) arises because the image field (since the tractions on the surface have to be zero) due to the defect gives rise to a dilatation that alters the normal mode frequencies. Using the Gruneisen equation relating change in normal mode frequencies f_i to volume change (the Gruneisen constant $\tau = - [\partial \ln f_i / \partial \ln V]$) the entropy contribution can be written as

$$S_3 = -3 \tau dV k \quad (3.4)$$

where k is the Boltzmann constant and dV , the volume change from the image field in atomic volumes. The value of Gruneisen constant is taken as 1.96, a value comparable in most metals.

The total entropy is the sum of S_1 , S_2 and S_3 .

3.1.1 Dilatation Due to the Disclination

From the Airy stress function of the disclination given in (Eq.2.5), the normal stresses can be written in cylindrical coordinates as

$$\begin{aligned} \sigma_{rr} = \Omega\mu/\pi(\kappa+1) \{ & 2\log r_1/r_2 \\ & - 2(1-\beta^2)a\cos\theta_2/\beta r_2 - (1-\beta^2)^2 a^2/\beta^2 r_2^2 \\ & - 2[\log\beta + 0.5(1-\beta^2)] \} \end{aligned} \quad (3.5)$$

$$\begin{aligned} \sigma_{\theta\theta} = \Omega\mu/\pi(\kappa+1) \{ & 2\log r_1/r_2 \\ & - 2(1-\beta^2)a\cos\theta_2/\beta r_2 + (1-\beta^2)^2 a^2/\beta^2 r_2^2 \\ & - 2[\log\beta + 0.5(1-\beta^2)] \} \end{aligned} \quad (3.6)$$

Using Hooke's law for a plane

$$e_{rr} = 1/2\mu [\sigma_{rr} - (3-\kappa)/4 (\sigma_{rr} + \sigma_{\theta\theta})] \quad (3.7)$$

$$e_{\theta\theta} = 1/2\mu [\sigma_{\theta\theta} - (3-\kappa)/4 (\sigma_{rr} + \sigma_{\theta\theta})] \quad (3.8)$$

it is given that

$$\begin{aligned} e_{rr} = \Omega(\kappa-1)/2\pi(\kappa+1) \{ & \log r_1/r_2 \\ & - (1-\beta^2)a\cos\theta_2/\beta r_2 \\ & - (1-\beta^2)^2 a^2/\beta^2 (\kappa-1) r_2^2 \\ & - [\log\beta + 0.5(1-\beta^2)] \} \end{aligned} \quad (3.9)$$

$$\begin{aligned}
e_{00} = & \Omega(\kappa-1)/2\pi(\kappa+1) \{ \log r_1/r_2 \\
& - (1-\beta^2) a \cos \theta_2 / \beta r_2 \\
& + (1-\beta^2)^2 a^2 / \beta^2 (\kappa-1) r_2^2 \\
& - [\log \beta + 0.5(1-\beta^2)] \} \quad (3.10)
\end{aligned}$$

The dilatation can be written as

$$\delta v = (e_{rr} + e_{00} + e_{zz}) \quad (3.11)$$

The net volume change is then, in plane strain condition

$$\begin{aligned}
dV &= \int \delta v \, dV \\
&= (1/2\pi) \int_0^{2\pi} \int_0^a (e_{rr} + e_{00}) r \, d\theta \, dr \quad (3.12)
\end{aligned}$$

since $e_{zz}=0$, for plane strain conditions. The integral of (Eq.3.12) was done numerically using trapezoidal rule for numerical integration and was found to converge for step lengths of $a/1000$ for the r and $\pi/500$ for θ variables. It was found that the entropy term due to the dilatation was small compared to the entropy contribution from the surface and stored elastic energy.

3.2 Free Energy Surfaces

The potential energy surface in section 2.2. was converted into Gibb's free energy surfaces using $G = E - TS$ and is shown in Fig.3.1 for a surface anisotropy value of 1.1.

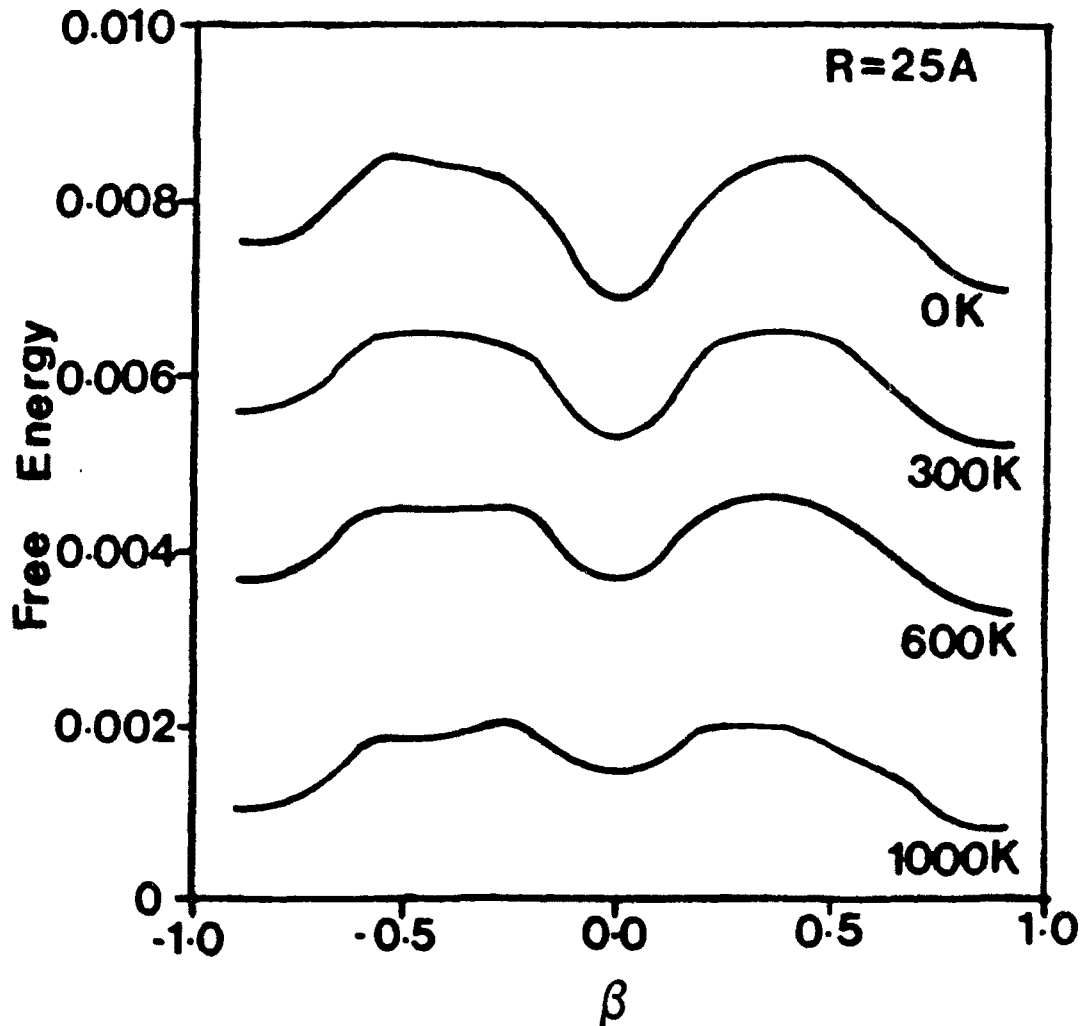


Fig.3.1 Plots of the Gibbs free energy as a function of β , for four different temperatures. The energy is plotted in reduced units and the scale is such that the maximum width of the 0 K energy curve correspond to approximately 0.0005 electron volts per atom. The energy axis between different curves are compressed for better visual comparison.

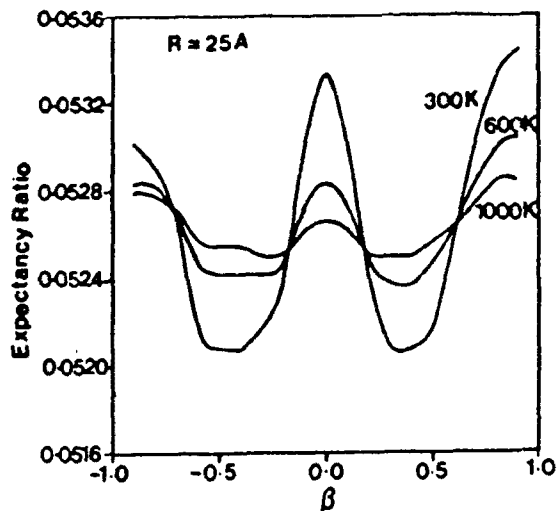


Fig.3.2 Boltzmann probability distributions to go with the free energy curves of Fig.3.1 at three different temperatures.

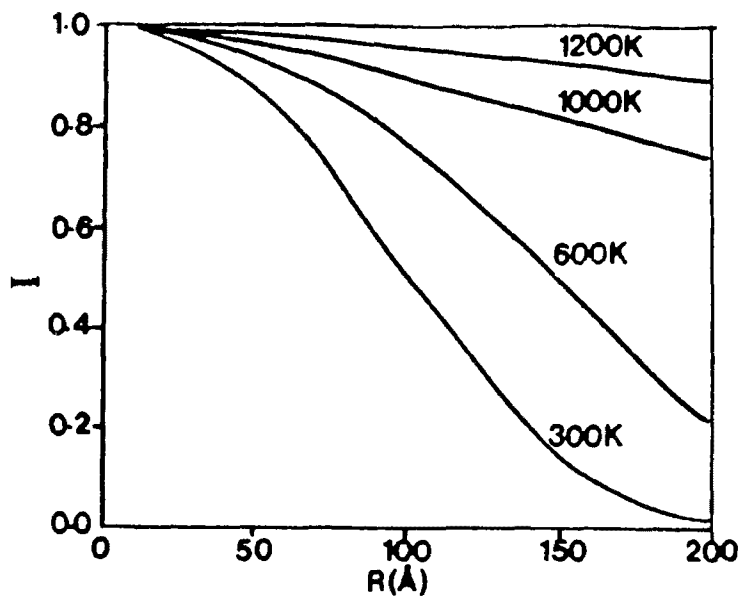


Fig.3.3 The index of quasi-melting, shown as a function of particle radius and temperature. True quasi-melting is defined at an arbitrary value of $I=0.98$.

Various features are evident from the figure. As the temperature is increased the activation energy barriers between different shapes decrease, similar to the anisotropy effect seen earlier. The value of the activation energy barriers decreased by about 30% to 70% for temperatures ranging from 300K to 1000K from the 0K potential energy surface. The decrease in the energy difference suggest that the addition of entropy has made the particles less stable with respect to any stable configuration. If the particle can gain enough energy to cross the activation energy barriers predicted by the free energy surface, it can move over the entire free energy surface structurally fluctuating between the various local minimum shapes. By analogy with quantum mechanics one could say that as the energy differences between various states are becoming smaller the uncertainties in finding the particle in a particular configuration is increasing. The instability should not be confused with the onset of melting, since the difference in the maximum activation energy for transition between any of the structural forms that we have considered, both at room temperature and higher temperatures, is orders of magnitude less than that for melting (this was evident from fig.2.8). The basic

phenomenological difference in the two instabilities will be treated in the discussion. The maximum activation energy barrier between the different shapes is very small and is decreasing with temperature. The maximum energy barrier corresponds to only about $\sim .0005$ ev per atom, a value orders of magnitude lower than kT above room temperature. This energy barrier is taken over the width of the entire energy surface, and the barrier between two neighboring configurations during any structural fluctuation sequence should be orders of magnitude smaller. Given the classical degrees of freedom for at least those atoms residing in the first few surface shells, one can say that thermodynamically the particle can undergo structural rearrangement with rather high probabilities.

3.3 'Quasi-Melting' in Small Particles

To understand how the particle morphologies populate the free energy surfaces, the easiest way is to look at the Boltzmann or probability distribution. This is defined as

$$d_{\beta} \approx \exp(-\xi E_{\beta}) / \sum_{\beta} \exp(-\xi E_{\beta}), \quad \xi = 1/kT \quad (3.13)$$

E_{β} corresponds to the free energy in the β state, where β defines a particular shape of the particle as before. Figure

3.2 shows the Boltzmann distribution of a series of particleshapes at different temperatures for a 25Å particle. At low temperatures the distribution is peaked at $\beta(0)$, since the symmetrical Dh particle is the lowest energy state. As the temperature is increased the distribution flattens out, and the existence of any global minimum is transformed into a multiplicity of local minima. In other words as the probability distribution flattens out, the particle becomes unstable with respect to any particular configuration and its trajectories begin to occupy larger volume of the configurational space.

This configurational instability suggested by the free energy curves of small particles and the corresponding Boltzmann distribution, distinct from thermodynamic melting, will be called "quasi-melting". This is the same type of phenomena found in small clusters by computer calculations and experimentally observed in small particles when a certain amount of energy is provided by an external source. Following authors such as Stillinger and Weber (1983), Berry, Jellenik and Natanson (1984), Honeycutt and Anderson (1987), this coexistence region of a 'group of inherent structures of similar energy' shall be treated as a separate phase occupying

a region of the configurational space. This raises questions about the possibility and nature of a phase transition as the size of a small particle is decreased. It should be quite clear by now that when one talks about the structure of a small particle one is only considering the statistical occupancy of the various local minima and the 'average' of these structures that populate the shallow energy surface.

In order to semi-quantify the idea of quasi-melting an index, I , is defined as the ratio of the Boltzmann probability factor of the most to the least probable particle shape on the energy surface for a particular particle size and temperature. Figure 3.3 shows a plot of the index as one varies the particle size and temperature. It should be noted that the index, although quite arbitrary, is representative of the instability of a particle in thermal equilibrium at temperature T . For a given value of the index, say 0.98, the configurational space has expanded 98% with respect to the occupancy of a single solid-like crystalline structure. It is interesting to see the index of quasi-melting in a reciprocal relation to the surface anisotropy ratio, α , which is the ratio of the energy of the (100) to (111) facet in a strong faceting model. For example, a value of $I=0.98$ would relate

to a value of 1.02 for α , whereas the starting value of the anisotropy ratio, 1.1, would correspond to a much smaller I value. Since the value of $\alpha=1$ (or $I=1$) corresponds to perfect isotropy, it can be said that the anisotropy has been reduced to such an extent that is suggestive of quasi-melting.

It is worthwhile to note that a particle with any arbitrary shape or size, if placed on any point on the free energy surface, aided by the energy fluctuations in a system, will move over and map the entire free energy surface, given enough time. But this time scale can be infinitely large and that is the reason why we do not see this phenomena in macroscopic systems. In the case of a small particle the activation energy barriers existing between the various shapes are extremely small and hence the phenomenon of quasi-melting occurs in observable time scales. The idea of quasi-melting is a statistical concept which relates the activation energy barriers existing on the configurational free energy surface of a free floating small particle to the mean energy and energy fluctuations in the system. The quasi-molten state should thus be a stable phase (although not in the thermodynamic sense) in the phase diagram of a small particle and it should be experimentally observable.

3.4 Phase Diagram of Small Particles

From the data of the free energies, the index of quasi-melting at different temperatures and sizes and the data for size dependent melting points [Couchman and Ryan 1978, Borel 1980], a phase diagram can be constructed for small particles as shown in Fig.3.4. The phase boundaries are derived semi-quantitatively and are far from rigorous. However, they indicate the stability regimes for the different important phases that are observed in materials (especially pertinent in fcc metals which readily form MTPs) at smaller particle sizes. The phase diagram describes a new phase, a coexistence region of many structures which are energetically unstable or rather metastable. In real situations this region should be modified to take care of the substrate-particle interaction, the energy supplied by the external observant etc. The latter point, the fluxional nature of clusters, has been discussed in a recent article by Halicioglu (1988). Similar types of phase diagrams have been proposed before dealing with the instability of the crystalline phase, see for example Wautelet, Laude and Antoniadis (1986) for thin films and wires, and Marks (1986) for polymorphs during thin film growth.

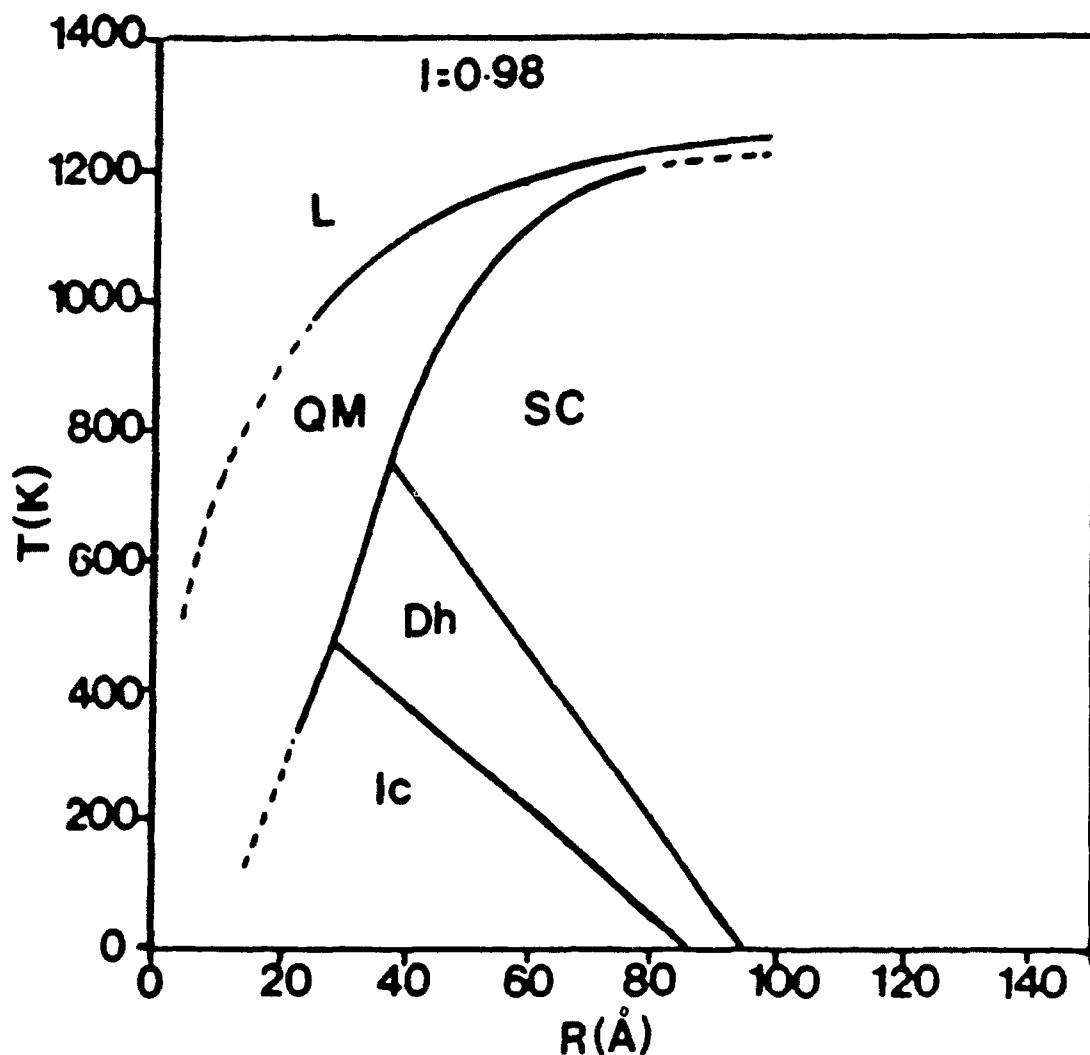


Fig.3.4 Phase diagram for small particles. Included in the figure is experimentally determined depression of the melting point in small particles (Couchman and Ryan, 1978). Stability regimes are: L, liquidus; QM, quasi-melt; Ic, icosahedral MTP; Dh, decahedral MTP; and SC, single crystal. The phase boundaries shown by dotted lines are extrapolated.

The phase diagram is important in predicting the nucleation and growth patterns in material systems as a function of temperature. The values used in the calculation are for gold but the general trend in the phase boundaries should not vary appreciably with other fcc materials. A unique feature in the phase diagram is a new phase (by phase it only mean a co-existence region of different structures of similar energy states and not the usual thermodynamic Gibbsian definition of the state of matter) for small particles, that has so far only been stated qualitatively. There are interesting ramifications of the phase diagram for small particle growth. As nucleation proceeds by atom addition the nuclei formed remain highly unstable not only against evaporation of the nascent atoms to decrease the free energy, but also due to the inherent structural instability. The latter instability remains even after the formation of a stable nuclei until the activation energy barriers become large and a single solid like structure is stabilized. This could be the first precursor of a crystalline solid state. It does not mean that this will be the final crystal structure of the infinite lattice. It only means that a particle with a strong global minimum on the energy surface is formed for

the first time.

The phase diagram could also predict the nature of epitaxy in different systems. For example, at higher temperatures where the quasi-molten phase is contiguous with the single crystal phase, good epitaxial growth can be expected. Experimental observations by Ino (1966), Ino and Ogawa (1967), Roos and Vermaak (1972), Heinemann et al. (1979, 1983) for noble metals on alkali halide substrates (KCl, NaCl) and palladium on MgO suggest that the predictions of the phase boundaries are consistent within limits with experimental results. The phase diagram may also be valuable in the field of catalysis since the shape and structure of particles influence the catalytic activity [see for example: Yacaman, Fuentes and Domenguez 1981, Freund, Lynch and Szymanski 1986]. The variability found in many supported catalyst systems could be due to the meta-stable structure-sensitive catalytic states [Spencer 1986] and their corresponding reactivity. The onset of quasi-melting in small particles could be related to the 'Huttig' temperature in catalysis at small particle sizes, which is suggestive of a soft transition between an equilibrated metal surface and a metastable metal surface of a small particle catalyst due to an appreciable change in the

mobility of the surface atoms.

Computer simulations by Honeycutt and Anderson (1987) and others predict that for large clusters (up to a few thousand atoms), the stable shape is icosahedral type clusters at lower temperatures but fcc or tetrahedral at higher temperatures. Farges et al. (1987) suggest that the transition of the icosahedral structure to fcc type lattice, at larger sizes, could be due to the addition of incomplete layers onto the icosahedral shell in order to avoid strains and compressions inside the particle, which increase as the number of the icosahedral shells are increased. The phase diagram shows the icosahedral structure as a low temperature phase and the decahedron with a narrow range of stability. For better quantitative results, which should include the effect of substrate and so on, the phase boundaries have to be tested and refined by carefully monitored experiments. An important point that should be stressed here is that the energy surfaces for small particles are strongly surface energy limited (similar to an increased manifestation of surface tension effect in liquids when they are constrained in a capillary), and should not vary much with different crystal structures. This is also borne out by the fact that the surface profiles

of small particles, when seen without strong substrate interaction (e.g. amorphous substrates) appear mostly rounded and close to spherical.

3.5 Statistical Energy Fluctuations

Since the systems that have been considered are small, the effect of statistical fluctuations is immense and the question arises whether equilibrium thermodynamics is valid in this range [Feshback 1987]. It should be noted that the results in the regime of "Quasi-melting" are only extrapolations and any attempt to define the system in terms of thermodynamic variables should be treated with caution. For particles with such small sizes the equilibrium thermodynamic variables have meaning only when the particle is coupled with a reservoir [Kittel 1988]. It looks promising to relate the phenomena to situations in which irreversible thermodynamics [Nicolis and Prigogine 1977, Prigogine 1980] plays a major role in self-organization and evolution of dissipative structures, where non-equilibrium may be a source of order, as seen in many physical and biological systems. In these situations when the system passes through a region of the configurational space where the energy is finely

distributed between the many 'eigenstates' (by analogy with quantum mechanics) the system may leave the thermodynamic branch and aided by macroscopic fluctuations, internal or imposed externally, may undergo bifurcations into an altogether new structure. This may introduce an extra entropic term, similar to a communal entropy during melting, of the order of a small fraction of $R \ln 2$ as discussed by Stishov, Makarenko, Ivanov and Nikolaenko (1973), and Tallon (1980). This new entropy term and the fluctuations in thermal energy of the system could more than offset the activation barriers, thus stabilizing the quasi-molten state. A major difference between the two is that whereas in dissipative structures the bifurcations are localized both in time and space (microscopic patterns are evolved in macroscopic systems), quasi-melting should be a phenomenon localized only in time. Such ideas can only be expressed qualitatively and work remains to be done.

A rough idea is obtained from the relative fluctuations in energy, with respect to a mean energy level, in configurational space as a function of temperature for different particle sizes. In situations where the system is assuming states at random the energy values of the individual

states lose meaning and the mean energy of the system becomes representative. The mean energy of the system is written as

$$\langle E^m \rangle = \sum_{\beta} E_{\beta} d_{\beta} \quad (3.14)$$

where E_{β} and d_{β} are the energy and probability of the β state. Since E_{β} assumes values different from $\langle E^m \rangle$, as the state of the system changes, the average width of the interval between the two can be used to calculate the statistical fluctuations in energy. This is done as

$$\begin{aligned} dE &= \sum_{\beta} d_{\beta} (E_{\beta} - \langle E^m \rangle)^2 \\ &= \langle (E_{\beta})^2 \rangle - \langle E^m \rangle^2 \end{aligned} \quad (3.15)$$

where $\langle \rangle$ is the same operation defined in (Eq.3.14). The ratio $dE/\langle E^m \rangle$ is known as relative fluctuation and gives a better idea of the fluctuations relative to a mean system energy. Figure 3.5 shows that at higher temperatures the relative energy fluctuations in a 10 \AA^0 particle become more than those for a 25 \AA^0 particle whereas the energy barriers are much lower for the former. This indicates that with decreasing particle size the system exhibits an increasing tendency for fluctuation dependent non-equilibrium processes.

An extension of the statistical method can be used to understand a random walk of the particle in configurational space (β -space), and this would give an idea of the phenomena

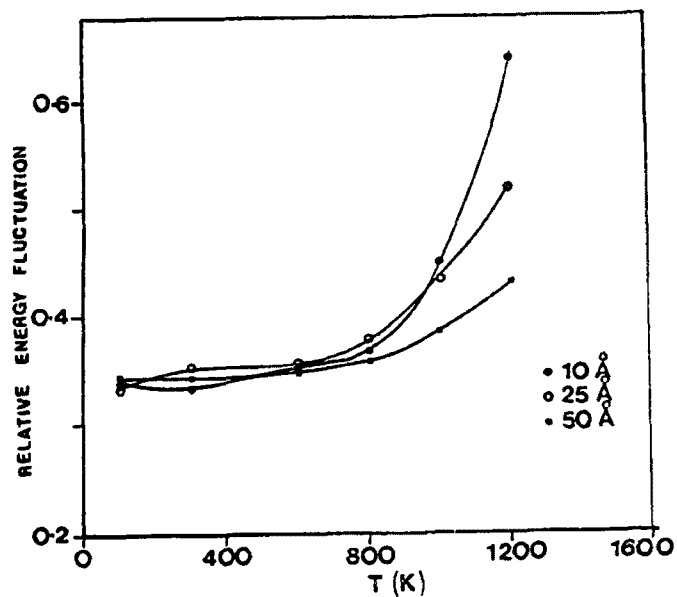


Fig.3.5 The relative statistical fluctuation in energy with respect to the mean energy level plotted as a function of temperature for three particle sizes.

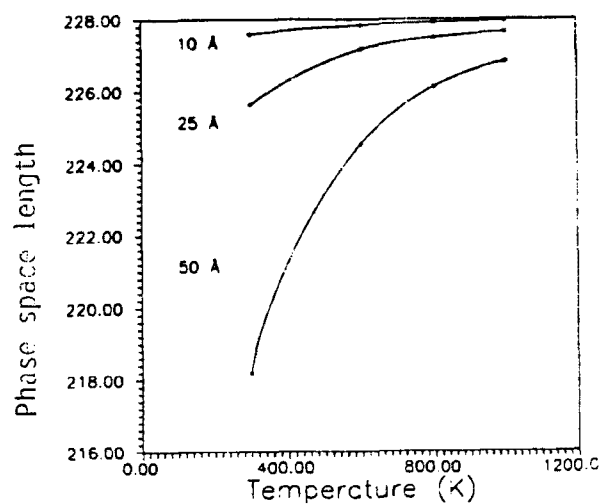


Fig.3.6 The phase space length spanned by particles of three different sizes, during a random walk in configurational space, plotted as a function of temperature. The units of length are arbitrary.

of quasi-melting. It will be assumed that the jumps between different states are determined solely by the energies of independent states. A particle with a higher energy (E_1) will jump to a lower energy state (E_2) with a probability

$$P_{12} \sim \exp [-(E_1 - E_2)/kT] \quad (3.16)$$

If there is an energy barrier (E_{barrier}) between the two states then the probability will be given as

$$P_{12} = \exp [-(E_{\text{barrier}})/kT] \quad (3.17)$$

The average displacement of a particle (in the β state) which is taking such jumps between various states can be written in arbitrary units of length as

$$\langle D \rangle = \sum_{\alpha} (\beta - \alpha) P_{\beta\alpha} \quad (3.18)$$

If all the configurational states are considered to be taking such jumps, then the dimension (length) of the configurational space (only a proportional quantity and not in correct units) could be represented by the sum of the displacements of all states with each state transforming into all the other possible states. This will give

$$\Phi = \sum_{\alpha} \sum_{\beta} (\beta - \alpha) P_{\beta\alpha} \quad (3.19)$$

A plot of Φ is shown in Fig.3.6 as functions of temperature and particle radius. At larger particle sizes, the

β -space dimension increases drastically as temperature is increased, but as for smaller particles this quantity is large and essentially remains unchanged at all temperatures. The plot should give us a qualitative idea of how a small particle evolves in configurational space (or structurally fluctuates between various shapes) as the size of the particle is reduced or the temperature is increased.

3.6 Discussion

The results from these theoretical calculations suggest that the same type of structural fluctuations observed for atomic clusters can be extended to larger particle sizes. The various anomalous properties observed at smaller sizes can be attributed to the fact that in that regime many new metastable and unstable phases appear, due to the fine distribution of energy levels and driven by external or non-equilibrium statistical forces. The environment could play an important role in deciding the exact structural configuration of these low-dimensional systems and any generalization of results on the properties of these materials should be treated very carefully.

The question of the nature of the phase transitions at

very small particle sizes is a curious one, and has yet to be resolved. Although melting itself is a complicated as well as a controversial phenomenon, the relationship between the two is worth examining. The simplest and probably the most successful model of melting is based on lattice instability, propounded over the years by Lindemann (1910), Herzfeld and Goeppert-Mayer (1934), Born (1939) etc. and recently reviewed by Boyer (1985), and has been used by authors like Takagi (1954), Buffat and Borel (1976), Couchman and Ryan (1978), Hasegawa, Hoshino and Watabe (1980) to calculate the depression in melting point in lower dimensional systems. It appears from these works that there is no unique way of defining the melting point in small particles. Moreover, work on small clusters predicts that there exists a range in the melting transition and the energy change in the vicinity of this range is a slowly varying function of temperature. The boundary of quasi-melting could be treated as an extension of this regime and hence the phase transition associated with it should be weaker compared to the melting transition in the corresponding real crystal. The Lindemann criteria in melting may be extended to a lower critical temperature for the instability range (from quasi-melting to melting) in small

particles. Quasi-melting could set in when the atomic vibration exceeds a certain fraction of the Lindemann's criterion (say, $T_{q.m.}/T_m$) with the actual melting taking place at the value given by the above criterion. This lower limit of instability could be due to the lower average coordination of atoms in a small particle resulting in a higher entropy and the lack of long range order which stabilizes the infinite crystalline lattice. Authors such as Eppers and Kaelberer (1977), Lee, Barker and Abraham (1976) and Briant and Burton (1975) have provided results, although inconclusive, for the nature and order of the structural phase transitions in clusters containing a few atoms. Statistical mechanical predictions suggest that sharp phase transitions cannot exist in small finite systems. This is also suggested by the fact that the activation energies involved during quasi-melting are much smaller than those for melting. The fact remains that the order of the solid-liquid and solid-quasi-solid phase transitions (for example surface melting) are controversial. It would be interesting to see the analogy between quasi-melting and displacive transformations [Boyer and Hardy 1981, a similar analogy is discussed by Boyer (1985) in the case of melting]. Here, above the transition temperature, the

parameter that defines the lattice undergoes a change from a static to a dynamically fluctuating one. The potential energy surface in the latter shows a distinct double well structure of a low and high symmetry crystal lattice whereas in the former the energy surface consists of many weak local minima with no preferred structure after the transition. The instabilities in the shape of a small particle was explained in terms of molecular motions associated with a redistribution in the vacancy concentration in different parts of the crystal by Searcy (1984). A dynamic equilibrium is established when the vacancies are so distributed that the molecular fluxes between various regions of different binding energies are equalized. Tholen (1981) suggested that structural changes in small particles could result from vibrational amplitudes during a martensitic type of transformation. He associated such a shear transformation with the passage of supersonic dislocations through the particle. It is worth noting that none of these models has any experimentally supported evidence.

An extension of the work on small particles has involved correlating the electronic instabilities when an electron beam in the microscope induces excitations inside a small particle

which provide the activation energy needed for it to quasi-melt. Most of the proposed mechanisms involve electronic excitations produced by the incident electrons, for example plasmon excitation, a coulomb explosion [Howie 1986], localized melting and recrystallization due to secondary auger electrons [Williams 1987]. But these violent electronic excitation events can be ruled out since it is experimentally demonstrated in chapter 5 that the energy needed to initiate quasi-melting in small particles is orders of magnitude higher than that needed to sustain it. It is found that the stable particle morphologies that one sees in any experimental situation are the trapped morphologies in large potential wells on substrates, due to stable interfaces (see next two chapters for experimental results). It should also be noted that a small particle is stable against ionization, especially at lower temperatures, due to the large gaps in the energy levels as suggested by Kubo (1962). Another question is whether the effect of temperature rise in a small particle is responsible for the instability. Calculations have indicated [Iijima 1985, Dundurs, Marks and Ajayan 1988] that the particle does not get thermally heated in the process of electron irradiation and remains canonical with the substrate.

Buxbaum and Marks (1987) proposed that the particle may be sensing an equivalent 'electronic temperature' which is localized in time and space. Thus the electron beam rather than indirectly transferring momentum and increasing the atomic vibrations and hence the temperature, could directly induce electronic excitations providing localized energy which can then be distributed to the material in short time scales.

What thermodynamics or the phase diagram predicts is the equilibrium structure and the position of the particle on a morphological energy surface. As the energy distribution becomes dense statistical and non-equilibrium forces assume importance. Quasi-melting will give the probability that a particle can jump the potential wells on the energy surface. The exact route for the energy gain and phase transformation remains unanswered and a fertile topic for future research.

Chapter 4 Experimental Observations of some Novel

Particle-Substrate Interactions

4.1 Small Particles and Substrates: Introduction

The thermodynamic equilibrium shape of a large crystallite can be determined using the Curie-Wulff construction, which is a mathematical procedure for minimizing the total surface energy at constant volume of the material. The construction predicts that any shape that is formed with constant values for the ratios of the energies of the surface planes to the distance of the planes to the geometric center is a local minimum in the energy diagram. But for small particles in the nanometer size ranges the volume transport across the particle becomes significant and the time scales for equilibration become small [Herring 1962]. In fact for a small free floating particle the particle remains in a structurally unstable state, fluctuating between various morphologies. This fluid-like state, which is distinct from the true molten state was termed, in the previous chapter, the quasi-molten state of a small particle. This state has been predicted theoretically by many authors for atomic clusters

and in the earlier chapters of this work in small particles, and its fingerprints observed in many experiments [Iijima and Ichihashi 1986, Bovin et al. 1986, Blumel et al. 1988].

The situation is a little different for small particles on relatively large solid substrates, which is the case in many systems which are technologically important, for example heterogeneous catalysts. Here the equilibrium shape of the particle can be more realistically predicted by the Wulff construction since the substrate behaves as an anchor and holds the particle in place, the difference being that now the interfacial free energy along the particle-substrate contact plane is different compared to the particle-vacuum interface. The actual shape and position of a particle with respect to the substrate can be predicted by considering the energy balance due to the change in area of the different facets and the new interface that is created. This is under ideal thermodynamic conditions which neglect the effects of diffusion, long range and vapor phase interactions with the substrate. In most real cases these effects can be dominating, and unavoidable, and the structure and shapes of the system can be altered dramatically; and in most theoretical calculations, the effect of the substrate interactions on the

structure of a small particle is not taken into account.

The easiest way to visualize the effect of substrate interactions, based on the ideas of Wulff construction, is to look at a Winterbottom construction [Winterbottom 1967, Pillar and Nuttig 1967, Heyraud and Metois 1980; also see Fig.4.1]. For a liquid droplet on the substrate, in the absence of any gravitational influence, the general shape of the droplet is uniquely defined by the equilibrium contact angle that the droplet makes with the substrate. For a solid particle this picture is complicated by the fact that the surface energy in solids is strongly anisotropic. In this case of an anisotropic surface tension, the contact angle can no longer be considered as a unique characterization of the balance of the horizontal components of the surface tension forces along the substrate plane and hence cannot uniquely define the particle shape since one or more of the intersecting interfaces adopt orientations corresponding to local surface energy minima. But still for the case of a planar interface, Winterbottom proved that it is possible to transform the complex problem of determining the equilibrium shape of the particle resting upon the interface to a much simpler problem of determining the equilibrium shape of an equivalent free particle with a

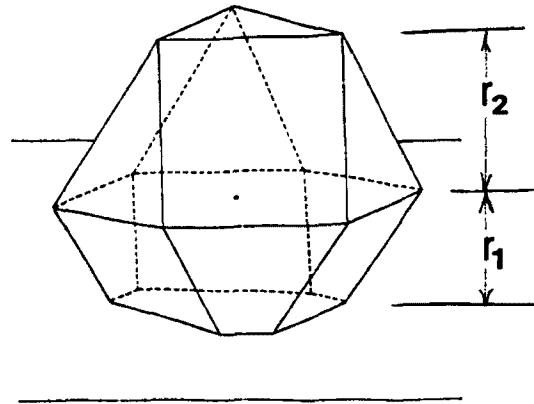


Fig.4.1a Schematic representation of equilibrated particle (truncated polyhedron shape) situated on substrate surface. Particle is made of $\{111\}$ triangular and $\{100\}$ square facets. (from Pillar & Nuttig, 1967).

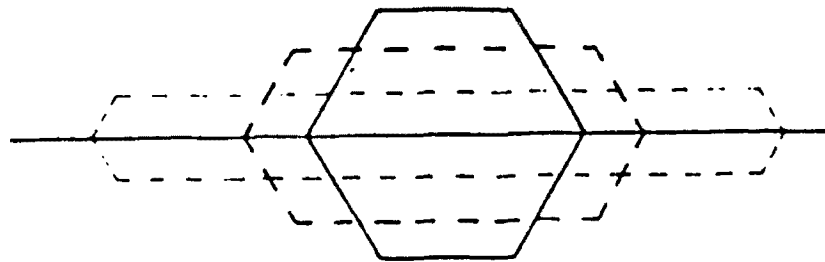


Fig.4.1b Schematic illustration of the influence of increased binding between particle and substrate when $(\gamma - \gamma^{ub}) < 0$; shown by dashed figures. Free particle shape is the solid figure. (from Winterbottom, 1967).

surface tension γ^* where

$$\gamma^* = (\gamma_{sp} - \gamma_{sv}) \quad (4.1)$$

Here γ_{sp} and γ_{sv} corresponds to the substrate-particle and the substrate-vacuum interfacial energies. So the Wulff construction for a particle on a substrate is the minimization of the integral

$$\int_p \gamma^* dS, \text{ for constant volume} \quad (4.2)$$

where the subscript p suggests that the integration has to be carried out over the total surface P of the particle. It should be noted that in this situation negative values for γ^* are possible, in which case the Wulff point will no longer fall inside the inner envelope of the construction.

The above construction physically means that the formation of an interface represents a lowering of the free energy of the system, and the planes which form the interface should by definition have lower free energies associated with them than their equivalent surface free planes. Hence the γ plot for a material forming an interface should be asymmetrical (as shown in Fig.4.1a), the solid state interfacial planes having lower free energy and hence being nearer to the Wulff point than their crystallographically equivalent solid-vapor interfacial planes. A regular

polyhedron shape for a small particle would thus change to a truncated and distorted polyhedron shape due to the substrate effect. In fact it is possible to get estimates of the solid-solid interfacial energy, knowing the surface energies associated with certain surface free planes. For example from Fig.4.1a, the total energy of the interface can be written as

$$\gamma_{\text{interface}} = \gamma_{\text{substrate}} + (r_1/r_2) \gamma_p^{(hkl)} \quad (4.3)$$

Depending on the value of γ , which characterizes the strength of the particle-substrate binding, a variety of particle-substrate configurations can result which correspond to various degrees of wetting of the particle by the substrate, see Fig.4.1b. It can be noted that the thermodynamic significance of the contact angle (which defines wetting in liquid systems) is ambiguous for solid particles since θ can not be related to a unique value of γ for the faceted particle. Experimental observations for these interactions for micron size particles sitting on solid substrates have been previously reported [Winterbottom 1967]. For very small particles in the nanometer size ranges, it can be shown that the free energy reduction in a particle-substrate system can also occur by the particle 'sinking' into the substrate rather than wetting. In fact the criterion for

sinking for such small particles sitting on solid substrates becomes stronger than wetting the substrate, and this will be discussed in a later section of this chapter. For larger particles, the activation energies for the former process could be quite large compared to the latter and wetting becomes the route for free energy reduction of the system.

4.2 Experimental Method

The specimen system used for the experiments consists of a distribution of gold clusters on magnesium oxide smoke particles. The reasons for choosing this system were many-fold. Magnesium oxide has a highly cusped γ plot due to a strong anisotropy in the surface energy, with the (100) surface plane having almost half the energy of any other low index planes of MgO. Thus the MgO smoke particles form well defined cuboids with almost flat (100) low energy facets. The smoke particles that are formed, by smoking magnesium ribbon in air, are in the micron or lower size ranges and look almost transparent in the electron beam inside a transmission electron microscope. The small size as well as the transparency of MgO smoke cubes is advantageous since the interactions between the particles distributed on the surface

and the substrate are in the field of view, and no unseen long range events need to be taken into consideration. The gold particles are useful because they are noble and the chances of any chemical reaction with the substrate is rather small. The sticking coefficients for gold is exceedingly small compared to many other metals for most of the contaminations that one finds in the microscope and they can be safely regarded as clean during most of the operations under the microscope vacuum (typically of the order of 10^{-6} to 10^{-7} torr). Gold also has a deep potential and hence strongly diffracts the electrons, giving very good image contrast.

The MgO smoke was directly caught on a 3mm copper grid, that is used in the TEM, placed above the smoke for a few seconds. The gold particles were distributed on the smoke particles by three different techniques.

1. The first method was to use a cluster solution which was prepared by the reduction of organometallic compounds, and the clusters stabilized by phenyl ligands [the method is detailed in Teo and Keating 1984]. The cluster solution was not prepared in our laboratory but supplied to us by Dr. Teo from the University of Illinois, Chicago. A drop of the solution was placed on the grid with MgO and the solvent



Fig.4.2 Distribution of two-dimensional rafts and single atoms of gold on the (100) surface and surface steps of magnesium oxide substrate (Courtesy of Professor L. D. Marks)

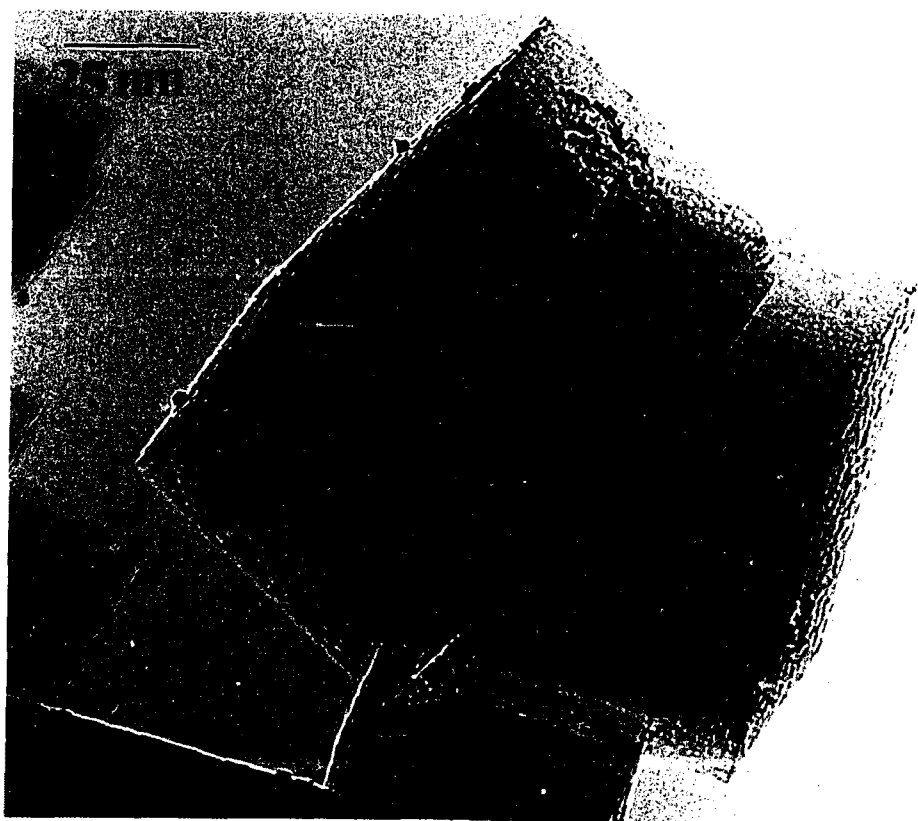


Fig.4.3 Low-magnification image showing cuboids of transparent magnesium oxide smoke particle with gold microclusters distributed on their (100) surfaces.

allowed to evaporate (the ligands evaporate off under the electron beam). This gave a very fine distribution of gold with mostly two dimensional atomic rafts and single atom distributions on the MgO surface steps [Marks et al. 1987], as seen in Fig.4.2. Under the electron beam these single atoms and rafts undergo surface diffusion and larger particles were formed giving a distribution (quite a sparse one and hence nice to work with) of gold clusters with a range of particle sizes, as seen in Fig.4.3. The specimens were clean during most operations including those at higher temperatures in a hot stage.

2. A second method consisted of evaporating gold particles on to copper grids with MgO, in a Danton high vacuum chamber at a base pressure of $\sim 10^{-6}$ torr. The distribution of gold clusters in this case on the MgO surface was similar to the above but thicker although a larger range of sizes could be obtained.

3. The third technique was to use laser evaporated gold clusters on MgO smoke supported on copper grids, at atmospheric pressure (Courtesy of Dr. Manfred Kappes).

The specimens were observed using the following atomic resolution transmission electron microscopes (a short

introduction to high resolution electron microscopy was given in chapter 1.5 and will not be repeated here):

1. HITACHI-9000 High Resolution Electron Microscope (HREM), at Northwestern HREM facility, where most of the work was done. The microscope was operated at 300 KV for all observations and had a point to point to resolution of $\sim 1.8\text{\AA}$. The microscope was equipped with a Gatan TV camera and an on-line facility for real time video recording using a 3/4" Sony VCR. There was also an on line image processing system, ITEX, connected to the TV camera, through which individual frames of the image could be grabbed and stored in an Apollo computer work station. ITEX, coupled with an image manipulation software package SEMPER, was also capable of performing many operations like taking the diffractograms of an area of the image, running average of many frames and so on.

2. JOEL-4000 HREM with a HOT STAGE (which was done at Bell Labs), in order to study the effects of temperature on the system.

The flux conditions used in the microscope were: 1. A low electron flux condition, with the condenser aperture inserted, and at spot size 3 corresponding to a current density of $\sim 1-5$ amps/cm². This corresponds to the normal flux used for

imaging in most microscopy experiments, and all the images were taken under this condition.

2. A high electron flux condition, with the condenser aperture removed, corresponding to a current density of 50-100 amps/cm². This can be converted to a flux density which corresponds approximately to 10⁵ electrons/Å²/sec. This flux is used mostly during electron irradiation studies to simulate kinetic conditions inside the microscope and to carry out radiation damage studies.

The specimens obtained from all three different techniques of sample preparation gave similar results as discussed in the following sections.

4.3 Sinking Small Particles

A series of observations during low flux and initial stages of the high flux electron irradiation conditions, suggest that for small gold particles sitting on the low energy faces of MgO there is a tendency to 'sink' in to overlayers of the substrate that diffuse and cover up the gold particles [Ajayan and Marks 1989a]. Figure 4.4 shows the first image of the sequence that illustrates the phenomena. Initially a gold particle, about 30Å in diameter, is seen



Fig.4.4 a) High resolution image of a gold particle on an MgO surface. Layers of MgO form on the particle following irradiation with an electron beam. The lattice layers in the substrate correspond to the (200) atomic planes. b & c show the same particle after low-flux electron irradiation for 10 and 60 minutes respectively. The particle sinks into the substrate and also undergoes some shear.

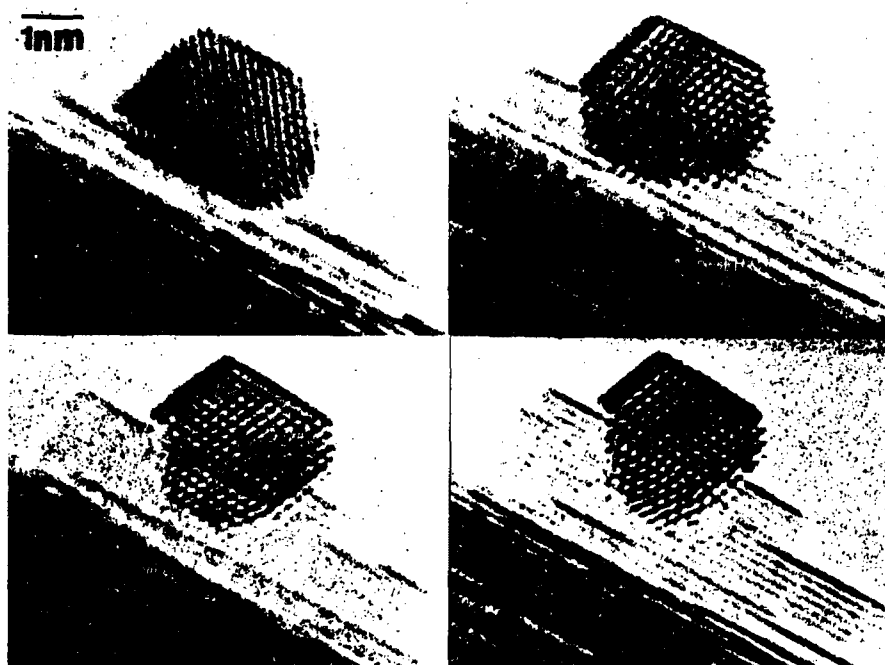


Fig.4.5 Irradiation sequence of a gold particle on the MgO surface. a) Initial particle b) After 10 minutes under low flux c) After 30 minutes under low flux d) After additional 10 minutes of high flux electron irradiation. Note that during the process of sinking a twin has developed in the lower part of the particle.

sitting on an almost flat MgO surface. The lattice fringes that are seen in the bulk of the MgO substrate correspond to the (200) spacing of the MgO lattice and are 2.1\AA apart. Approximately, one can calculate as mentioned in section 4.1, the total energy of the gold-MgO interface and such a calculation is given in Appendix 4.A.

Under low electron fluxes, with time, an interesting transformation occurs to the gold-MgO system (Fig.4.4). One can see that with time the substrate material slowly diffuses and covers up the gold particle surface, or effectively the particle sinks into a capsule of the substrate that has formed around the gold particle. The lattice spacing of the overlayer that has formed corresponds to the (200) spacings similar to the bulk. In this particular case, where the particle is very small, the sinking is complete and the whole of the gold surface is covered with MgO. During this process of encapsulation or reversely speaking, sinking, the particle shape has also undergone a change due to some kind of shear. Similar shape changes are a characteristic feature of small particle structures, as have many times previously been mentioned. Figure 4.5 shows the sequence of another particle (better images of the gold particle) slowly sinking into the

diffusing MgO layers. It is seen that during the process the particle has rotated slightly with respect to the original substrate and also a twin boundary has formed in the lower part of the particle. Here sinking does not proceed to completion and the particle is seen to be slowly getting pushed out from the original substrate plane. This process of decoupling of the particle from the substrate under the electron beam, which is independent of the phenomenon of sinking will be the subject of discussion in the next section. It is also seen from many observations that the initial orientation of the particle affects the process and rate of sinking. Sinking appears to occur much faster if the initial orientation of the particle with the substrate is close to epitaxial. It is also seen that whenever there is some contamination on the surface of the gold particle, like amorphous carbon or other hydrocarbons, sinking slows down and some times is even halted. Diffusion of these hydrocarbons and cleaning of the gold surface by the electron beam resumes sinking. For larger particles (above 50Å in size) the process is very slow and never proceeds to completion. At larger electron fluxes, sinking occurs much faster as seen from Fig.4.6. It is possible to roughly calculate the diffusion

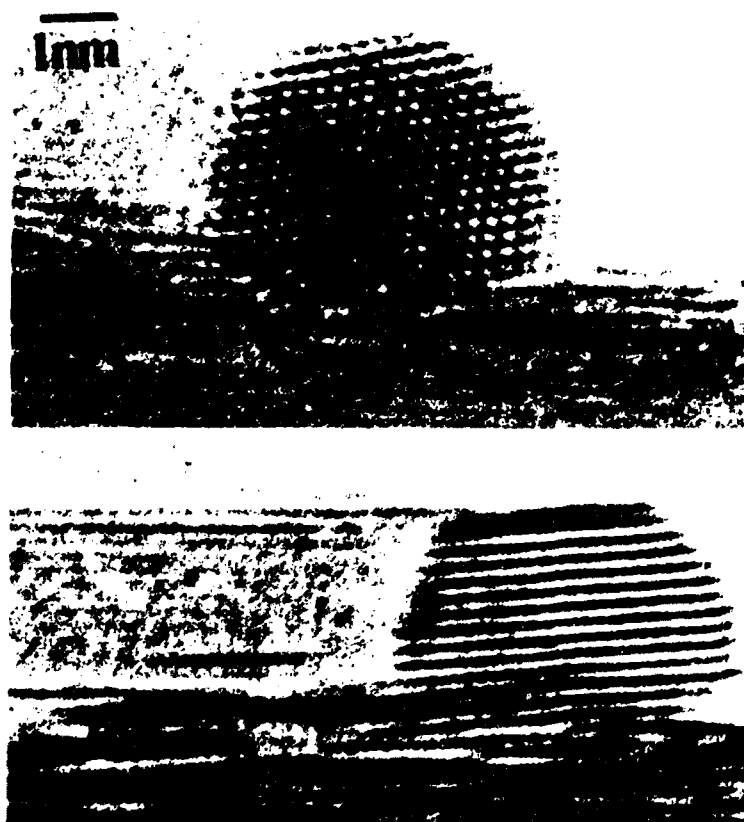


Fig.4.6 a) High resolution image of the original gold particle sitting on MgO substrate. b) After 10 minutes of high flux electron irradiation. It shows sinking occurs much faster at high electron fluxes.

coefficient for the encapsulation process and compare it with those in systems that exhibit strong metal substrate interaction (SMSI) which is an important effect in most catalyst systems. Using a one-dimensional diffusion relationship $l = \sqrt{2Dt}$, where l is the diffusion length and t the diffusion time, one arrives at a value for the diffusion coefficient of $10^{-17} \text{ cm}^2 \text{ sec}^{-1}$. This value is quite comparable with that for SMSI systems (at low temperatures), as will be discussed in the next paragraph, the difference being that here it is the electron irradiation rather than any thermal effects that provide the driving force for diffusion; this is consistent with the observation, during irradiation, of roughening of the MgO surface far from the gold clusters.

It is quite a well known phenomenon that strong metal-support interaction (SMSI) in catalyst systems can inhibit chemisorption and catalysis depending on the nature of the particle and substrate material [see for examples and characteristic features, Tauster et al. 1978, Tauster and Fung 1978, Galvagno et al. 1980, Chen and White 1982, Spencer 1985, Wang et al. 1988]. A famous example for this is the transition metal/titania systems which show strongly reduced uptake of hydrogen and carbon monoxide due to SMSI. Models to explain

this effect suggest that the interaction occurs through electron transfer from the substrate to the metal either through interfacial metal-metal bonds or through electrons tunneling through substrate layers [see Horsley 1979]. It is also suggested that metal particles distributed on oxide substrates form Schottky joints which can change the nature of the interaction [Boudart 1989]. In most of the systems studied the supported metal systems are subjected to high temperature reduction when the SMSI state is strongly initiated, and in many systems the state is reversed on oxidative treatments. Many models suggest formation of intermetallic compounds due to the reaction of the metal ions with the reduced state of the metallic oxide. But in none of the above models is the simple thermodynamic possibility investigated that a small metal particle sitting on the oxide substrate can sink into the substrate material in order to reduce the free energy of the system. Such evidence is provided here and in the following model a criterion will be derived for sinking, which may help to predict the SMSI state in many systems. It should be added in passing that although gold-MgO is not a real catalyst system; it was recently suggested that a strong metal substrate interaction in this

system could be responsible for some catalytic activity in a hydrogen dissociation reaction [Boudart 1989].

4.3.1 Theoretical Model for Sinking Small Particles

Figure 4.7a shows schematically a particle that forms a non-planar interface with the substrate. Assuming that the strain energies at the interface are negligible compared with the surface energies (which holds if the interface is nearly epitaxial or the boundary is coherent) the potential energy of the system can be written as

$$E = (r_2 + 2a) (\gamma_p + \gamma_s^{sub} + \gamma_i) + (2r_1 + r_2 - 2a) \gamma_s - r_2 \gamma_s^{sub} \quad (4.4)$$

Here γ_p is the energy of the particle-vapor interface, γ_s^{sub} that of the substrate-vapor interface, and γ_i the bonding energy of the interface; the distances r_1 , r_2 and a are defined in Fig.4.7.a. Actually the configuration seen in fig.4.7.a is the final result of sinking and there could be many intermediary geometries assumed by the sinking particle. Two such constructions are shown in fig.4.7.b in which the free energy change will be little different compared to that assumed in (Eq.4.4) due to the extra ledges of the substrate appearing. But these will disappear by diffusion around the

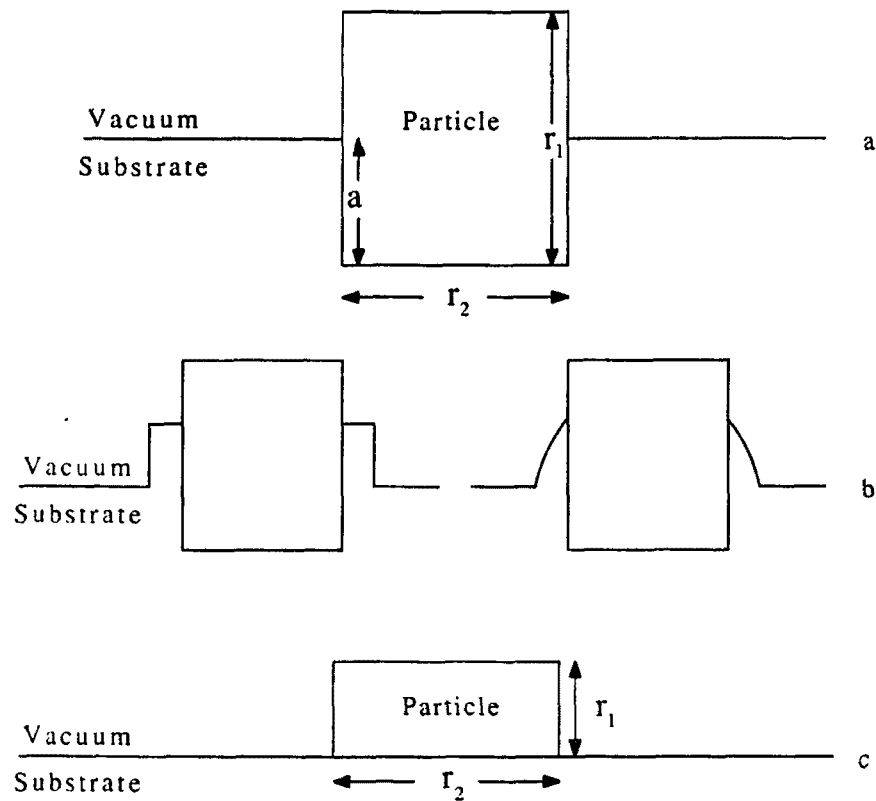


Fig.4.7 a) Schematic diagram of a particle that is partially immersed in a substrate. b) Intermediary configurations of the particle on the substrate during sinking which finally leads to the geometry shown in (a). c) A particle on a planar substrate. It is assumed for simplicity that the particle is of unit length normal to the figure and that the substrate surface is semi-infinite.

particle resulting in the situation shown in fig.4.7.a. By definition, γ_s^p and γ_s^{sub} are positive and γ_i , the energy released when the two surfaces are brought together, is negative. The change in total energy with respect to a is

$$\partial E/\partial a = 2(\gamma_s^{sub} + \gamma_i) \quad (4.5)$$

If $\partial E/\partial a < 0$ (corresponding to a particle that forms a high energy interface on a low energy substrate-facet, as may be the case in gold-MgO) the particle will sink; if $\partial E/\partial a > 0$, it will float. The system is thus thermodynamically unstable with respect to sinking or floating. Note that if the particle and the substrate consist of the same material the problem reduces to that of conventional sintering, and sinking becomes equivalent to heterogeneous sintering or ostwald ripening. The criterion can be applied to other geometries and may be extended to three dimensions.

For a planar interface (Fig.4.7c) energy balance can similarly be written, by setting $a=0$, as

$$E = 2\gamma_s^p (r_2 + r_1) + r_2\gamma_i, \quad r_1 r_2 = C \quad (4.6)$$

Finding $\partial E/\partial r_2$, it is found that

$$\partial E/\partial r_2 = 2\gamma_s^p (1 - C/r_2^2) + \gamma_i \quad (4.7)$$

Complete wetting of the particle on the substrate will occur if

$$\partial E / \partial r_2 < 0; \text{ ie}$$

$$2\gamma_s^p + \gamma_i - 2C\gamma_s^p / r_2^2 < 0; \text{ ie. when}$$

$$2\gamma_s^p + \gamma_i < 0 \quad (4.8)$$

If the inequality become positive, then you have a positive solution for r_2 , and incomplete wetting will occur. Similarly, the substrate will wet the particle if

$$2\gamma_s^{\text{sub}} + \gamma_i < 0 \quad (4.9)$$

And complete drying will occur if

$$\gamma_i > 0 \quad (4.10)$$

Note that the propensity of a particle to sink will be sensitive to changes in the surface free energies, as might be induced, for example, by chemisorption of impurities. It should be also noted that in solid-solid systems the criterion for sinking that have been derived is much easier to satisfy compared to the wetting criterion. The γ_i that is used here for the energy gained in forming an interface is similar to the energy of adhesion (but of opposite sign) that is used in most surface science literature. Since γ_s^{sub} is constant for a particular substrate facet on which the particle is sitting, the chances of sinking increases with increasing value of γ_i .

In general one can represent schematically, how the energy of the system changes as any particle of arbitrary

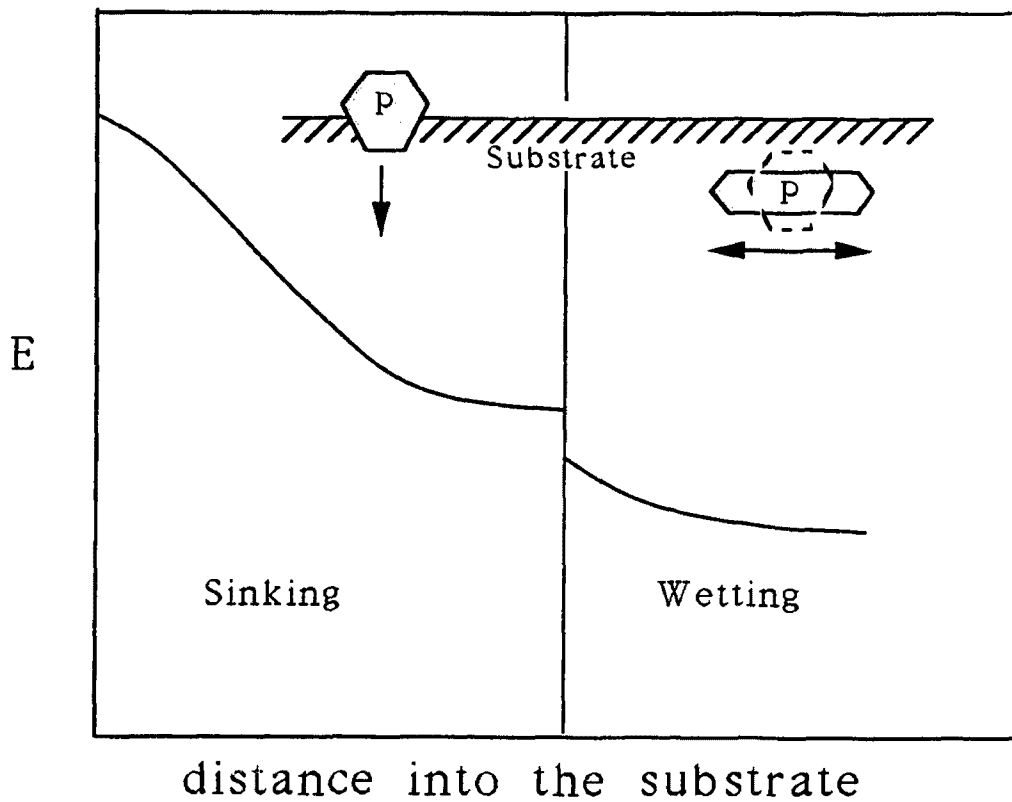


Fig.4.8 Schematic of the free energy function as the particle of any arbitrary shape sinks into a substrate. Once the particle is completely sunk, energy reduction can occur only by the substrate wetting the particle.

shape sinks more and more into the substrate (see Fig.4.8). Initially as the particle is incompletely sunk the γ_s^p is being replaced by $(\gamma_s^p + \gamma_i)$ but once sunk γ_s^{sub} will be replaced by $(\gamma_s^{sub} + \gamma_i)$ which is usually smaller than the former. Hence the change in energy decreases and levels off completely once the particle is sunk into the substrate and further reduction can occur only by the substrate wetting the particle.

The results of sinking that is seen could be of Figure importance in small particle catalyst systems. The stability of a particle with respect to sinking, and hence reactivity, can be changed by chemisorption of impurities, which will change the surface free energies. Surface free energies could also be drastically altered by a change in temperature, although data for such variations are difficult to find in the literature. A plausible model for catalyst deactivation is that the particle sinks diffusively into the substrate in the course of time. Regeneration of the catalyst could require changing the surface free energy by chemisorption or thermal treatments, causing the particle to float back onto the substrate surface. Thus during the kinetics of a catalytic reaction, the catalysts can remain on the surface or get buried under the substrate depending on the environment and

the surface free energy relations thereby greatly changing the activity and productivity of the reaction.

4.4 Microscopic Pillar Growth Instabilities

In macroscopic dimensions and dissipative systems the formation of delicate patterns and structures is common. This is due to non-linear forces acting on the system to produce non-equilibrium perturbations that grow rather than decay as in linear systems. Famous examples are the formation of hexagonal snowflakes [Nakaya 1954], fingering instabilities during the mixing two viscous fluids [Benismon et al. 1986, Langer 1989] and growth of dendritic solidification fronts [Langer 1980]. These unique and complex spatial patterns are the results of kinetic processes due to competing forces of chemical or thermal gradients against surface tension and crystalline anisotropy. In these growth patterns the moving interface generates latent energy which is conducted away by thermal diffusion. This is done by having large interfacial areas and large thermal gradients at the interface; both of which are achieved by the interface forming protrusions in the direction of heat dissipation.

What is found in the experiments, at high flux electron

irradiation and as a sequel to the sinking of small particles into substrates, is a similar problem of a moving interface [Ajayan and Marks 1989b], not due to thermal dissipation but due to competing forces of surface energy reduction and interfacial surface stress. The results presented in this section are also important from the point of view of radiation damage of solid surfaces where impurities on the surface of solids could lead to drastic modification and corrosion of surfaces which would prove undesirable in many practical applications. These effects could be important in semiconductors and materials used in space applications which are incessantly subjected to high doses of radiation. As far as the author knows this is the first time anybody has reported such radiation induced interface driven pattern formation at the microscopic scale; some interfacial instabilities have been reported during laser annealing [Poate and Brown 1982] and recrystallization of GaAs films [Licoppe 1988].

Figures 4.9 to 4.13 show the experimental results obtained during the electron irradiation of gold-MgO system, which show various sequences on the formation of microscopic pillars from MgO underneath the gold particles. Figure 4.9

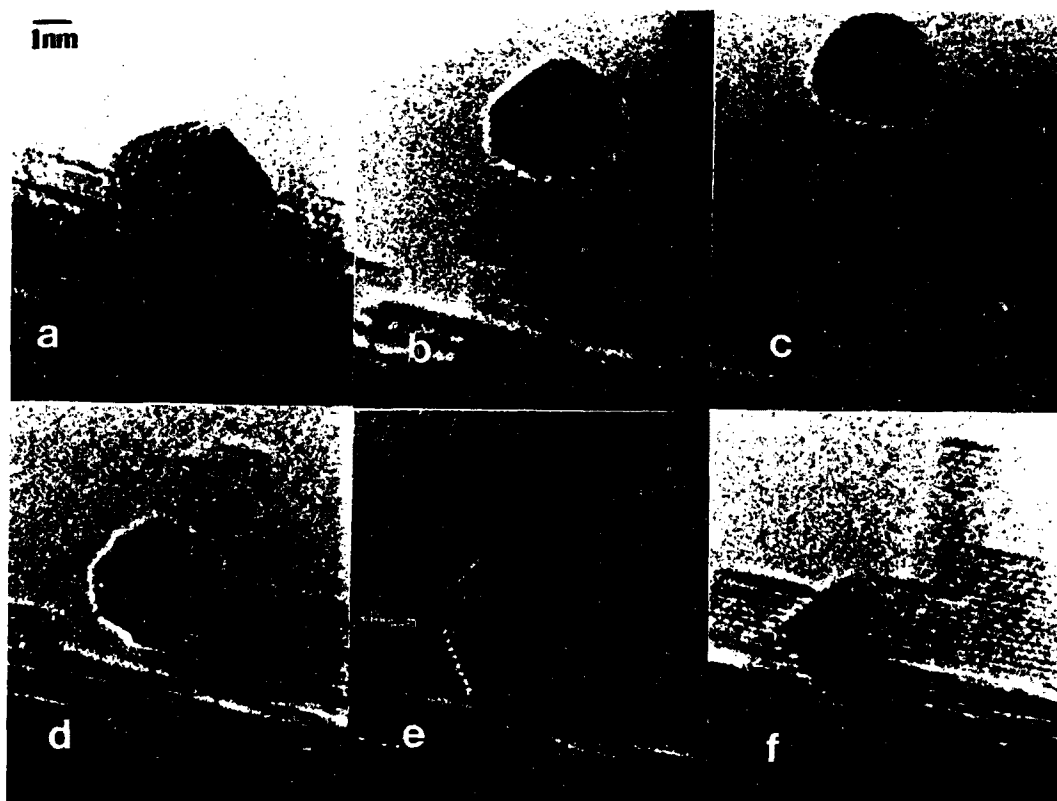


Fig.4.9 Electron microscopy images for a time sequence of the pillar growth phenomena. a) Original particle on the substrate. b) 20 minutes; particle on top of a short pillar that has grown out of the encapsulation. c) 40 minutes; pillar has grown to its maximum height with particle floating (quasi-melting) on top. d) 48 minutes; particle has flipped down onto the side of the pillar. e) 52 minutes; similar to that in (d) but the particle has a different shape f) 55 minutes; final state of the particle which has fallen down onto the substrate and stabilized. The pillar has partially collapsed but not completely disappeared.

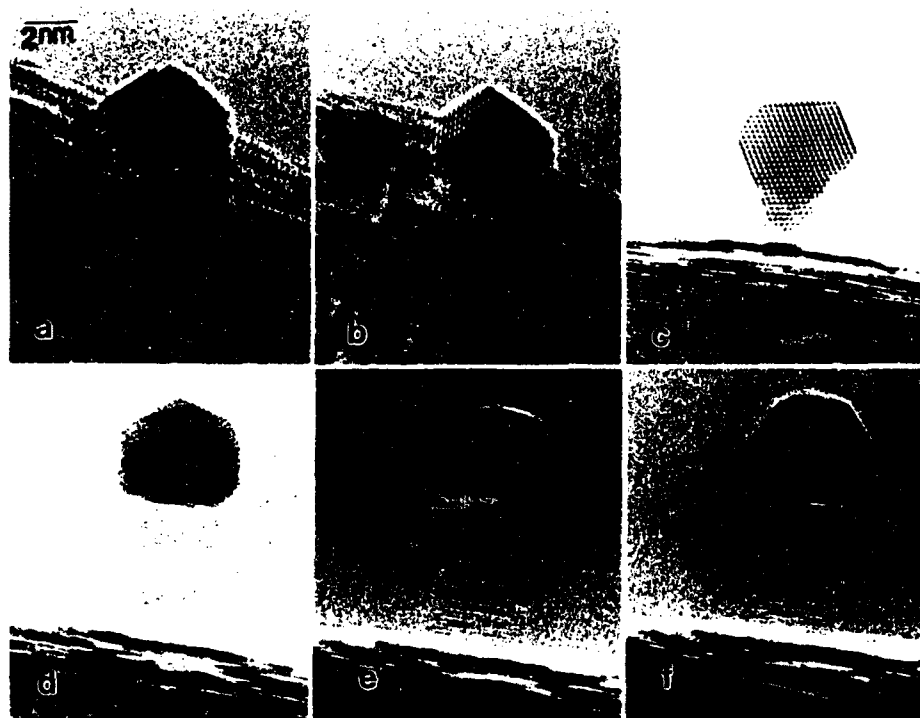


Fig.4.10 Another time sequence of microscopic pillar growth. a) Original particle; b) 60 minutes of high flux irradiation; c) 80 minutes, the particle is almost decoupled from the substrate; d, e, f) 100, 110 and 120 minutes, particle floating on pillars in a structurally unstable state. In the last 20 minutes the pillar height has only increased very slightly, indicating that a steady state has been reached.

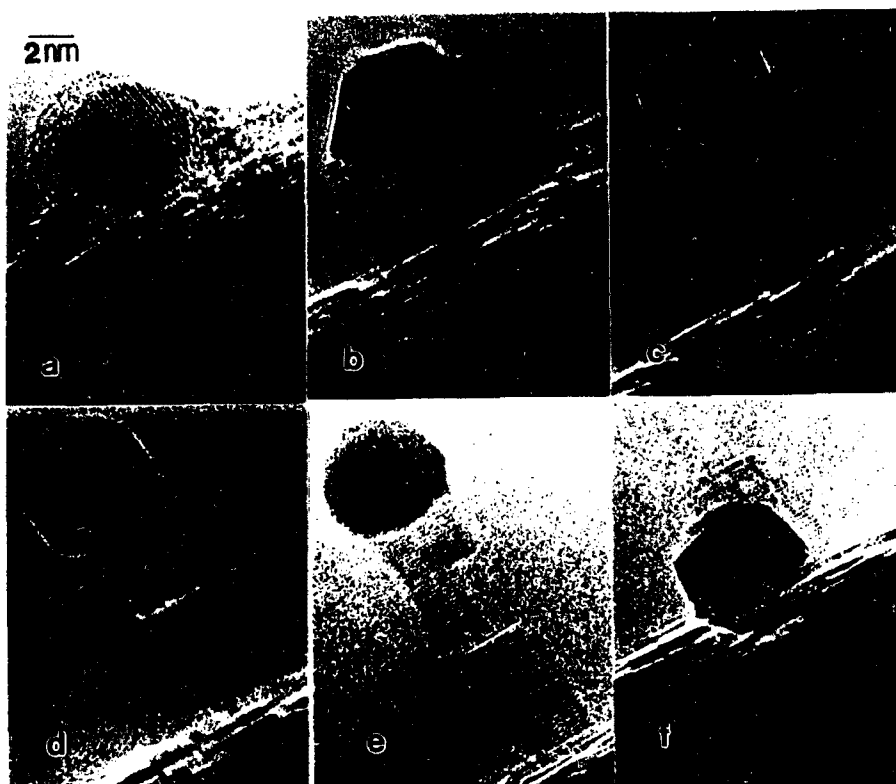


Fig.4.11 The formation of a pillar which is indented in the middle. a) Original particle with some carbon contamination. b) 15 minutes; the carbon has disappeared due to the beam but the particle has grown a short pillar beneath it. c) 25 minutes; larger pillar grown with a non-uniform structure. d) 30 minutes; the pillar has grown in height and the particle has become quasi-molten. e) 35 minutes; a chunk of mass has been transported from the middle of the pillar to the top increasing the height. f) 40 minutes; particle has fallen down and formed a stable shape.

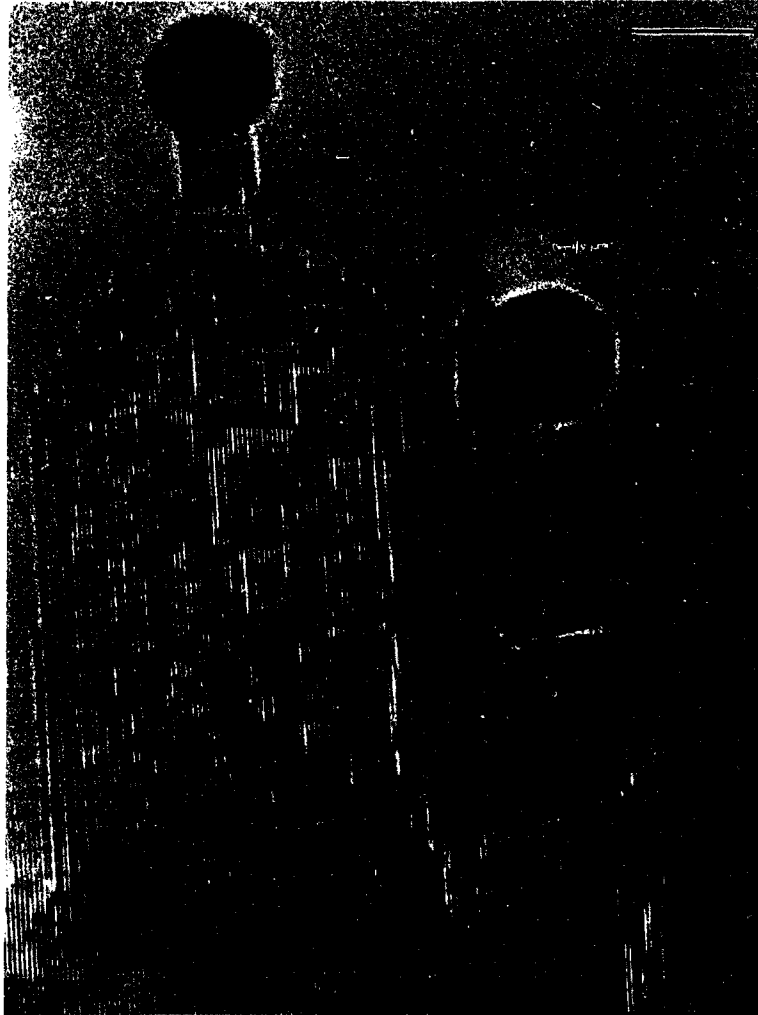


Fig.4.12 An extreme case of pillar growth where two pillars have grown out of a small crystallite of MgO with two gold clusters in structurally fluctuating state, floating on top. The growth occurred during high flux electron irradiation for ten minutes.

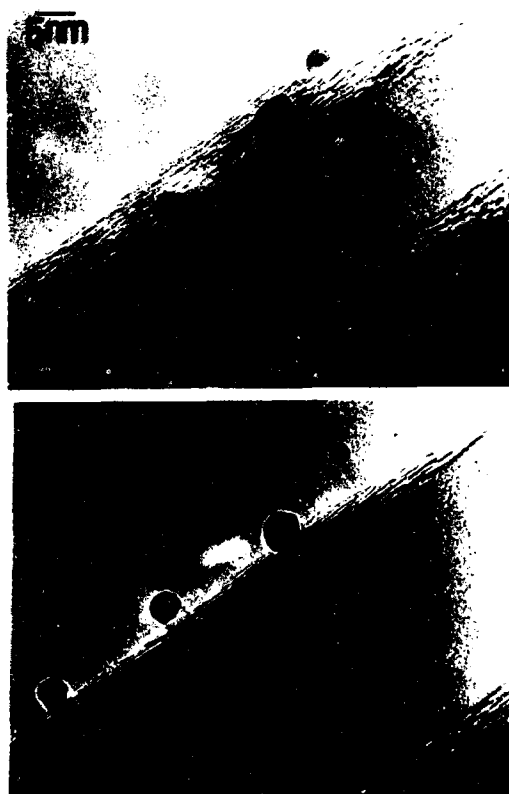


Fig.4.13a Experimental images of pillars grown to different heights varying inversely as the particle size, for particles irradiated under similar conditions.

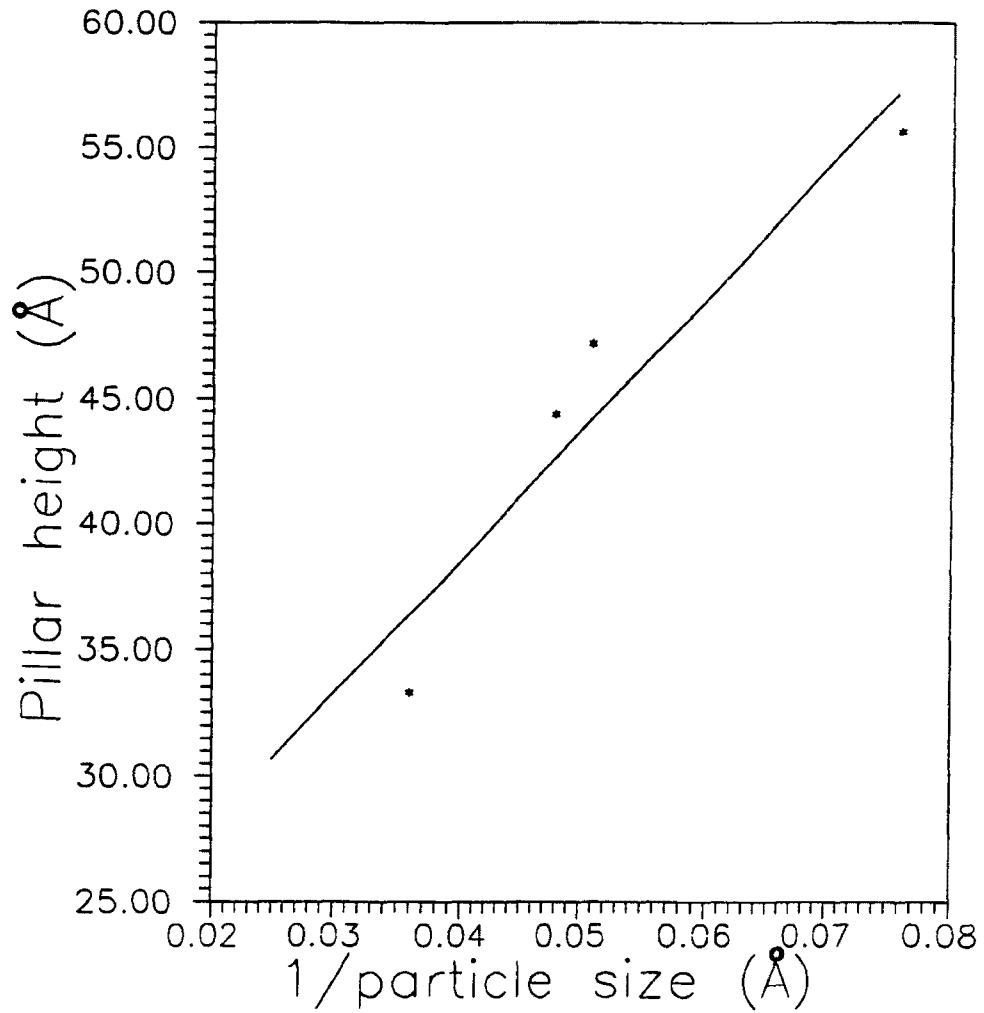


Fig.4.13b Plot of the pillar height as a function of particle radius, for the experimental images in fig.4.13.a

shows a typical time sequence of a gold particle sitting on the MgO substrate, depicting this phenomenon in detail. It reveals the gradual transformation of a stable particle on the MgO substrate with a stable interface, getting decoupled and lifted up to the top of a microscopic pillar. An extreme case of this is apparent in Fig.4.12, the result of 20 minutes of high flux electron irradiation of gold clusters dispersed on the (100) face of a small magnesium oxide cube. The fringes in the main body of the image are the (200) lattice fringes of magnesium oxide. The arms sticking out are also magnesium oxide, grown from the main body during irradiation. The arm on the right side can be thought of as grown almost perpendicular to the MgO surface since the MgO layers remain parallel to the bulk fringes whereas the directionality in the top arm is difficult to interpret (since the fringes are seen perpendicular to the bulk, it could have grown as a staircase inclined to the original surface). The blobs at the end are the gold clusters which are in a structurally unstable state, fluctuating between various twinned morphologies, which is the quasi-molten phase of small particles (this observation, experimental evidence of quasi-melting, will be the subject of chapter 5).

At some point in time, when the pillars are high enough that the particle-substrate interactions are reduced below some critical value, the particle becomes quasi-molten. The pillar growth continues, but slows down with time, and stops when it reaches a certain height. Increasing the electron flux resumes the pillar growth but finally it reaches a critical height, beyond which it will not grow any further (fig.4.9.d). Pillar growth has been observed for particles up to 100 Å in diameter, the height of the pillars decreasing with increasing particle size (this can be seen in Fig.4.13 which clearly shows this inverse relation). It is seen from many observations that the pillar growth eventually comes to a stop and the maximum height of a pillar that would grow under a 25Å particle is less than 100Å. This is an indication of a dynamic steady state reached in the system, unlike in a dendritic growth front which shows no such steady state. A scatter plot of all the data so far obtained on pillar growth is presented in Fig.4.14. The plot shows the relationship between particle size and pillar height. Although the data obtained are for different electron fluxes and time scales, it gives an idea of the active size of the particle size below which pillar will grow. It can also be seen approximately that the pillar

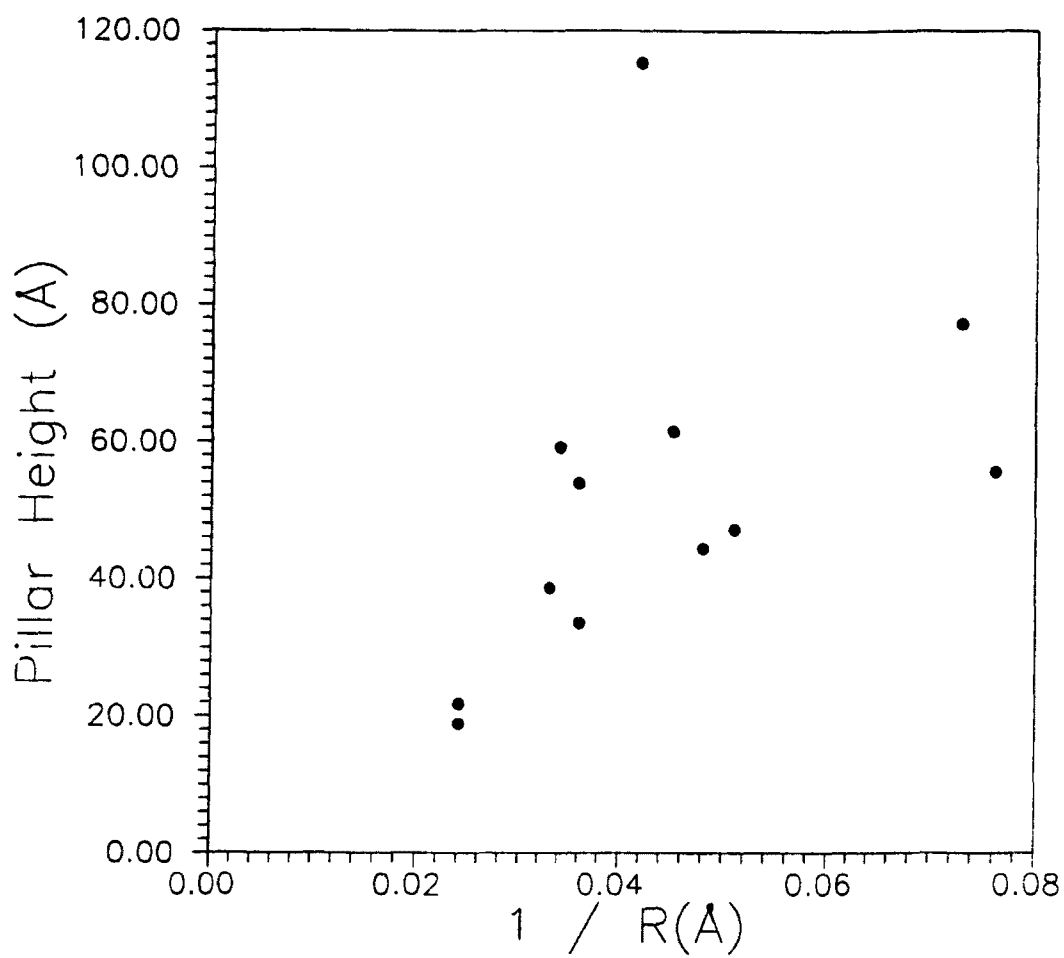


Fig.4.14 Scatter plot of all the data for the height of pillars formed on particles of different sizes.

height decreases with increasing particle size.

It should be noted that the pillar grows before the gold particle becomes structurally unstable and hence is not a direct consequence of the latter. Small particles floating on these pillars are mobile and may flip sideways (Fig.4.9.e) or fall directly onto the substrate (Fig.4.9.f) where they stabilize into stable shapes. The shape of the pillars formed are not always smooth and cylindrical but many times corrugated and indented and this should precisely depend on the nature of local diffusion fields and kinetics of growth. This is illustrated in fig.4.11.d,e where the pillar grown from an almost flat MgO surface during the process gets indented in the middle due to the transport of a chunk of mass to the top from the side of the pillar. This is an indication of the fact that once a certain height of the pillar is reached mass transport from the original substrate is negligible and continued diffusion occurs from the pillar that is already formed.

How does one explain this phenomenon of pillar growth? It is known that the temperature rise during electron irradiation in crystals is negligible [Gale and Hale 1961, Fisher 1970, Luzzi 1986, Curzon 1989] and hence thermal

gradients are not the driving force for the growth patterns seen in this system. Observations on many particles suggest that it is a two step process. As was pointed out in the previous section, a small particle sitting on a solid substrate can be unstable, thermodynamically, with respect to 'sinking' into the substrate material if this leads to a reduction in the total surface free energy and this is truly the case in Au/MgO system. At low electron fluxes the MgO species on the surface diffuse and cover up the gold surface leading to a surface energy reduction.

A dynamic equilibrium is reached for the sinking particle when the activation energy barrier for surface diffusion becomes too large. Apart from the tendency for surface energy reduction there are two other forces acting along the Au/MgO interface; first, due to the curvature of the interface and second, due to the interfacial surface stress. Strains exist at the interface due to the lattice mismatch of gold and MgO lattices and hence the chemical potential is a varying function of position. The curvature exerts a force of the order of gK where g is the interfacial surface stress and K , the average curvature. It should be noted that interfacial surface stress rather than interfacial free energy should be

used for solids [Cahn 1980]. The strain energy for the interface (the Au/MgO interface is almost coherent) is proportional to the second power of the difference in the two lattice spacings [Hilliard 1966]. This strain is similar to that in the nucleation problem where there is an energy barrier for the formation of a new phase due to the energy of the interface between the nucleus and the exterior phase. Thus the interface between the two solid phases tends to deform elastically in order to lower the free energy. But this process is energetically much more difficult than in a dendrite growth front where deformation of the interface into the liquid phase takes place with ease, since the former involves long range diffusion and extensive atomic rearrangements. This is facilitated by increasing the electron flux which increases the bulk diffusion coefficient by the creation of a large number of point defects (vacancy-interstitial pairs) inside the material [see for instance Itoh and Tanimura 1986, Murphy 1989]. Recent work carried out in our lab [Singh and Marks 1989, Fan and Marks 1989] has provided strong evidence for electron beam induced diffusion, and it is therefore quite reasonable that at higher beam fluxes the relative diffusion rate is sufficiently changing

such that the particle can switch from sinking to pillar growth. In the latter case extrusion of MgO takes place leading to deformation and motion of the interface which pushes the gold particle out of the encapsulated MgO layer to the top as seen typically in Fig.4.9.c.

4.4.1 Theoretical Model for Microscopic Pillar Growth

A semi-quantitative model will be presented to explain the diffusion of the interface, under kinetic conditions, which pushes the gold particle to the top of these microscopic pillars. Here only the bulk diffusion which extrudes the MgO around the interface will be considered, assuming that the surface diffusion has already created an encapsulation around the gold particle. The model presented here is similar to the one discussed by Shewmon (1983). One can consider that the gold-MgO interface is moving under its own force field which sets up an uneven diffusion current on both sides of the interface. The inverse of this problem is the segregation of lattice defects at a phase boundary (grain boundary or stacking fault) or dislocation due to the potential field of the latter.

Consider here the effect of the elastic stress gradient

on diffusion due to the interface. This elastic potential here is due to the strain due to a coherent gold-MgO interface which is short range but effective in the vicinity of the interface. One can consider that the gold particle is sitting strained and there is a stress gradient along the length of the pillar. The potential due to this elastic gradient can set up a diffusion flux in the direction of the interface, thus initiating the growth of pillars. The effect of the hoop strain existing across the surface of the pillar is neglected, although this could influence the morphology of the pillars formed. The energy of the final configuration with the interface located away from the original substrate plane becomes smaller than that of the interface being in the plane of the substrate until an equilibrium position for the interface is reached. This is the steady state condition for pillar growth.

The potential gradient produces a flux and this must be added to the flux produced by concentration gradient of point defects in the vicinity of the interface for the equation of total flux which can be written (strictly for short times but extended to this case) as

$$J = -D(\nabla c + c\nabla V/kT) \quad (4.11)$$

where D is a constant diffusion coefficient, c the concentration of point defects at temperature T , k the Boltzmann constant and V is the potential due to the interface. This gives the time dependent diffusion equation

$$\frac{\partial c}{\partial t} = D \nabla \cdot (\nabla c + c \nabla V / kT) \quad (4.12)$$

The potential due to the interface at a radial distance r away can be written as

$$V(r) = -\alpha g K; \quad K = 1/(R+r) \quad (4.13)$$

where R is the radius of curvature of the interface, r the distance of the interface from the original substrate plane (after the initial state $r \gg R$), g the interfacial surface stress in reduced units (interfacial surface stress multiplied by the atomic volume) and α a parameter which should depend on the geometry and solid angle of the interface, which for convenience will be taken as unity. Note that this is similar to the force field of a screw dislocation. It follows that

$$\nabla_r V = g K^2 \quad (4.14)$$

Rewriting the diffusion equation (4.13), and assuming that $\nabla^2 V$ is small

$$\frac{\partial c}{\partial t} = \nabla \cdot (D \nabla c + D c g K^2 / kT) \quad (4.15)$$

Also the gradient moves the interface with a velocity (assuming that the velocity at which the point defects reach

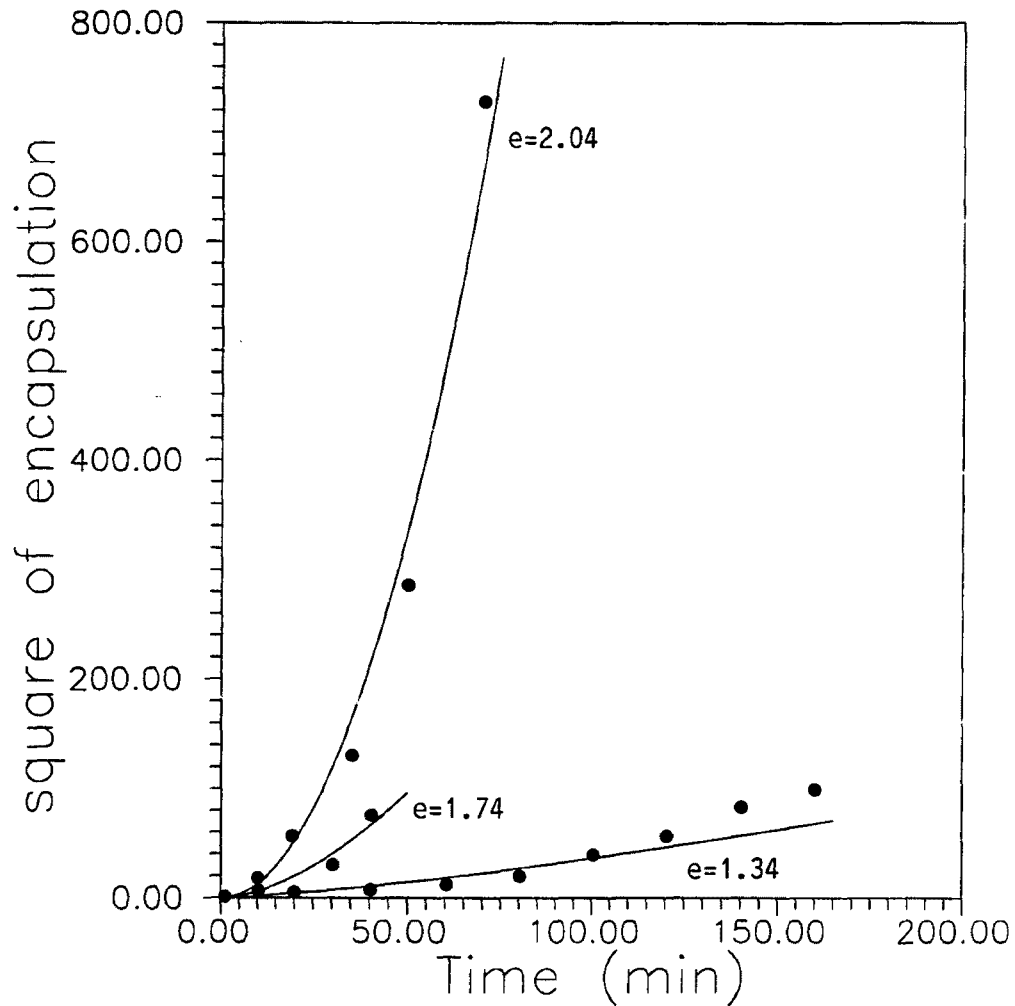


Fig.4.15 Data for rate of encapsulation. Square of the encapsulation width is plotted as a function of time and power fitted. Average of three different sequences show that encapsulation increases as $t^{0.85}$. Note that the data is only for the interval during which encapsulation increases. After this interval the particle start extruding out, decreasing the effective width of encapsulation.

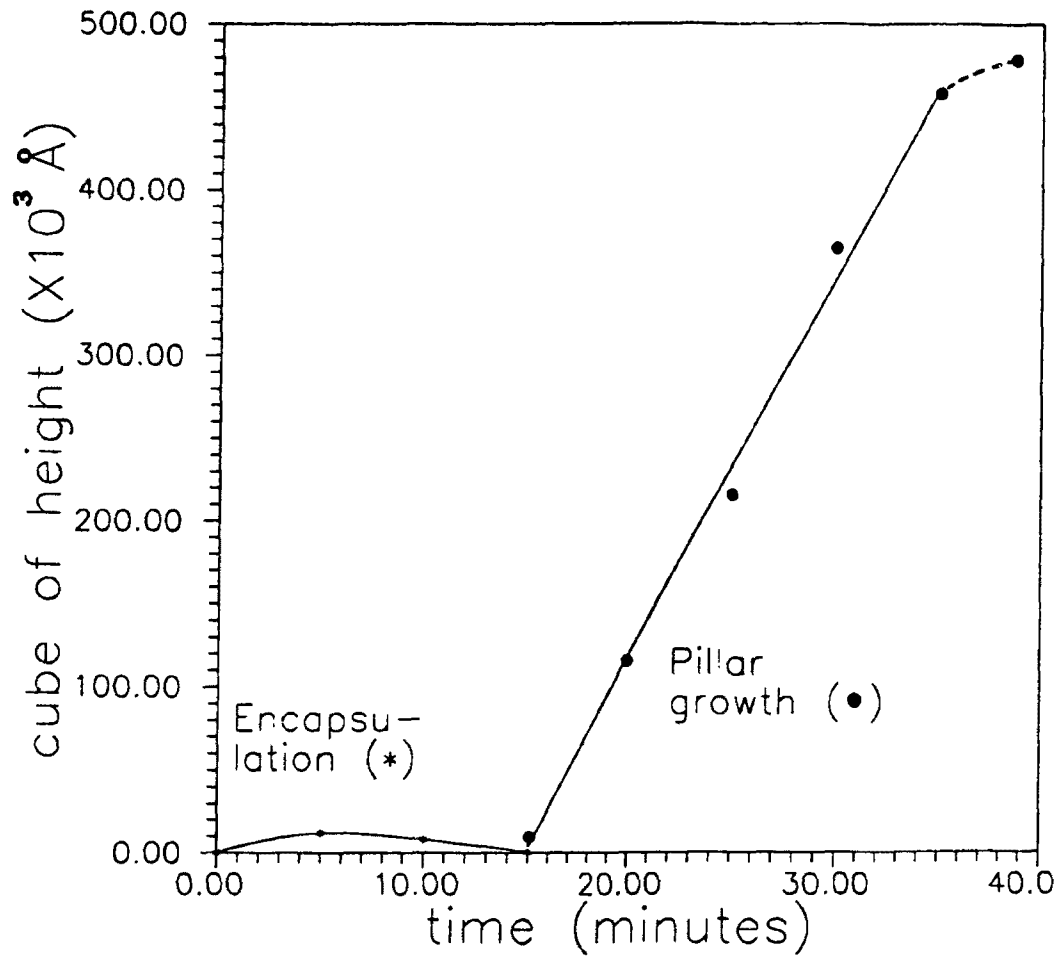


Fig.4.16 Experimental data for pillar growth. Graph shows cube of the pillar height plotted against time, until the pillar has reached maximum height, for a particular electron flux. Dotted lines represent deviation from linearity as the pillar growth slows down before coming to a stop. Data shows two regimes, one for encapsulation and the pillar growth regime where the height increases as $t^{1/3}$.

the interface is the same as the velocity of the interface; it will also be assumed that during diffusion there is a net flow of interstitials towards and vacancies away from the interface, so that the mass of the pillar is built up continuously)

$$\begin{aligned} v &= dr/dt = -D\nabla V/kT \\ &= DgK^2/kT \end{aligned} \quad (4.16)$$

Integrating between $r=0$ at $t=0$ and $r=r'$ at $t=t'$, it is obtained that (for $r \gg R$)

$$r' = (3Dgt'/kT)^{1/3} \quad (4.17)$$

which only means that the interface has moved a maximum distance r' through a $t^{1/3}$ relation. This can be compared with the experimental data for diffusion during the two distinct stages of encapsulation and pillar growth. Figure 4.15 shows a plot of the square of the encapsulation width against time power fitted numerically. The average of three different encapsulation sequences (different fluxes) gives a value for the exponent of time in the diffusion relation as 0.85. In other words diffusion occurs during the first stage approximately through the relation $l \sim Ct^{0.85}$ where C is a constant related to the diffusion coefficient. Plots of the cubes of linear dimension against time for the complete



Fig.4.17 Experimental image of pillar that has grown in two perpendicular directions during growth resulting in a bent pillar.

process of encapsulation and pillar growth is presented in Fig.4.16; the result shown in this plot was repeatable. It is seen from both sequences that after the initial stage the relation is linear which shows the diffusion during the growth of pillars is controlled by a relation of the form $l \sim C't^{1/3}$ where C' is again a constant similar to C . This is a direct confirmation of the diffusion model which actually predicted a $t^{1/3}$ relation. Nevertheless it should be noted that the first region, or the initial stage of pillar growth involves surface diffusion, encapsulation and extrusion of the interface and does not present a simple relationship with time. The diffusion in this process depends on many factors such as the electron flux, nature of the surface (since surface diffusion is predominant here) etc. An order of magnitude calculation of the diffusion coefficient (using $l = \sqrt{2Dt}$) gives values of 10^{-15} - 10^{-16} cm²/seconds. Comparing with Values in Literature [Vieira and Brook 1984] it can be easily seen that the rate determining process here is the diffusion of oxygen which is much slower than the diffusion of magnesium in the MgO lattice for a range of operating temperatures.

The inverse size dependence of the pillar height can also be understood from the integration of the velocity equation.

At any given time $(h+R)^3 - R^3 = \text{constant}$, suggesting that as the particle size increases pillar height decreases. The $1/R$ dependence of the pillar height, where R is the effective particle size, can be seen from Figs.4.13 & 4.14 which show the experimental data of pillar height for a distribution of particle sizes which were under similar substrate and irradiation conditions. The sample is quite small (only four) but it is extremely difficult to obtain similar conditions for range of particle sizes. The above observations strongly suggest that the effect is due to capillary forces similar to surface tension effects that are so common at macroscopic dimensions in fluid systems. A direct confirmation of the volume diffusion model can also be seen from fig.4.17 which shows the experimental image of a bent pillar. After an initial growth in one direction the diffusion direction here has got switched, probably due to the particle flipping to one side and the pillar growth proceeded in that direction. It should be noted in this case that the particle is not touching the substrate since a the moire fringe between the particle and the substrate is clearly visible.

For $t > t'$, there is an equilibrium steady state with $\partial c / \partial t = 0$. For steady state (Eq.4.13) becomes

$$\nabla^2 c + gK^2 \nabla c / kT = 0 \quad \Rightarrow \quad \nabla c = \exp(-gK^2 r / kT)$$

or

$$gK^2 / kT = (1/r) \ln\{1/(\partial c / \partial r)\} \quad (4.18)$$

The solution in (Eq.4.16) will be valid over a period of $r < r'$ when the potential gradient due to the interface can exert an influence on the moving point defects. It is impossible to provide experimental data to check Eq.4.18 because it would involve the measurement of the concentration gradient during steady state. But it is experimentally seen that a steady state exists for the growth of pillars. The significance of r' is similar to the 'capture radius' for precipitation of a solute on a dislocation [Ham 1959]. A physical interpretation would be that the influence of the interface and hence its motion will continue until the potential become smaller than the thermal energy of the vacancy; ie.

$$-V(r) < kT \quad (4.19)$$

This effective 'h' or the maximum height of the pillar that could form is then approximately equal to

$$h = g/kT - R \quad (4.20)$$

For a g value of $\sim 10^{-19}$ - 10^{-20} dynes-cm² (for a typical interfacial energy of ~ 1500 ergs/cm² and a particle radius of

25 Å) one gets reasonable values of ~20-200Å for critical pillar height, which seems to correlate quite well with experimental values.

So depending on the relative rate of surface, bulk and interfacial diffusion as well as the magnitude of the two terms, the particle will either sink or a pillar will grow. This on and off process can finally lead to a critical height of the pillar when the activation barriers for diffusion become too large and the electron beam can no longer provide enough energy to surmount the barrier. Also when the gold particle becomes unstable above a certain pillar height, there is no clear interface and the curvature and the interfacial stresses become insignificant. The two steps mentioned above could also occur simultaneously if a surface layer of MgO is pulled along by a constantly deforming Au/MgO interface. As the particle size increases, the energy for deformation increases drastically and the effect of surface tension decreases (lower curvature) and pillar growth becomes harder to realize.

It should be noted that the idea of thermal gradients producing pillar growth does not work. Considering the effect of a small fin protruding out from a planar surface and

applying radiative heat transfer (Stefan-Boltzmann law) to calculate the temperature drop, assuming a constant power input into the material, one gets temperature gradients of the order of 10^{-15} K/Å² across the fin. This is obviously not sufficient to select pattern formation like the pillar growth. Similarly arguments based on the work done by a capillary force versus the energy of new MgO surface created do not appear to give valid results.

Thus it has been demonstrated that at the atomic scale delicate and unique growth patterns can arise in a system when kinetic conditions prevail. The uniqueness of these results is that the only forces that drives the pattern formation are surface stress and curvature. These differ from other instabilities like dendritic growth in that in the latter there is no dynamic equilibrium steady state as is found in this system. The reason is that in the latter instabilities the growth front is always surrounded by an infinite supply of the source material (the molten metal during solidification) whereas the pillar growing into vacuum faces an uphill diffusion with the supply of the diffusing mass diminishing with time. Nevertheless the similarities between the two are self-evident.

Assuming that pillar growth is analogous to a gravity field, a pillar would grow until the capillary pressure is balanced by the weight of the pillar. For the experiments mentioned in here the analogue of gravity will be the concentration gradient along the length of the pillar which, at some pillar length, will balance the capillary pressure. Clearly this is a problem which merits detailed numerical simulation as well as further experimental work; for instance, it could be speculated that temperature may play the same role as the electron beam in enhancing the different diffusion rates but from (Eq.4.20), the temperature would also decrease the critical pillar height (at higher temperatures the defects created by the electron beam in the material will be annealed out; see Waite (1957) for reference). However, such speculations need to be substantiated with systematic experiments which are beyond the scope of this thesis.

4.5 Effect of Temperature on Gold-MgO System:

In order to understand the effect of temperature, the hot stage facility available in a JOEL 4000 high resolution electron microscope at the AT&T Bell laboratories in New Jersey was utilized. The idea was to look for temperatures at



Fig.4.18 Image showing the roughening of MgO surface at around 300°C and the start of encapsulation of the gold particles by MgO.



Fig.4.19 Completely encapsulated gold particles sitting on MgO surfaces after the system was heated to 600°C. Note that spherical shells of MgO has formed around gold particles and the configuration remains intact even after weeks of sitting at room temperature.

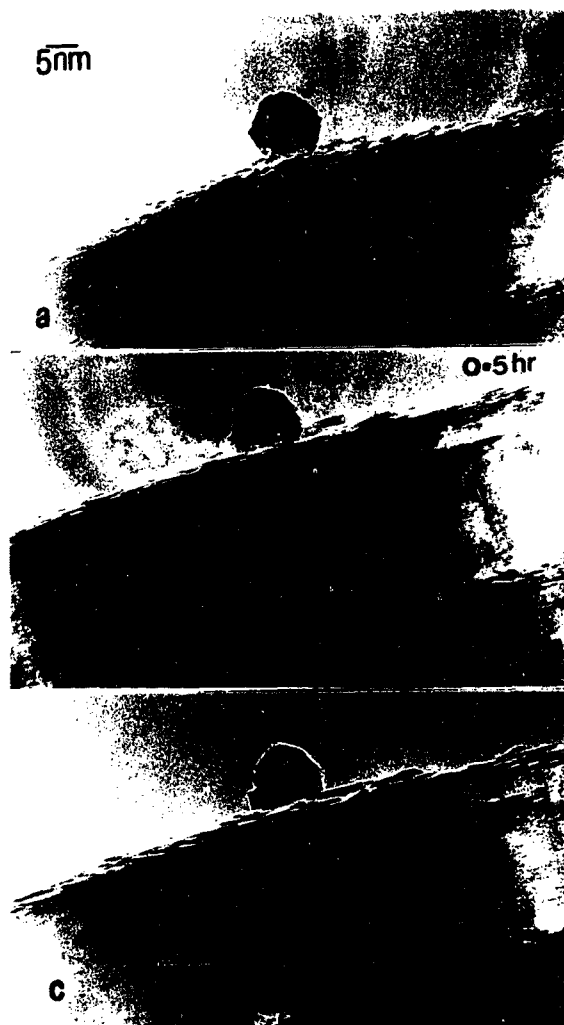


Fig.4.20 Images showing the effect of high flux electron irradiation on completely encapsulated gold particles. No microscopic pillar growth is seen after the particles have been heated above the encapsulation temperature.



Fig.4.21 Rounded surface profiles of gold-MgO-hydrocarbon system after the system was heated above $\sim 150^{\circ}\text{C}$.

which different sized particles became structurally unstable and also to see any such particle-substrate interactions like sinking and pillar growth as a function of temperature. At 300 KV, the microscope had a point to point resolution of $\sim 2\text{\AA}$ with the temperature in the hot stage ranging from room temperature to 800°C .

Observations during heating gave one important and interesting result. It was seen that around 400°C ($\pm 50^{\circ}\text{C}$) the MgO started strongly encapsulating the gold particle and finally formed a shell structure around the gold particle (600°C). This was about the temperature, 300°C , when the MgO surface started roughening due to the temperature and this suggests that the encapsulation was a result of strong surface diffusion. Figure 4.18 shows gold particles sitting on the MgO substrate getting encapsulated at 300°C and the MgO surface starting to roughen with formation of a large number of surface steps. The encapsulation is strong and this is shown in Fig.4.19 where the gold particles sitting on MgO surfaces are completely covered by substantial quantities of MgO. The shell that is formed around the gold particle is seen to be stable even when the temperature was turned down to room temperature. This configuration remained stable even under

high flux electron irradiation except that the volume of encapsulation increased slightly during the irradiation (see Fig.4.20). There was no growth of pillars during irradiation, once the MgO shell was formed. This could be because the surface diffusion was fast enough that the shell formed exceeded a certain critical thickness ($\sim 20 \text{ \AA}$) of the encapsulation above which the particle can not extrude out. It was also observed that when one uses a dirty specimen (gold evaporated to MgO at a base pressure of 10^{-4} torr) during heating the contaminants diffuse anisotropically over the MgO and gold giving the overall surface a rounded profile (isotropic surface energy for amorphous hydrocarbons) as shown in Fig.4.21.

The heating experiments showed the effect of kinetics of MgO diffusion and the nature of strong particle-support interaction. Since the resulting configuration of MgO over gold is stable to electron irradiation, one cannot study the structural stability of gold particles as a function of temperature and size when they are supported on MgO, and this was definitely a disappointment. One has to select a particle-substrate system which shows minimum substrate effects in order to study this, and to find such a system would be beyond

the scope of this thesis. Nevertheless it is worth mentioning that the gold-MgO system did provide exciting results both in understanding some of the novel particle-substrate interactions as well as the structural stabilities of small particles as they were decoupled during high flux electron irradiation. The sinking problem as a modified Wulff construction is discussed further in Appendix 4.B. The pillar growth still lacks from a rigorous theoretical model. The experiments of structural stability and onset of quasi-melting in gold clusters on MgO will be the topic of the next chapter.

Chapter 5 Experimental Evidence for Quasi-Melting

5.1 Experimental Search for Quasi-Melting

It has been demonstrated, both theoretically and experimentally, that small particles of many materials tend to form icosahedral, dodecahedral and various multiply twinned states rather than their stable bulk structure. It has also been pointed out that the configurational space of these small particles is densely populated [Berry 1987, Honeycutt and Anderson 1987] due to their shallow free energy surfaces [for example, Hoare and Pal 1971] with a multiplicity of local minima. From part of the Gibbs free energy surface for small particles and the corresponding Boltzmann distributions it was found that particles (size range of a few nanometers) can escape into a 'quasi-molten' state at low temperatures compared to their true thermodynamic melting points, due to the low activation energy barriers between the various states. This and other theoretical results [Fukano and Wayman 1969, Hoare and Pal 1972, Gordon et al. 1979, Beck et al. 1988] were to some extent experimentally verified [Bovin et al. 1985, Humphreys 1985, Iijima and Ichihashi 1986] when a small

particle was found to fluctuate between various shapes under an intense electron beam, in an electron microscope, with frequencies of the order of 30-60 Hz per second. However it has been suggested that the source of these fluctuations is violent events such as core excitations [Williams 1987] or a Coulomb explosion [Howie 1986]; the fluctuations being due to the particle recrystallizing from a highly excited, possibly molten state many times per second. A fundamental physical problem is which of these models is correct since experimental proof for neither exists so far; and why does it take such large amounts of energy in the form of high flux electron beam to induce structural fluctuations in a small particle if the activation energy barriers between various shapes are so small?

5.1.1 How Does a Small Particle Absorb Energy from

Electron Irradiation

There has been some attempts to characterize the generation and dissipation mechanisms for electron beam excitations in small particles, but none with quantitative details to answer unequivocally all the questions raised by the experimental observations. The most probable process [says

Howie 1986] is the excitation of valence electron density oscillations (plasmons) which have characteristic energy losses of $\sim 20\text{eV}$. For this order of magnitude energy it would involve only about 2% of the fast electrons moving through the particle and hence should be low cross section events. Howie adds that plasmons are generated at such a high rate (10^5 per second on each particle) that on the time scale of video recording, there could possibly be an effective temperature rise of 100°C . The plasmon excitations could decay radiatively or by the emission of secondary electrons if the specimen is well grounded. Another possibility which will lead to drastic movements of atoms in a small particle is some rarer inner-shell excitations which could involve the transfer of considerable amounts of energy and momentum to the particle, or substantial charging effects via Auger cascade processes. This can indirectly lead to the Coulomb explosion [Knotek 1981] when the energy released by filling the inner shell vacancy causes injection of two or more less strongly bound electrons from the atom. Although the latter type of phenomenon is usually observed in ionic and organic materials (whereas in metals the excitations are rapidly screened out), it was assumed that the special features of small particles

may be susceptible to this dramatic type of excitation.

Another explanation for the phenomena was based on charging of the particles during electron irradiation. Iijima and Ichihashi (1986) explain that the small particle and the local area of the substrate may temporarily deviate from electrical neutrality. These charges present on the particle (if the substrate is an insulator, the particle will have a positive charge) could impose coulombic repulsive forces between different regions of the particle which will set up the structural fluctuations. Similar forces between the particle and the substrate can also result in translational and rotational motions of the particle and these have been observed. It was also observed that when one used a conductive substrate the fluctuations in small particles slowed down considerably, which was a point in favor of this model. The major objection to this idea is that it is extremely difficult to ionize a small particle (Kubo) since there are very few electrons that are tightly bound to the core of positive charges, and even if such an event occurs the decay times should be very small. Also there is no direct evidence to show that the particle remains charged all the time although the structural changes continue to occur and this would mean that

the charging effect persists for long intervals of time which is quite improbable. In fact it will be shown in the next section that the quasi-molten state of the small particle is retained even when the electron beam is turned down to a minimum value. In the next chapter evidence will be presented to show that the coalescence of gold particles under electron irradiation form structures that resemble diffusion limited aggregation (DLA) growth suggesting that the particles do not carry charges [Lin et al. 1989] during electron beam irradiation and aggregation.

Although it is widely accepted that the reason for the structural instability in small particles is not thermal (average temperature rise) it was suggested [Williams 1988] that it could be the result of localized spikes of temperature bursts due to inner shell electronic excitations. One such process which was suggested to be a prime candidate was the ionization of an M-shell level in an atom in a gold particle. Depending on the ionization cross-section of this event and an electron current density of $\sim 15 \text{ A/cm}^2$, it was estimated that a 2 keV MNN Auger electron is produced in the gold cluster about 100-200 times per second. Since only a fraction of these electrons is produced on the surface, approximately 10-20

times a second, a 2 keV electron traverses the cluster, imparting energy of the order of 0.3-0.4 eV per atom in the cluster. If this energy is coupled into atomic motion more rapidly than heat can be conducted out of the particle into the support, the result would be a rapid temperature rise of $\sim 1000^\circ\text{K}$. Then the particle could transiently melt even if its steady state temperature is not much above room temperature. It was explained based on this idea that the shape changes that are observed in a small particle are the results of these transient melting and subsequent recrystallization events, occurring 10-20 times per second for a 2 nm cluster at a current density of 15 A/cm². Although this model could qualitatively explain many of the features of the structural instability in a small particle, it was more or less based on speculations and approximations and as will be seen in the next section of this chapter, the actual current densities needed to sustain the unstable phase is much lower and the model given above will give much lower frequencies of fluctuation than those that are observed.

5.2 Experimental Evidence for Quasi-Melting

The purpose of this section is to present experimental

observation that although a large dose of electrons, and hence quite large amounts of energy, is needed to initiate the state in which a small particle sitting on a substrate (trapped in a deep potential energy well) starts fluctuating, the energy needed to sustain that state is orders of magnitude smaller [Ajayan and Marks 1989c]. This is in agreement with the earlier prediction that a quasi-molten state distinct from the thermodynamic molten state exists in small particles and appears to rule out the violent event models discussed in the previous sections.

Figures 5.1 and 5.2. as well as Figs.4.8-4.12 show small gold particles sitting on a MgO substrate, with stable shapes, evolving through the process of sinking into diffusing substrate overlayers, decoupling from the substrate and finally going into a state where they start changing shapes between various twinned structures. The energy needed to initiate this unstable phase was provided in the form of high flux electron beam (~ 10 - 100 amps per cm^2) irradiation for long periods of time (1-4 hours). The final image (for example, in Fig.5.1.f), when the particle is in the quasi-molten phase, is the ensemble average of many particle shapes which occurred during an exposure time of 3 seconds. The details of the

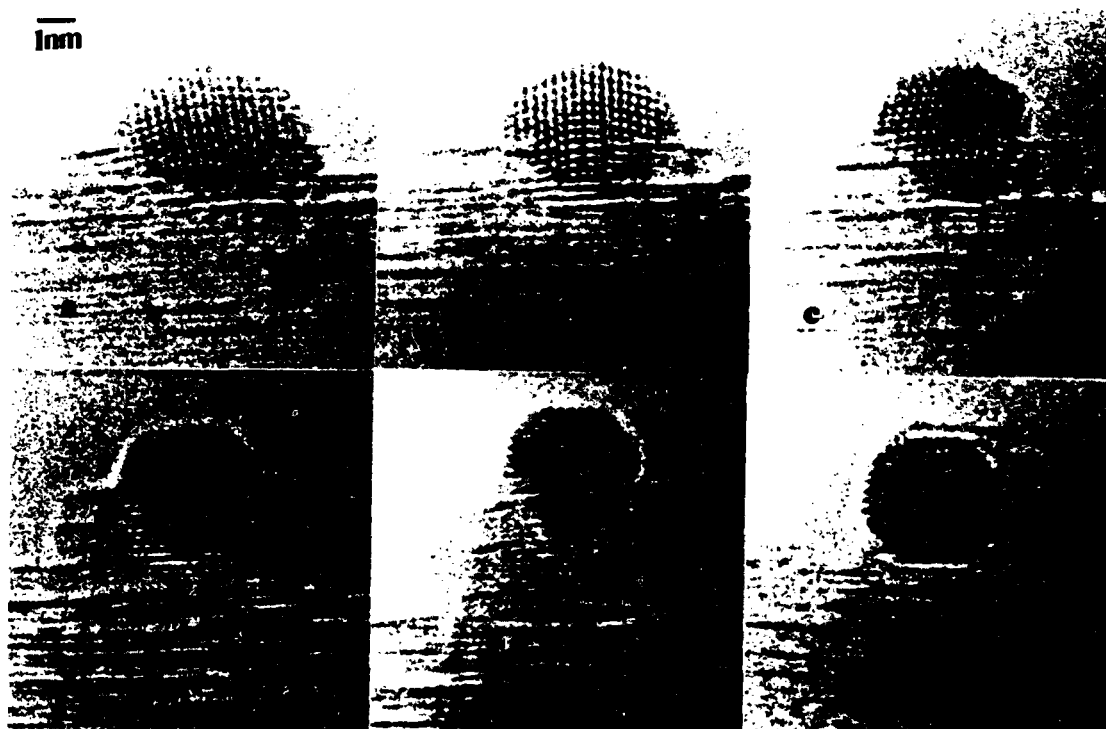


Fig.5.1 Sequence of images showing a small gold particle on MgO substrate changing, during electron irradiation, from a stable shape to the quasi-molten phase. a) Original particle; b),c),d) after 60, 120 and 180 minutes of irradiation. The particle is slowly being encapsulated by substrate overlayers; e) 220 minutes. The particle has been lifted off the original substrate plane; f) 240 minutes. quasi-molten state. The final image is the average structure of an ensemble of particle shapes that occurred during an exposure time of three minutes.

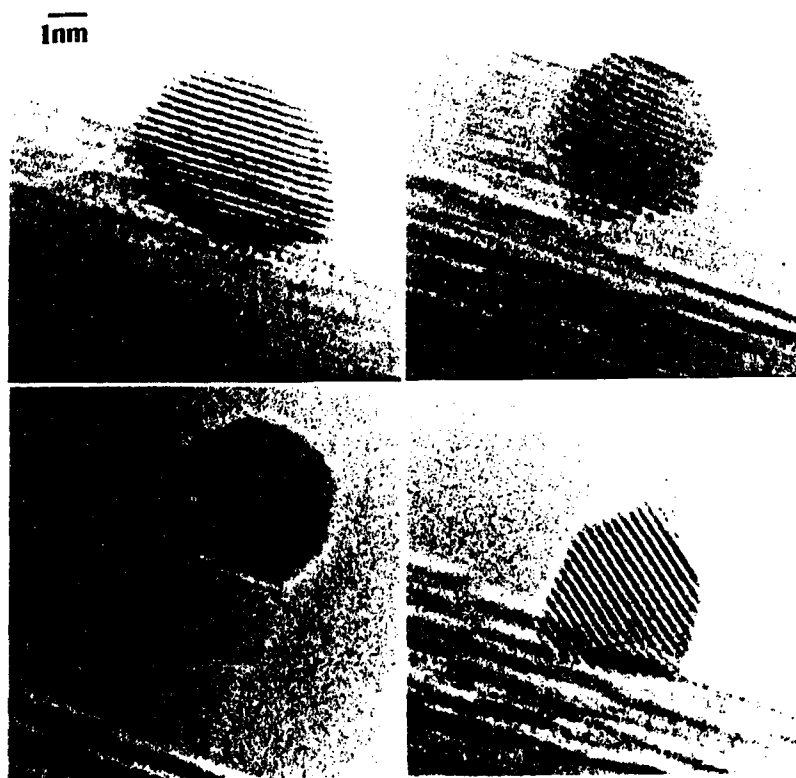


Fig.5.2 A small particle of gold on MgO support, evolving under electron beam irradiation. a) Original particle; b) 230 minutes, just before being lifted off the substrate plane; c) 260 minutes, particle sitting on a pillar grown from the substrate, quasi-melting; d) 270 minutes, the pillar has partially collapsed and the particle fallen off onto the substrate and crystallized into a stable Wulff polyhedron with well defined facets.

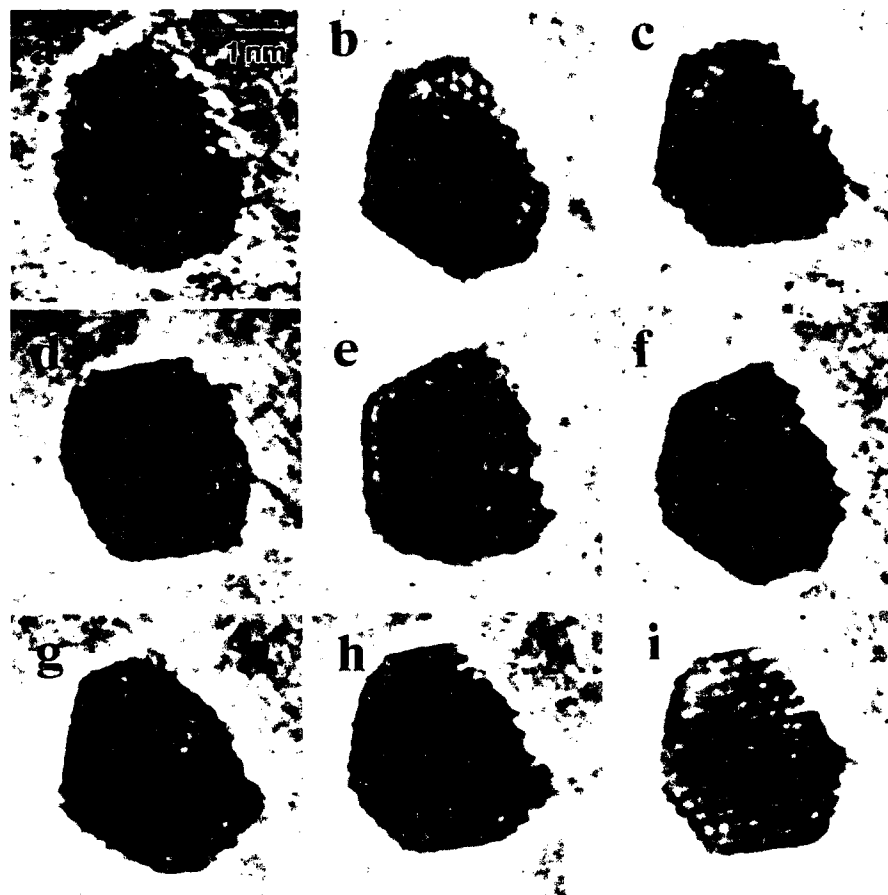


Fig.5.3 Sequence of particle shapes that occur during the quasi-melting of a small particle, during a time scale of 3 minutes, taken from real time video recording (each image correspond to eight frames from the video image). a) original particle b) 20 sec., strongly faceted cuboctahedral shape c) 35 sec., reentrant surfaces appearing d) 1 min., twinned, close to icosahedral e) 1.5 min., irregular shape with rounded surface profiles, f) 2.1 min. g) 2.4 min., twinned and faceted h,i) 2.8 and 3 min., single crystal shapes with slightly different orientations.

particle morphologies that occur during these structural fluctuations have already been reported and a typical sequence taken from single frames of a real time video recording is shown in Fig.5.3. It is clear from Fig.5.1 that the original stable particle on the substrate has a large contact area (the formation of the interface reduces the free energy of the system) whereas in the fluctuating state the particle seems decoupled from the substrate with almost spherical surface profile and a negligible area of interface. In some cases, the decoupling of the particle from substrate takes another route. As seen from Fig.5.2, the particle gets lifted off from the original substrate plane, moves to the top of a pillar like structure that has grown from the substrate overlayers, before becoming unstable (as discussed in the last chapter). The one dimensional nature of the pillar suggests that the particle-substrate interactions have been reduced to a minimum and the conditions simulate that of a free floating cluster in vacuum.

Since the theoretical predictions demanded only small activation energy barriers between different particle morphologies in a small particle, a crucial question is does it need such a high flux electron beam to transport the particle between various states. It was observed that this is

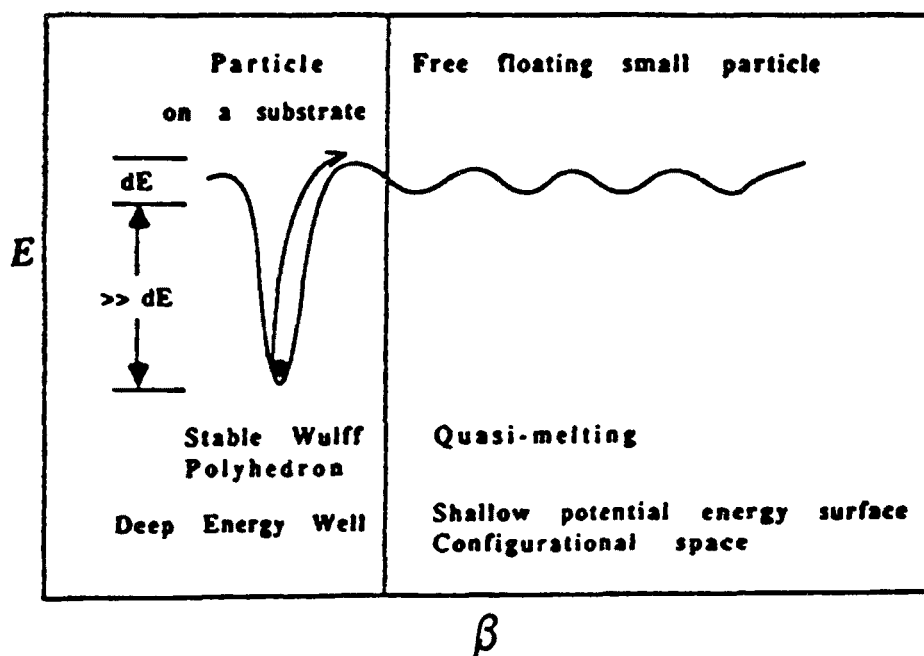


Fig.5.4 Schematic showing the deep energy wells in which a small particle on a substrate gets trapped as a familiar Winterbottom shape. Once out of the well, the particle can hop easily over the shallow morphological potential energy surface. β , here denotes the parameter that defines a particular configurational state.

not true. True, it needs large amounts of energy to push the particle out of a large potential well in which the particle is trapped in as a familiar Winterbottom shape, see Fig.5.4. for the schematic. But, once initiated, the particle quasi-melts even after the electron beam intensity is turned down to almost zero. The fluctuations in the particle were observed at the lowest possible flux conditions in the microscope to see an image (using a TV intensifier with the gain on the intensifier at the maximum value), which corresponds to a flux of < 0.1 amps per cm^2 . This unstable phase of a small particle persisted for long periods of time, a maximum of 40 minutes observed so far. Even when the electron beam was completely turned off for about five minutes, and then turned on at the lowest flux for observation, the particle was still fluctuating. This means that either the particle was fluctuating when the beam was off or the activation energy needed to form the quasi-molten phase in small particles is much lower than previously reported. It was noticed that as the height of the pillar increased, the frequency of fluctuations of the particle increased suggesting that the stability in structure of the small particle decreases with decreasing interaction with the substrate. The particle became

stable again only when it found another potential well on the substrate, as seen in Fig.5.2.d, when the pillar like structure partially collapsed and the particle crystallized on the substrate into a familiar Wulff polyhedron shape with well defined surface facets.

The above observations are also partially confirmed by recent results obtained by Lewis and Smith (1989). They reported initial efforts to quantify some of the experimental factors involved in the quasi-melting process. Data was obtained for gold particles of different sizes supported on three different substrates (amorphous carbon, graphitized carbon and amorphous silicon) for the quasi-melting at different beam currents. Their data is reproduced in Fig.5.5 which shows the relationship between particle size and beam current density for quasi-melting to occur. It is interesting to note that if one extrapolates the curves they all cross the X-axis (ie. zero current density) at some finite value of particle size, which shows that there is a critical particle size below which quasi-melting would occur even in the absence of the beam. Also, on changing the particle-substrate interactions (decreasing) the curves shift to the right suggesting much larger particles would quasi-melt if the

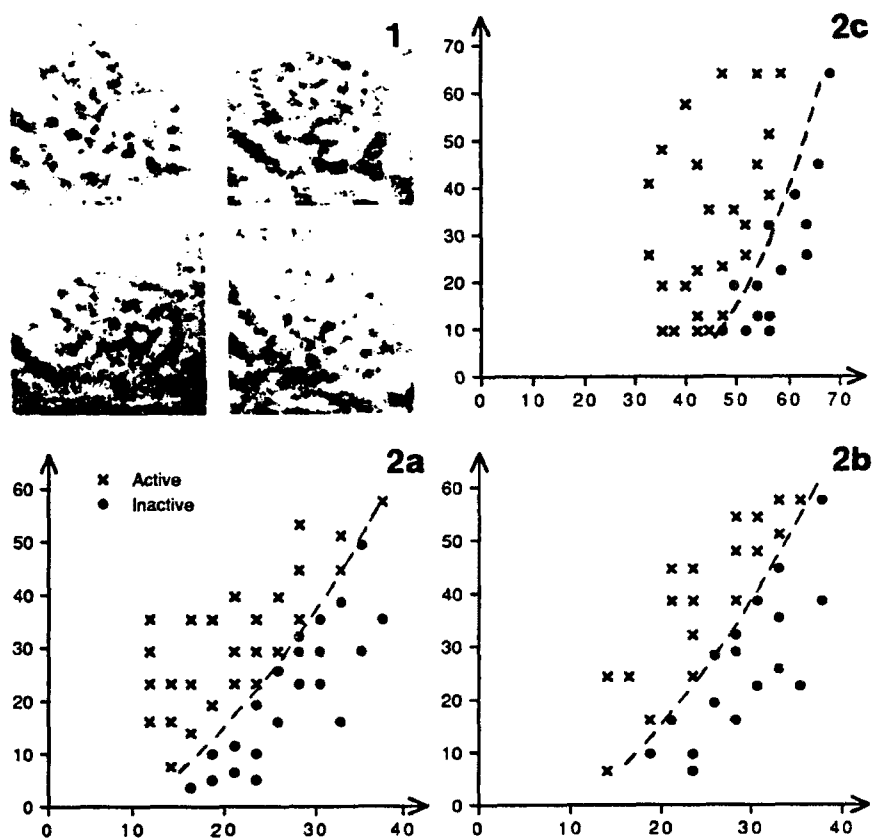


Fig.5.5 1. Gold particle on graphitized carbon support showing structural fluctuations as a result of electron irradiation at 400 KV. 2. Behavior of small gold particles on different substrates for irradiation at 400 KV: a) amorphous carbon b) graphitized carbon c) amorphous silicon. Horizontal axes correspond to particle size (Å), vertical axes to beam current density (A/cm²). (from Lewis and Smith, 1989).

interactions are reduced to a minimum, like what was observed in the case of particles floating on one dimensional pillars. The observations also correlate well with the size of the particle in the phase diagram which would quasi-melt.

These observations confirm earlier predictions on the free energy surfaces and Boltzmann distributions in small particle structures. A particle of any size should theoretically follow a Boltzmann type distribution in the interval of infinite time scales, due to the statistical fluctuations in the system. But, in small particles where the activation energy barriers between various states is extremely small, the dwell times of individual states could be small and the Boltzmann distribution could evolve in observable times. The probabilities of these changes in particle morphologies predicted such an unstable state and this state was named quasi-molten. In this chapter, experimental conditions of an almost free floating cluster was simulated and demonstrated that the particle left to itself is unstable and random walks in configurational space between various morphological states. It should be noted at this point that similar ideas about the coexistence of various isomeric forms in clusters containing large number of atoms have been predicted recently by Berry

and Wales (1989).

Other possible causes of the quasi-molten state are not consistent with our experimental results. A thermal origin for the process, which was reported elsewhere [Bovin et al. 1985, Williams 1987] can be ruled out. Using Stefan-Boltzmann law for radiative heat transfer from an MgO particle of radius R and using an emissivity of 0.6, one gets an order of magnitude value of $\sim 10^{-5} R$ seconds for the temperature to drop from 1400°K to room temperature. The time for gold will be smaller since thermal conductivity is higher. For MgO particles a few ten thousand Å in size (an average value), the temperature drop will occur in a few milli-seconds. Local melting and recrystallization does not seem to be a viable route since at fluxes as low as have been reported, the frequency of structural rearrangements given by this model will be too low (frequencies of the order of 1-10 Hz for a 20Å particle were observed even at low fluxes). Energy gain through channels involving core excitations could still be possible but in that case the critical flux for such events should be much lower than previously reported. Since these excitations have decay times of less than fractions of seconds, the persistence of the unstable phase cannot be

explained by the same model. These violent models are highly improbable since they are high flux and hence low cross section events and need not be invoked for sustaining the quasi-molten phase; as mentioned below they may play a role in initiating the quasi-molten phase but not in sustaining it.

The way the electron beam deposits energy into a small particle through electronic excitations is not clear as yet. It is found that the large amounts of energy needed goes to break the bonds at the particle substrate interface and free the particle from the potential well, and this could involve violent electronic excitations. Charging of the particle or the MgO does not seem to be taking place since this would have created problems in imaging, which was not observed. The fact is that the energy fluctuations due to the smallest number of electrons that can be used for imaging in an electron microscope are enough to make the particle structurally unstable; indeed, there is a good probability that in the absence of the beam the particle is quasi-molten although, of course, it can not be proved. An increase in the mean energy (thermal or electronic) may increase the system fluctuations. It has been observed that when the electron flux is increased the particle starts changing shapes at a faster rate,

essentially flattening the probability distribution.

The results presented here are clear experimental proof for the existence of a quasi-molten phase in a free small particle. The stable particle morphologies that one find in experiments are the trapped morphologies in deep potential energy wells on the substrate. The amount of energy needed to float the particle out of the well will depend on the strength of short range interactions that stabilize the particle / substrate interface. But this energy is orders of magnitude higher than that needed to sustain the quasi-molten phase in small particles.

5.3. Conclusions

As evident from this and previous chapters, the conclusions that can be derived from our experiments are many-fold. The most important of all is the experimental proof for the theoretical prediction that a quasi-melting phase exists for small particles at temperatures much below the thermodynamic melting point. This should have far reaching implications both in understanding the physics of microclusters as well as in industry.

The evidence of instability seen in small clusters

suggest that one has to look at these quite differently compared to the conventional ways, for example in catalysis. Usually catalysis works by a lock and key mechanism in which the particle, having a certain surface structure is the lock and the incoming molecule the key. But one has to realize that the lock is actually changing in structure, it is varying its code all the time. Of course in the time scales of a chemical reaction one may still see a solid but if one looks at these particles for longer time, there no more would be a fixed structure. This also leads us to a philosophical problem; take for instance a car sitting in a valley. From statistical and quantum mechanics it is evident that if one watches long enough one could see the car half way up the valley. But how long is this long enough? it purely depends on the potential energy of the car; we know from experience that it will be infinitely long and this unusual phenomena can never be seen. But for small particles our experimental predictions tell us that this time scale is only fractions of a second and one can actually see the evolution that takes place.

Although the experimental part of this result is based on induction (since the particle remains structurally unstable even as the beam current is decreased to a minimum value that

is experimentally observable, and the unstable state persists even after the beam is turned off and on again to this value of beam current, it was extrapolated to say that the particle was in the unstable state even when the beam was off) it is to be believed that this is probably the closest one can get experimentally at the present state of affairs. With improved sensitivity of the detector system one could probably go to still lower beam currents and observe if the particle is quasi-molten, but one will always have to supply energy to the system (however small it is) in order to observe it. A free floating cluster is also experimentally an impossibility and the author was lucky to have a system that lends itself favorably by forming microscopic pillars under electron irradiation and thus reducing the substrate interactions by many orders of magnitude.

The particle substrate interactions that were observed in the system studied are themselves very interesting; for example, sinking of small particles into solid substrates could have enormous implications in the catalysis industry. The formation of pillars was more of a novelty although there is some interesting physics involved and it is still uncertain as to whether the problem has been completely solved. More

systematic studies involving obtaining data for pillar height against time and flux need to be done. The experiments that involved heating of the specimens gave few results since the MgO readily encapsulated the gold particles, thereby failing to provide any interesting results, for example some data points for the structural instability as a function of temperature (in other words mapping parts of the Boltzmann distribution experimentally). One has to look for a different system for such experiments which would give valuable data; but this in itself would be another PhD project. It is hoped that the results that were presented in this thesis have generated enough ideas and implications for further research on small particles, the scope of which the author believes remains still unfathomable.

Chapter 6 Electron Irradiation of Small Particles

6.1 Fluxional Dependence of the Structure

From the previous chapters it would have become quite evident that the electron flux density used for imaging in the microscope plays an important role in the structural stability of small particles. Figure 6.1 shows the irradiation sequence of a small gold particle at three different electron flux densities. It is clear from the images that the changes in the structure is a function of the electron flux (although qualitatively). As the current density or the net flux of electrons falling on the particle per second is increased the particle morphology start changing with time. In small particle research structural non-rigidity of particles is an important consideration and this is fluxional in nature. For larger particles where the structure is more stable the dose of electrons (flux times time) may become important. This dependence could be the result of many diffusional as well as electronic phenomena; for example flux dependent surface diffusion, flux dependent defect creation inside the material, structural rearrangement due to indirect electronic

excitations or even increased background noise (contrast) which makes the precise determination of the structure, a difficult task. Although the images in fig.6.1 provide only a qualitative result, it shows that the phase boundary of quasi-melting that we predicted before (phase diagram in chapter.3) is flux dependent. This point has been recently demonstrated by Lewis and Smith (1989). The dependence can not be said to be linear and the phase change is not abrupt but continuous, at least in the presence of strong substrates.

An electron microscopist, especially one who works with small particle structures which are so transient in nature, has to be careful in reporting structures without mentioning the flux or current densities used in the experiments since there is a definite correlation between the two. For an increase in the signal to noise ratio one tends to work at lowest beam current; whereas in order to observe and record images at very high magnifications and better contrasts one needs higher beam currents. It is always a compromise between the two that gives reliable as well as good images of structures that one can interpret unequivocally.

6.2 On the Structure of Larger Particles Under Electron Irradiation

As mentioned in chapter 3 the activation barriers between various particle shapes increase almost exponentially with particle size and hence for larger particles there should be a global energy minimum shape (/structure) which should be stable under a range of conditions. This fact is also experimentally seen since the structural fluctuations in small particle become sluggish as one increases the particle size. A quantitative estimate of the particle size for the cross-over between a stable and unstable state in small particles is difficult, since the stability depends on many parameters like the temperature and electron flux, but from many of our experimental observations it is reasonable to say that this cut-off falls around 80-100Å; this is also quite in accordance with our theoretical phase diagram prediction. But apart from the morphological changes which involves structural rearrangements over the entire particle, various other effects which involves changes in localized structure occurs during the irradiation of larger particles.

Figure 6.2.a shows the image of a larger particle containing two parallel twin boundaries and Fig.6.2.b-d,

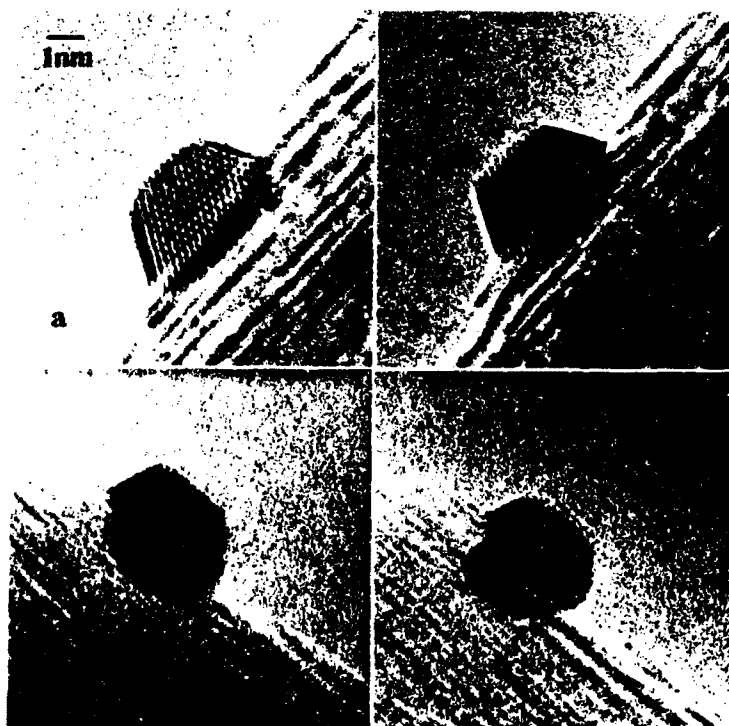


Fig.6.1 a) Shows an equilibrium shape of a small gold cluster on MgO. b-d show structures of the same particle at three different electron fluxes corresponding to emission currents of 8, 16 and 24 micro-amperes. It is seen that the structure deteriorates faster at higher current densities.

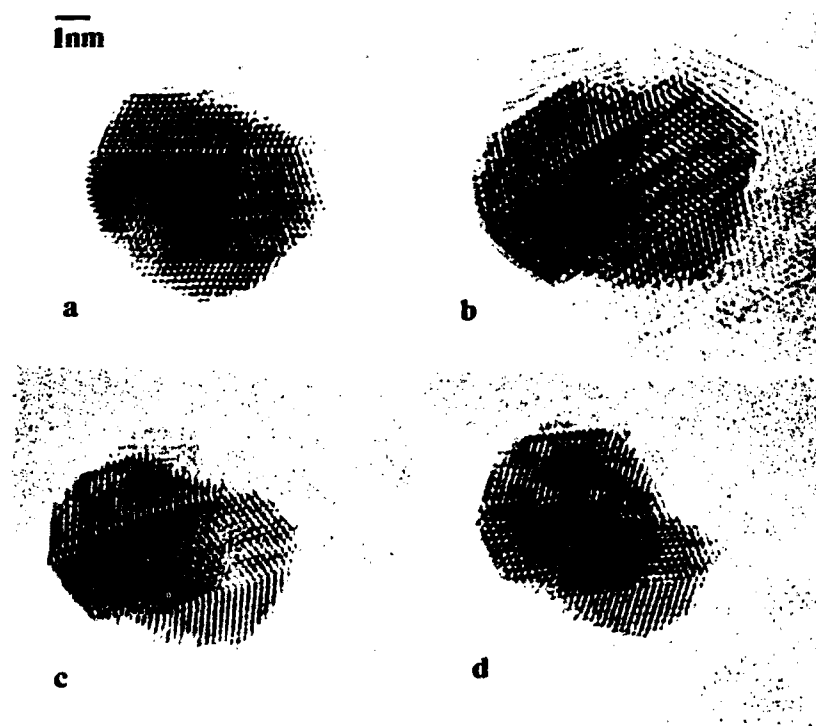


Fig.6.2 Sequence of images showing the effect of 30 minutes of electron irradiation on a large gold particle, supported on MgO, with two parallel twin boundaries. During irradiation it is seen that the particle has suffered some mass loss (primarily due to surface diffusion), the twin boundaries have moved closer to each other, and undergone a shear along the twin plane.

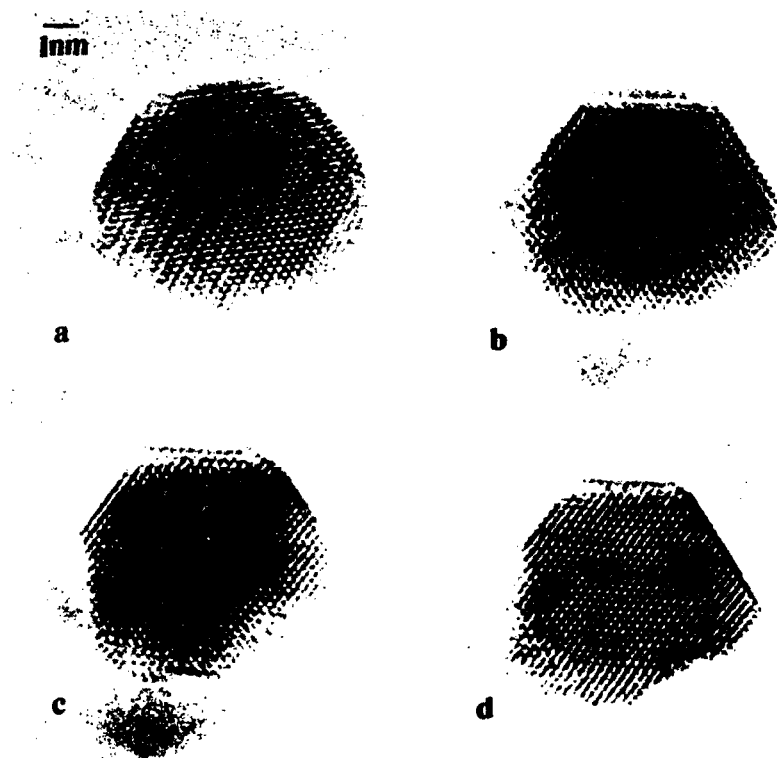


Fig.6.3 A large cuboctahedral particle of gold on MgO, under 30 minutes of electron irradiation undergoing volume shrinkage from areas adjoining the substrate and changes in the facet structure.

and sequence of changes occurring during the high flux electron irradiation of thirty minutes. Some features are clear from the picture. Apart from a small volume shrinkage of the particle it has undergone small shear along the twin boundaries. The twins have moved closer to each other and steps and microfacets have formed on the surface of the particle. Figure 6.3.a-d shows another sequence of a particle undergoing surface faceting and volume shrinkage. During the faceting it is seen that some of the low index facets that are on the original particle are retained whereas volume loss occurs from regions which are in contact with the substrate; a reason to believe that most of the material loss occurs through surface diffusion. If one assumes that the volume shrinkage took place through evaporation, one can calculate the rate of evaporation and match with the vapor pressure data for gold. An order of magnitude calculation shows that the temperature for the evaporation rate seen here corresponds to $\sim 800-850^{\circ}\text{C}$, quite an improbable value which again suggests that surface diffusion is the major mechanism of mass transport for particles supported on solid substrates. Rather than an increase in the thermal energy of the system the electron beam could probably induce an effective electronic

temperature rise [Buxbaum and Marks 1986] where the electron beam, instead of creating a thermal effect by the succession of electron-hole pair formation and decaying into a phonon bath, is driving the evaporation process through some direct electronic excitation channels. This could increase the surface diffusion coefficients resulting in mass loss.

The difference between a small particle and larger particle under electron beam irradiation is striking. For a small particle, surface diffusion induces the support material to diffuse and cover up the particle to reduce free energy. They also undergo structural rearrangements under the electron beam. For larger particles this latter phenomena is never seen. Surface diffusion in this case produces diffusion of gold atoms from edges and surfaces of the particle towards the surface of the support. The activation barrier for sinking for larger particles is too high and this does not happen. Also the loss of mass occurs relatively easily from larger particles supported on substrates whereas in smaller particles this seldom occurs since the atoms on the surfaces easily exchange positions with the interior and undergo structural fluctuations.

The movements of twin boundaries and other defects like

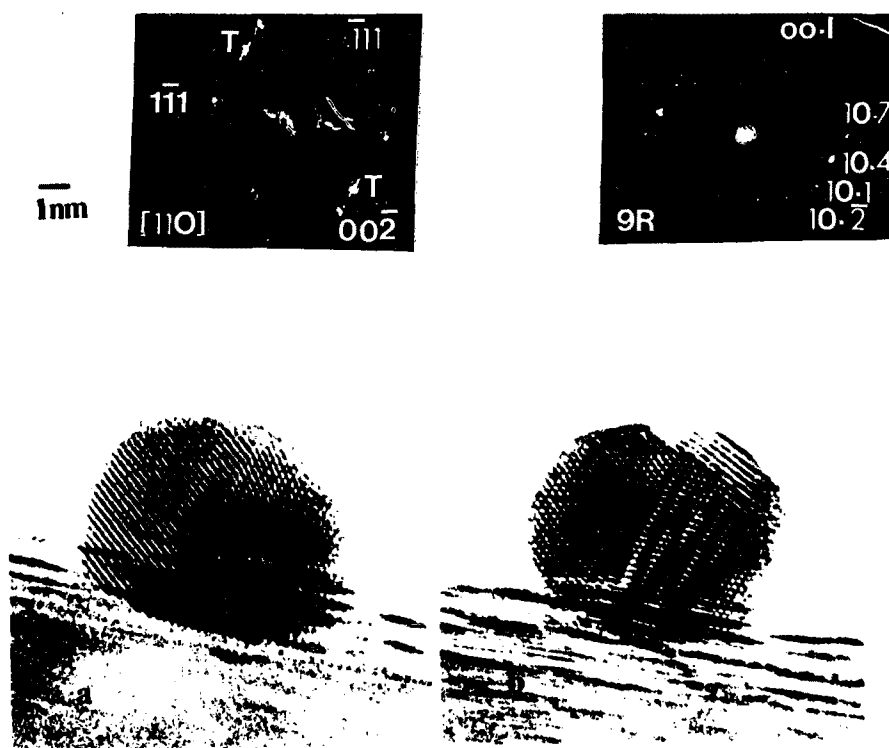


Fig.6.4 A larger particle of gold on MgO, during 60 minutes of high flux electron irradiation, undergoes local changes in stacking from an fcc to a hexagonal or distorted 9R type of structure. Shown also on the top corners of the images are the optical diffractograms which indexes the structures. The changes occurring in the structure can also be explained as resulting from multiple twinning and re-orientation giving rise to moire fringe contrast from the twinned structure.

stacking faults have been reported in both small and large particles elsewhere [Iijima, Ichihashi 1988]. It should be noted that the energy deposition process during irradiation is a statistical process and hence there must be some distribution of the excitation events which could result in the random creation or movement of defects like a twin boundary or stacking fault.

For still larger a particle (Fig.6.4.a,b), with one twin boundary, other structural transformations are seen to occur. This can be explained either as the stacking of the gold fcc lattice slowly changing to a distorted 9R type hexagonal structure locally (the optical diffractograms taken from the particle are shown in the insets which show the introduction of the psuedo-hexagonal stacking) or as a result of moire fringes that result from multiple twinning and re-orientation of the particle. In many of the larger particles similar localized changes in stacking and structure are visible during electron irradiation. These observations suggest that in larger particles, when the energy needed for complete restructuring of the particle morphology is too large the energy deposited through radiation induces local changes in structure like changes in stacking order or introduction of

lattice defects which may require smaller activation energies since the volume involved in these changes are much smaller relative to the particle volume.

6.3 Electron Beam Induced Diffusion Limited Aggregation

An interesting result is obtained when a uniform distribution of small particles (gold particles supported on NaCl support) is irradiated under high flux and they diffuse and coalesce under the electron beam. Figure 6.5 shows the initial distribution and the final structure of the growth that has resulted from the coalescence. It should be noted that the nature of coalescence of small particles is liquid-like when two approaching clusters will suddenly merge (the necking regime usually seen in large particles are almost absent at smaller sizes) resulting in an almost new spherical cluster. The observations of small particle coalescence during electron beam irradiation has been reported before [Flueli and Borel 1988]. These imply that atomic rearrangements over the entire volume of small particles takes place easily and it is not necessary to go through the different stages of coalescence or sintering like a neck formation where diffusional mass transport can occur slowly and the reduction

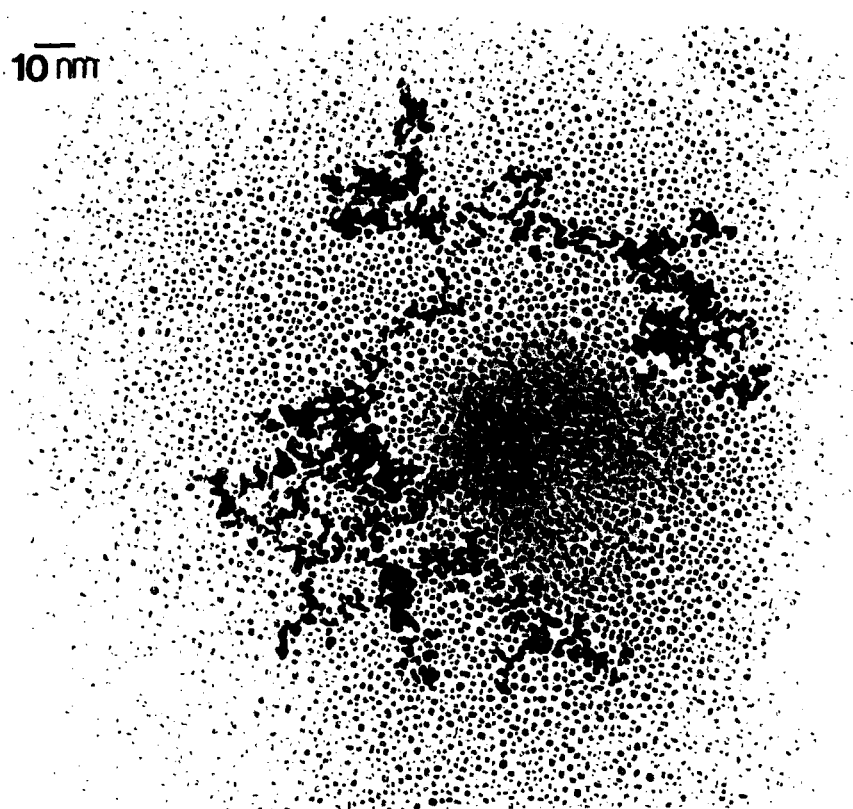


Fig.6.5 Image of the fractal structure of cluster-cluster coalescence during electron beam irradiation of gold clusters evaporated onto NaCl substrate.

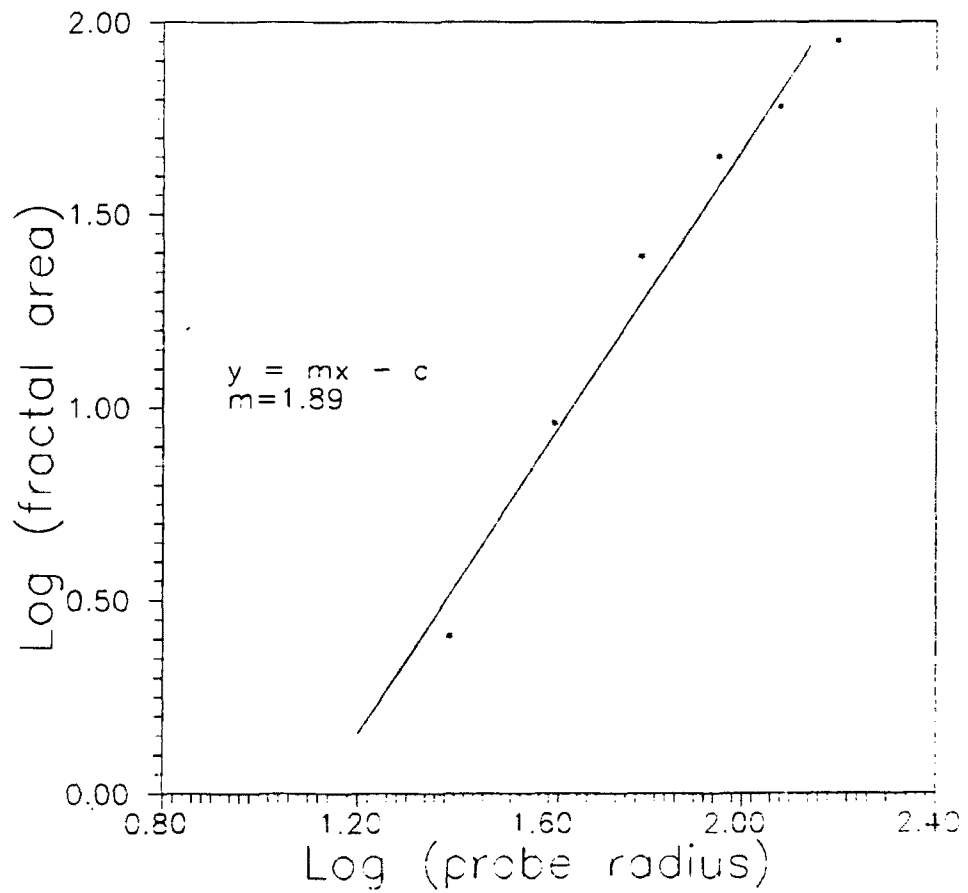


Fig.6.6 Area encompassed by the fractal structure inside uniform probes (circular) of increasing sizes plotted against the size of the probe on a log-log scale. Slope of the curve gives the fractal dimension of the structure in Fig.6.5.

of free energy occurs in steps.

Another important feature of Fig.6.5. is the fractal nature of the coalesced structure. One can compare this with the micrographs given by Lin and coworkers (1989) of colloids of gold clusters prepared by diffusion limited aggregation [Witten and Sander 1981, Vicsek 1984]. Diffusion limited aggregation occurs when there is negligible coulombic repulsive forces between the particles, so that the aggregation or coalescence rate is limited solely by the time taken by the clusters to encounter each other by diffusion. This also suggests that the gold clusters carry negligible charges during irradiation (in which case a DLA type growth will not occur) and the charging mechanisms which tries to explain the quasi-melting in small particles can be safely avoided. DLA is also characterized by the varying sticking probabilities along the profiles of individual particles and this is quite applicable to small particles which has a varying surface energies around the profile due to faceting and continuously changing surface stresses. The fractal structures thus formed have the property of invariance under dilatation and are solely characterized by a single quantity known as the fractal dimension.

The usual way to calculate the fractal dimension of two dimensional random fractals, such as in Fig.6.5, is to superimpose regular probes of varying sizes and measuring the area encompassed by the fractal structure in each. Since the area covered scales with the size of the probe as the fractal dimension (a characteristic of the dilatancy property of fractals) the fractal dimension can be determined by plotting the first two variables. Circular probes of uniformly increasing radii were applied to the structure in Fig.6.5 and the areas counted manually (for better accuracy the image intensity should be digitized and each pixel related to the structure should be counted using a computer). The areas are plotted against probe sizes in Fig.6.6 using a log-log scale. The slope of the curve gives the fractal dimension which is approximately equal to 1.9. This value corresponds reasonably to a diffusion limited aggregation growth [Schaffer 1989]. This proves semi-quantitatively that the cluster-cluster aggregation under electron beam induced surface diffusion is DLA and refutes the argument that the clusters get charged during radiation. If charging had occurred one would expect to see much thicker structures from coalescence as discussed in the previous paragraph.

The results that have been presented in this section are only a preliminary one on this topic, although an interesting one, and work remains to be done. This can give several features of electron beam enhanced diffusion of species.

Chapter 7 Summary and Suggestions for Future Research

7.1 Summary

The major accomplishments of this study are as follows:

1. The energetics of small fcc metal particles have been worked out using a continuum theoretical model and a phase diagram constructed showing the stability regimes for multiply twinned particle structures as a function of particle size and temperature. The phase diagram can provide valuable information and impetus for further studies involving the structure and growth sequences of small metal particles leading to formation and epitaxy of thin film structures.

2. The theoretical model predicted that particles in the size range of 1-10 nanometers can exist in a quasi-molten state where various particle structures and morphologies can co-exist and transform between one another with high probabilities.

3. It was seen that small gold particles can sink into magnesium oxide substrate due to strong metal substrate interaction and this phenomena can be explained on the basis of thermodynamics based on the reduction of free energy of the

system. A more sophisticated analysis based on the idea of modified Wulff construction also proves that the path taken by a sinking particle is the lowest energy path since the static points in the path can be shown to be true minimum equilibrium shapes. The phenomenon of sinking can be of substantial importance in real catalyst systems.

4. Under high flux electron irradiation conditions, it was noticed that microscopic pillars can grow from the magnesium oxide support beneath gold particles due to strong capillar forces that can localize the diffusion field.

5. The existence of the quasi-molten phase in small particles was experimentally observed when small particles sitting on microscopic pillars, and almost freely floating in vacuum, continued to structurally fluctuate even after the electron beam was turned down to a minimum value and then completely off. It was proposed that small particles on substrates sit in deep potential wells and once floated out of these wells can quasi-melt on shallow morphological energy surfaces between the various local minimum energy configurations.

6. Larger particles sitting on substrates did not undergo structural fluctuations under electron beam irradiation, but

changed structure locally either by faceting, surface reconstructing or changing local stacking from fcc to distorted hexagonal type structure.

7. Electron beam induced cluster-cluster aggregation produced fractal structures suggesting that the growth occurs by diffusion limited aggregation.

7.2 Suggestions for Future Research

As far as the theory of the structure and energetics of small particles, especially the MTP structures are concerned, it seems that a conclusive stage has been reached. It would be interesting to consider the kinetics and time evolution of particle structures but this would necessitate the knowledge of the dwell times of the particle in each individual state. Also an effective mass of the quasi-molten state have to be considered, which at the moment is not comprehensible. It should be noted that we have used continuum models throughout, whereas pair-potential calculations would be more accurate. With the availability of faster computers and more efficient molecular dynamics programs it would be conceivable to perform such calculations.

But on the other hand, the experimental work on the

subject is far from closed. The major work that can be done is in the refinement of the phase diagram with experimental data. One can hope to get data points for quasi-melting as a function of particle size and temperature by using a hot stage and a support that does not readily encapsulate the particle at higher temperatures. Graphite or SiO_2 may be such a substrate. It can also be attempted to map the Boltzmann distribution of particle structures experimentally, but this will be extremely tedious.

There is a lot of scope to studying the effect of particle / substrate interactions by looking at various different systems. The criterion of sinking can be tested since the surface energy balance will be different in different systems. The observation of microscopic pillars was the first of its kind as far as the author knows, and the field is now open for various different experiments like video recording of the pillar growth under various flux conditions and deducing the nature of diffusion and so on. The phenomenon can also be tested in other particle / substrate systems.

So far the study undertaken in this thesis has only dealt with the structure of small particles in the microscope vacuum. But in real catalysis and practical systems different

gaseous and thermodynamic environments are encountered. With the acquisition of the new UHV microscope equipped with a side chamber, one should think of developing an environmental cell which can simulate the conditions of real reactions and compare the results with the those seen in UHV conditions. For example, various gaseous species can be leaked into the chamber and the changes in structure and surface morphologies can be observed after the gases are adsorbed on the surface.

Finally, it is hoped that the results presented in this thesis would prove valuable to the scientific community and would serve as an impetus for development of new ideas and models in the field of small particle research.

References

Ajayan, P. M., and Marks, L. D., "Quasimelting and Phases of small particles", *Phys. Rev. Lett.* 60, 585-587 (1988).

Ajayan, P. M., and Marks, L. D., "Evidence for sinking of small particles and implications for heterogeneous Catalysis", *Nature* 338, 139-141 (1989).

Ajayan, P. M., and Marks, L. D., "Experimental evidence for quasi-melting in small particles", *Phys. Rev. Lett.* 63, 279-282 (1989).

Ajayan, P. M., and Marks, L. D., "Experimental observation of microscopic pillar growth instabilities", *Appl. Phys. Lett.*, Submitted.

Allpress, J. G., and Sanders, J. V., "The structure and orientation of crystals in deposits of metals on Mica", *Surf. Sci.* 7, 1-25 (1967).

Bagley, B. G., "A dense packing of hard spheres with five-fold symmetry", *Nature* 208, 674-675 (1965).

Badzian, A. R., Badzian, T., Roy, R., Messier, R., and Spear, K. R., "Crystallization of Diamond crystals and Films by microwave assisted CVD-II", *Mat. Res. Bull.* 23, 531-549 (1988).

Beck, T. L., Leitner, D. M., and Berry, R. S., "Melting and Phase space transitions in small clusters: Spectral characteristics, dimensions and K entropy", *J. Chem. Phys.* 89, 1681-1694 (1988).

Benison, D., Kadanoff, L. P., Liang, S., Shraiman, B. I., and Tang, C., "Viscous flow in two dimensions", *Rev. Mod. Phys.* 58, 977-999 (1986).

Bernal, J. D., "Geometry of the structure of monatomic liquids", *Nature* 185, 68-70 (1960).

Berry, R. Stephen, Jellenik, J., and Natanson, G., "Melting of clusters and melting", *Phys. Rev. A.* 30, 919-931 (1984).

- Berry, R. Stephen, and Wales, J. David, "Freezing, melting, spinodals and clusters", *Phys. Rev. Lett.*, 63, 1156-1159 (1989).
- Blackman, M., and Sambles, J. R., "Melting of very small particles during evaporation at constant temperature", *Nature* 226, 38-38 (1970).
- Blaisten-Barojas, E., Garzon, I. L., and Avalos-Borja, M., "Melting and freezing of Lennard-Jones clusters on a surface", *Phys. Rev. B* 36, 8447-8455 (1987).
- Blumel, R., Chen, J. M., Peik, E., Quint, W., Schleich, W., Shen, Y. R., and Walther, H., "Phase transitions of stored laser-cooled ions", *Nature* 334, 309-313 (1988).
- Borel, J. P., "Thermodynamic size effect and the structure of metallic clusters", *Surf. Sci.* 106, 1-9 (1981).
- Born, M., "Thermodynamics of crystals and melting", *J. Chem. Phys.* 7, 591-603 (1939).
- Boudart, M., "Metal-support interaction: From weak to strong", 11th North American meeting of the Catalysis society (Dearborn, Michigan), Presented (1989).
- Bouligand, Y., in "Dislocation in solids", ed. Nabarro, F. R. N., Vol. 5, North-Holland Publishers, Amsterdam, (1980).
- Boyer, L. L., and Hardy, J. R., "Theoretical study of the structural phase transition in RbCaF_3 ", *Phys. Rev. B* 24, 2577-2591 (1981).
- Boyer, L. L., "Theory of melting based on lattice instability", *J. Phase Transitions* 5, 1-48 (1985).
- Briant, C. L., and Burton, J. J., "Molecular dynamic study of the structure and thermodynamic properties of argon micro-clusters", *J. Chem. Phys.* 63, 2045-2058 (1975).
- Buffat, Ph., and Borel, J. P., "Size effect on the melting temperature of small particles", *Phys. Rev. A* 13, 2287-2298 (1976).

Burton, J. J., "Configuration, energy, and heat capacity of small spherical clusters of atoms", *J. Chem. Phys.* 52, 345-352 (1970).

Buxbaum, A., and Marks, L. D., "The electronic temperature in TEM", *Proc. XIth Int. Cong. on Electron Microscopy, Kyoto*, 1441-1442 (1986).

Cahn, J. W., "Surface stress and the chemical equilibrium of small crystals-I. The case of the isotropic surface", *Acta Met.* 28, 1333-1338 (1980).

Chen, Bor-Her, and White, J. M., "Properties of platinum supported on oxides of titanium", *J. Phys. Chem.* 86, 3534-3541 (1982).

Couchman, P. R., and Karasz, F. E., "The effect of particle size on debye temperature", *Phys. Lett.* 62A, 59-61 (1977).

Couchman, P. R., and Jesser, W. A., "Thermodynamic theory of size dependence of melting temperature in metals", *Nature* 269, 481-483 (1977).

Couchman, P. R., and Ryan, C. L., "The Lindemann hypothesis and the size-dependence of melting temperature", *Phil. Mag.* 37, 369-373 (1978).

Curtis, A. C., Duff, D. G., Edwards, P. P., Jefferson, D. A., Johnson, B. F. G., and Kirkland, A. I., "The preparation and structure characterization of an unprotected copper solution", *J. Phys. Chem.* 92, 2270-2275 (1988).

Curzon, A. E., "A closed expression for the increase in specimen temperature produced during transmission electron microscopy", to be published.

Dahmen, U., and Westmacott, K. H., "Observations of pentagonally twinned precipitate needles of germanium in aluminum", *Science* 233, 875-876 (1986).

de Heer, W. A., W. D. Knight, M. Y. Chou, and M. L. Cohen, "Electronic shell structures and metal clusters". *Solid state Physics* (ed: Ehrenreich, H., and D. Turnbull), 40, 93 (1987).

- de Wit, R., "Relation between dislocation and disclinations", *J. Appl. Phys.* 42, 3304-3308 (1971).
- de Wit, R., "Partial disclinations", *J. Phys. C: Solid state Phys.* 5, 529-534 (1972).
- Dhere, A. G., De Angelis, R. J., Reucroft P. J., and Bentley, J., "Twinned colloidal gold particles", *Ultramicroscopy* 18, 415-418 (1985).
- Dickey, J. M., and Paskin, A., "Phonon spectrum changes in small particles and their implications for superconductivity", *Phys. Rev. Lett.* 21, 1441-1443 (1968).
- Ding, A., and Hesslich, J., "The abundance of Ar and Kr microclusters generated by supersonic expansion", *Chem. Phys. Lett.* 94, 54-57 (1983).
- Dinghas, V. A., "Uber einen geometrischen sat von Wulff fur die gleichgewichtsform von kristallen", *Z. Kristallogr.*, 105, 304-314 (1943).
- Dundurs, J., *Mathematical theory of dislocations*, Mura, T. (ed.), *Am. Soc. Mech. Engg.*, 70-115 (1969).
- Dundurs, J., "Theory of Elasticity", *Lecture Notes*, Northwestern University, (1987).
- Dundurs, J., Marks, L. D., and Ajayan, P. M., "Structural fluctuations in small particles", *Phil. Mag.* 57, 605-620 (1988).
- Echt, O., Sattler, K., and Recknagel, E., "Magic numbers for sphere packings: Experimental verification in free Xenon clusters", *Phys. Rev. Lett.* 47, 1121-1124 (1981).
- Etters, R. D., and Kaelberer, J., "Thermodynamic properties of small aggregates of rare-gas atoms", *Phys. Rev. A* 11, 1068-1079 (1975).
- Etters, R. D., and Kaelberer, J., "On the character of melting transition in small atomic aggregates", *J. Chem. Phys.* 66, 5112-5116 (1977).

Fan, H., and Marks, L. D., "On the electron beam induced radiation damage of V_2O_5 ", to be published in *Ultramicroscopy*.

Farges, J., de Feraudy, M. F., Raoult, B., and Torchet, G., "Noncrystalline structure of argon clusters-I: Polyicosahedral structure of Ar_N clusters", *J. Chem. Phys.* 78, 5067-5080 (1983).

Farges, J., de Feraudy, M. F., Raoult, B., and Torchet, G., "Surface arrangements on multilayer icosahedra", *Dynamics of surfaces*, B. Pullman et al. (eds.), 425-430 (1984).

Farges, J., de Feraudy, M. F., Raoult, B., and Torchet, G., "Noncrystalline structure of Argon clusters, II-multilayer icosahedral structure of Ar_N clusters $50 < N < 750$ ", *J. Chem. Phys.* 84, 3491-3501 (1986).

Farges, J., de Feraudy, M. F., Raoult, B., and Torchet, G., "From five-fold to crystalline symmetry in large clusters", *Large Finite Systems*, J. Jortner et al. (eds.), 113-119 (1987)

Feshback, H., "Small systems: when does thermodynamics apply", *Physics Today*, 9-11 (1987 November).

Fisher, S. B., "On the temperature rise in electron irradiated foils", *Radiation effects* 5, 239-243 (1970).

Flueli, M., and Borel, J. P., "Surface energy anisotropy measurements on small cuboctahedron of gold observed by HREM", *J. Cryst. Growth* 91, 67-70 (1988).

Freund, E., J. Lynch, and R. Szamanski, "Small particles in the field of industrial supported catalysts", *Ultramicroscopy* 20, 107-110 (1986).

Fukano, Y., and Wayman, C. M., "Shapes of nuclei of evaporated fcc metals", *J. Appl. Phys.* 40, 1656-1664 (1969).

Gale, B., and Hale, K. F., "Heating of metallic foils in an electron microscope", *Brit. J. Appl. Phys.* 12, 115-117 (1961).

Galvagno, S., Schwank, J., and Parravano, G., "Cyclopropane hydrogenation of Ru and Ru-Au catalysts", *J. Catal.* 61, 223-231 (1980).

- Gillet, M., "Structure of small metallic particle", *Surf. Sci.* 67, 139-157 (1977).
- Giorgio, S., and Urban, J., "Fivefold and threefold symmetries in silver clusters", *Appl. Phys. Lett.* 52, 1467-1468 (1988).
- Gordon, M. B., Cyrot-Lackmann, F., and Desjonqueres, M. C., "Relaxation and stability of small transition metal particles", *Surf. Sci.* 80, 159-164 (1979).
- Griffin, G. L., and Andres, R. P., "Microscopic capillary approximation: free energies of small clusters", *J. Chem. Phys.* 71, 2522-2530 (1979).
- Halicioglu, T., and White, P. J., "Structures of microclusters: an atomistic approach with three body interactions", *Surf. Sci.* 106, 45-50 (1981).
- Halicioglu, T., "Fluxional nature of gas-phase clusters", *Surf. Sci.* 197, L233-L236 (1988).
- Halicioglu, T., and Bauschlicher, C. W., "Physics of microclusters", *Rep. Prog. Phys.* 51, 883-921 (1988).
- Halperin, W. P., "Quantum size effects in metal particles", *Rev. Mod. Phys.* 58, 533-606 (1986).
- Ham, Frank S., "Diffusion limited growth of precipitate particles", *J. Appl. Phys.* 30, 1518-1525 (1959).
- Harris, W. F., and Scriven, L. E., "Intrinsic disclinations as dislocation sources and sinks in surface crystals", *J. Appl. Phys.* 42, 3309-3312 (1971).
- Hasegawa, M., Hoshino, K., and Watabe, M., "A theory of melting in metallic small particles", *J. Phys. F: Metal Phys.* 10, 619-635 (1980).
- Hayashi, C., "Ultrafine particles", *Phys. Today*, 44-51 (1987 December).
- Heine, V., and Marks, L. D., "Competition between pairwise and multi-atom forces at noble metal surfaces", *Surf. Sci.* 165, 65-82 (1986).

Heinemann, K., Yacaman, M. J., Yang, C. Y., and Poppa, H., "The structure of small vapor deposited particles, I. experimental study of single crystals and particles with pentagonal profiles", *J. Crystal growth* 47, 177-186 (1979).

Heinemann, K., Osaka, T., Poppa, H., and Avalos-Borja, M., "In-situ TEM studies of Pd on MgO", *J. Catalysis* 83, 61-78 (1983).

Heinemann, K., and Soria, F., "On the detection and size classification of nanometer-size metal particles on amorphous substrates", *Ultramicroscopy* 20, 1-14 (1986).

Herring, C., "Some theorems on the free energies of crystal surfaces", *Phys. Rev.* 82, 87-93 (1951).

Herring, C., "The use of classical macroscopic concepts in surface-energy problems", *Structure and properties of solid surfaces* (eds Gomer, R., and Smith, C. S., University of Chicago press), 5-72 (1953).

Herzfeld, K. F., and Goeppert-Mayer, M., "On the theory of fusion", *Phys. Rev.* 46, 995-1001 (1934).

Heyraud, J. C., and Metois, J. J., "Equilibrium shape of gold crystallites on a graphite cleavage surface: Surface energies and interfacial energy", *Acta Met.* 28, 1789-1797 (1980).

Hilliard, J. E., "Nucleation with crystalline phases", *Nucleation phenomena* (American chemical society publication, Washington, D.C.), 79-85 (1966).

Hirth, J. P., and Lothe, J., "Theory of Dislocations" Wiley interscience publication, NewYork, (1982).

Hoare, M. R., and Pal, P., "Physical cluster mechanics: statistical thermodynamics and nucleation theory for monoatomic systems", *Advan. Phys.* 24, 645-678 (1975).

Hoare, M. R., and Pal, P., "Statistics and stability of small assemblies of atoms", *J. Crystal Growth* 17, 77-96 (1972).

Hofmeister, H., "Habit and Internal structure of multiply twinned gold particles on silver bromide films", *Thin Solid*

Films 116, 151-162 (1984).

Honeycutt, J. D., and Anderson, H. C., "Molecular dynamics study of melting and freezing of small Lennard-Jones clusters", *J. Chem. Phys.* 91, 4950-4963 (1987).

Horsley, J. A., "A molecular orbital study of strong metal-support interaction between platinum and titanium dioxide", *J. Am. Chem. Soc.* 101, 2870-2874 (1979).

Howie, A., and Marks, L. D., "Elastic strains and energy balance for multiply twinned particles", *Phil. Mag.* 49, 95-109 (1984).

Howie, A., "Coulomb explosion in metals?", *Nature* 320, 684-684 (1986).

Humphreys, J. J., "Hopping atoms in crystal growth", *Nature* 317, 16 (1985).

Huntington, H. B., Shirn, G. A., and Wajda, E. S., "Calculation of entropies of lattice defects", *Phys. Rev.* 99, 1085-1091 (1955).

Iijima, S., "Electron microscopy of small particles", *J. Electron Microsc.*, 34, 249-265 (1985).

Iijima, S., and Ichihashi, T., "Structural instability of ultrafine particles of metals", *Phys. Rev. Lett.* 56, 616-619 (1986).

Iijima, S., and Ichihashi, T., "Grain boundary migration in small gold particles", *Surf. Sci.* 192, L872-L878 (1987).

Iijima, S., "The 60-carbon cluster has been revealed!", *J. Phys. Chem.* 91, 3466-3467 (1987a).

Iijima, S., "Fine particles of silicon. I. Crystal growth of spherical particles of Si", *Jap. J. Appl. Phys.* 26, 357-364 (1987b).

Iijima, S., "Fine particles of Silicon. II. Decahedral Multiply Twinned Particles", *Jap. J. Appl. Phys.* 26, 365-372 (1987c).

Ino, S., "Epitaxial growth of metals on rocksalt faces cleaved in vacuum II - Orientation and structure of gold particles formed in ultrahigh vacuum", *J. Phys. Soc. Japan* 21, 346-362 (1966).

Ino, S., and Ogawa, S., "Multiply twinned particles at early stages of gold film formation on alkali halide crystals", *J. Phys. Soc. Japan* 22, 1365-1374 (1967).

Ino, S., "Stability of multiply-twinned particles", *J. Phys. Soc. Japan* 27, 941-953 (1969).

Itoh, N., and Tanimura, K., "Radiation effects in ionic solids", *Radiation effects* 98, 269-287 (1986).

Jellenik, J., Beck, T. L., and Berry, R. S., "Solid-liquid phase changes in simulated iso-energetic Ar₁₃", *J. Chem. Phys.* 84, 2783-2794 (1986).

Khlyustikov, I. N., and Buzdin, A. I., "Twinning-plane superconductivity". *Adv. Phys.* 36, 271-329 (1987).

Kimoto, K., and Nishida, I., "Multiply twinned particles of FCC metals produced by condensation in Argon at low pressures", *J. Phys. Soc. Japan* 22, 940-940 (1967).

Kimoto, K., and Nishida, I., "A study of lithium clusters by means of a mass analyzer", *J. Phys. Soc. Japan* 42, 2071-2072 (1977).

Kirchner, H. O. K., and Chadwick, G. A., "Surface entropies of Cadmium and Zinc", *Phil. Mag.* 22, 449-453 (1970).

Kittel, C., "Temperature fluctuation: an oxymoron", *Physics Today*, 93-93 (1988 May).

Kleman, M., "Points, Lines and Walls in liquid crystals, magnetic systems and various ordered media". Wiley-Interscience publication, (1983).

Knight, W. D., Clemenger, K., de Heer, W. A., Saunders, W. A., Chou, M. Y., and Cohen, M. L., "Electronic shell structure and abundance of sodium clusters". *Phys. Rev. Lett.* 52, 2141-2143 (1984).

- Knotek, M. L., "Stimulated desorption from surfaces", *Physics Today*, 24-32 (September 1984).
- Komoda, T., "Study on the structure of evaporated gold particles by means of high resolution electron microscopy", *Jap. J. Appl. Phys.* 7, 27-30 (1968).
- Kubo, R., "Electronic properties of metallic fine particles", *J. Phys. Soc. Japan* 17, 975-986 (1962).
- Landman, U., Barnett, R. N., Cleveland, C. L., Scharf, D., and Jortner, J., "Electron excitation dynamics, and solvation in small clusters", *J. Phys. Chem.* 91, 4890-4899 (1987).
- Langer, J. S., "Instabilities and pattern formation in crystal growth", *Rev. Mod. Phys.* 52, 1-28 (1980).
- Langer, J. S., "Dendrites, Viscous fingers, and the theory of pattern formation", *Science* 243, 1150-1156 (1989).
- Laue, M. Von, "Der Wulffsche satz fur die gleichgewichtsform von kristallen", *Z. Kristallogr.* 105, 124-133 (1943).
- Lee, J. K., Barker, J. A., and Abraham, F. F., "Theory and Monte Carlo simulation of physical clusters in imperfect vapor", *J. Chem. Phys.* 58, 3166-3180 (1973).
- Lewis, J., and Smith, D. J., "Structural rearrangements in small gold particles", *Proceedings of the 47th annual meeting of EMSA*, 640-641 (1989).
- Li, J. C. M., and Gilman, J. J., "Disclination loops in polymers", *J. Appl. Phys.* 41, 4248-4256 (1970).
- Licoppe, C., Nissim, Y. I., and Anterroches, C. D., "Growth front instabilities in solid-state recrystallization of amorphous GaAs films", *Phys. Rev. B* 37, 1287-1292 (1972).
- Lin, M. Y., Lindsay, H. M., Weitz, D. A., Ball, R. C., Klein, R., and Meakin, P., "Universality in colloid aggregation", *Nature* 339, 360-362, (1989).
- Lindemann, Von F. A., "Uber die Berechnung Molecularer Eigenfrequenzen-Concerning the calculation of molecular

- fundamental frequencies". *Z. Physik*, 11, 609-618 (1910).
- Linford, R. G., "Surface thermodynamics of solids", *Solid State Surface Science*, Vol-II, Green, M. (ed.), Marcel Dekker, New York, 1-152 (1973).
- Long, N. J., Marzke, R. F., Mckelvy, M., and Glaunsinger, W. S., "Characterization of Pt Microcrystals using HREM", *Ultramicroscopy* 20, 15-20 (1986).
- Luzzi, D., "Electron beam induced amorphization in materials", PhD thesis, Northwestern University, Evanston, IL, (1986).
- Mackay, A. L., "A dense non-crystallographic packing of equal spheres", *Acta. Cryst.* 15, 916-918 (1962).
- Malm, Jan-Olle, Bovin, J. O., Petford-Long, A., Smith, D. J., Schmid, G., and Klein, N., "Real-time atomic-resolution imaging of polymorphic changes in ruthenium clusters", *Angew. Chem.* 27, 555-558 (1988).
- Marks, L. D., "The structure of small silver particles", PHD thesis, University of Cambridge, England, (1980).
- Marks, L. D., and Smith, D. J., "High resolution studies of small particles of gold and silver, I. multiply twinned particles", *J. Cryst. Growth* 54, 425-438 (1981).
- Marks, L. D., and Smith, D. J., "HREM and STEM of defects in multiply twinned particles", *J. Microscopy* 130, 249-261 (1983).
- Marks, L. D., "Modified Wulff constructions for twinned particles", *J. Cryst. Growth* 61, 556-566 (1984a).
- Marks, L. D., Heine, V., and Smith, D. J., "Direct observation of elastic and plastic deformations at Au(111) surfaces", *Phys. Rev. Lett.* 52, 656-658 (1984).
- Marks, L. D., "Surface structure and energetics of multiply twinned particles", *Phil. Mag.* 49, 81-93 (1984b).
- Marks, L. D., "Particle size effects on Wulff constructions", *Surf. Sci.* 150, 358-366 (1985a).

- Marks, L. D., "Inhomogeneous strains in small particles". *Surf. Sci.* 150, 302-318 (1985b).
- Marks, L. D., "Imaging small particles", *Ultramicroscopy* 18, 445-452 (1985c).
- Marks, L. D., "Image localization", *Ultramicroscopy* 18, 33-38 (1985d).
- Marks, L. D., "Solid-like growth", *Thin solid films* 136, 309-315 (1986a).
- Marks, L. D., "High-Resolution electron microscopy of surfaces", *Structure and dynamics of surfaces I: Topics in current physics*, ed. Schommers, W., and von Blanckenhagen, P., 71-109 (1986b).
- Marks, L. D., Hong, M. C., Zhang, H., and Teo, B. K., "Structure and epitaxy of silver-gold microclusters on MgO", *Materials Research Society symp. proc.* 111, 213-218 (1988).
- Martins, J. L., Car, R., and Buttet, J., "Variational spherical model of small metallic particles", *Surf. Sci.* 106, 265-271 (1981).
- Matsubara, T., Iwase, Y., and Momokita, A., "Theory of anharmonic lattice vibration in metallic fine particles", *Prog. in The. phys.* 58, 1102-1113 (1977).
- Matsui, Y. "Small Particles of cubic Boron Nitride prepared by electron irradiation of hexagonal Boron Nitride in a TEM", *J. Cryst. Growth* 66, 243-247 (1984).
- Matsumoto, S., and Matsui, Y., "Electron microscopic observation of diamond particles grown from the vapor phase", *J. Mat. Sci.* 18, 1785-1793 (1983).
- Matthews, J. W., and Allinson, D. L., "A mechanism for the formation of twins in evaporated fcc metal films", *Phil. Mag.* 8, 1283-1303 (1963).
- Mays, C. W., J. S. Vermaak, and D. Kulhmann-Wilsdorf, "On surface stress and surface tension II", *Surf. Sci.*, 12, 134-138 (1968).

- McGinty, D. J., "Vapor phase homogeneous nucleation and thermodynamic properties of argon clusters", *J. Chem. Phys.* 55, 580-588 (1971).
- Melmed, A. J., and Hayward, D. O., "On the occurrence of five-fold rotational symmetry in metal whiskers", *J. chem. Phys.* 31, 545-546 (1959).
- Menon, S. K., and Martin, P. L., "Determination of the anisotropy of surface free energy of fine metal particles", *Ultramicroscopy* 20, 93-98 (1986).
- Messmer, R. P., "Theoretical treatment of the electronic structure of small particles", *Surf. Sci.* 106, 225-238 (1981).
- Metois, J. J., and Heyraud, J. C., "SEM studies of equilibrium forms; roughening transition and surface melting of indium and lead crystals", *Ultramicroscopy* 31, 73-79 (1989).
- Michell, J. H., "The flexure of a circular plate", *Proc. Lon. Math. Soc.* 34, 223-229 (1902).
- Mihama, K., and Yasuda, Y., "Initial stage of epitaxial growth of evaporated gold films on Sodium Chloride", *J. Phys. Soc. Japan* 21, 1166-1176 (1966).
- Mindlin, R. D., and Salvadori, M. G., *Handbook of experimental stress analysis*, Hetenyi, M. (ed.), Wiley publications, New York, 775 (1950).
- Mort La Brecque, "Opening the door to forbidden symmetries", *Mosaic* 18, 3-20 (1987).
- Murphy, S. M., "Kinetic theory of diffusion in the presence of irradiation", *Phil. Mag.* 59, 1163-1179 (1989).
- Nakaya, U., *Snow Crystals*, Harvard University press, Cambridge, Massachusetts, (1954).
- Natanson, G., Amar, F., and Berry, R. S., "Melting and surface tension in microclusters", *J. Chem. Phys.* 78, 399-408 (1983).
- Nicolis, G., and Prigogine, I., *Self-Organization in non-equilibrium structures*, Wiley-Interscience publication, John

Wiley and Sons, New York, (1977).

Nimtz, G., Marquardt, P., and Weiss, W., "Raoult's law and melting point depression in mesoscopic systems", *Science* 243, 708-712 (1989).

Oberli, L., Monot, R., Mathieu, H. J., Landolt, D., and Buttet, J., "Auger and X-ray photoelectron spectroscopy of small Au particles", *Surf. Sci.* 106, 301-307 (1981).

Ogawa, S., Ino, S., Kato, T., and Ota, H., "Epitaxial growth of FCC metals on Alkali halide crystals cleaved in UHV", *J. Phys. Soc. Japan* 21, 1963-1972 (1966).

Ogburn, F., Paretzkin, B., and Peiser, H. S., "Pseudopentagonal twins in electrodeposited copper dendrites", *Acta Cryst.* 17, 774-775 (1964).

Pillar, R. M., and Nuttig, J., "Solid-solid interfacial energy determinations in metal-ceramic systems", *Phil. Mag.* 16, 181-188 (1967).

Poate, J. M., and Brown, W. L., "Laser annealing of Silicon", *Physics Today* 24(6), 24-30 (1982).

Prigogine, I., *From being to becoming: time and complexity in the physical sciences.* W. H. Freeman and company, Sanfransisco, 1980.

Rao, B. K., Khanna, S. N., and Jena, P., "Ab initio studies of the electronic structure of micro-clusters", *Ultramicroscopy* 20, 51-54 (1986).

Reimer, L., *Transmission electron microscopy*, Springer series in optical sciences, Springer-verlag, (1984).

Roos, J. R., and Vermaak, J. S., "On the growth process of Au and Ag on various air- and vacuum-cleaved alkali halide crystals", *J. Cryst. Growth* 13/14, 217-224 (1972).

Ross, J., and Andres, R. P., "Melting temperature of small clusters", *Surf. Sci.* 106, 11-17 (1981).

Rottman, C., and Wortis, M., "Statistical mechanics of

equilibrium crystal shapes: Interfacial phase diagrams and phase transitions", *Physics Reports* 103, 59-79 (1984).

Saito, Y., Yatsuya, S., Mihama, K., and Uyeda, R., "Multiply twinned particles of Germanium", *Jap. J. Appl. Phys.* 17, 1149-1150 (1979).

Schaeffer, D. W., "Polymers, fractals and ceramic materials", *Science* 243, 1023-1027 (1989).

Schwoebel, R. L., "Anomalous growth of gold from vapor phase", *Phys. Rev.* 151, 2515-2516 (1966).

Searcy, A. W., "The influence of molecular motions on the stabilities and shapes of solid particles", *J. Chem. Phys.* 81, 2489-2491 (1984).

Shechtman, D., Blech, I., Gratias, D., and Cahn, J. W., "Metallic Phase with long range orientational order and no translational symmetry", *Phys. Rev. Lett.* 53, 1951-1953 (1984).

Shewmon, P. G., *Diffusion in solids*, J. Williams Book Company, Jenks, OK., (1983).

Singh, S. R., and Marks, L. D., "Diffusion during electron beam induced reduction of WO_3 ", *Phil. Mag. Lett.* 60, 31-36 (1989).

Smith, D. J., and Marks, L. D., "High resolution studies of small particles of gold and silver, II. Single crystals, lamellar twins and polyparticles", *J. Cryst. Growth* 54, 433-438 (1981).

Smith, D. J., Petford-Long, A. K., Wallenberg, L. R., and Bovin, J. O., "Dynamic atomic-level rearrangements in small gold particles", *Science* 233, 872-875 (1986).

Solliard, C., "Structure and strain of the crystalline lattice of small gold and platinum particles", *Surf. Sci.* 106, 58-63 (1981).

Spence, J. C. H., *Experimental high-resolution electron microscopy*, Monographs on the physics and chemistry of materials, Oxford science publications, (1981).

Spencer, M. S., "Models of strong metal-support interaction (SMSI) in Pt on TiO₂ catalysts", *J. Catal.* 93, 216-223 (1985).

Spencer, M. S., "Stable and metastable metal surfaces in heterogeneous catalysis", *Nature* 323, 685-687 (1986).

Stephens, P. W., and King, J. G., "Experimental investigation of small helium clusters: magic numbers and the onset of condensation", *Phys. Rev. Lett.* 51, 1538-1541 (1983).

Stillinger, F. H., and Weber, T. A., "Hidden structure in liquid", *Phys. Rev. A* 25, 978-989 (1982).

Stishov, S. M., Makarenko, I. N., Ivanov, V. A., and Nikolaenko, A. M., "On the entropy of melting", *Phys. Lett.* 45A, 18-18 (1973).

Takagi, M., "Electron-diffraction study of liquid-solid transition of thin metal films", *J. Phys. Soc. Japan* 9, 359-363 (1954).

Tallon, J. L., "The entropy change on melting of simple substances", *Phys. Lett.* 76A, 139-142 (1980).

Tauster, S. J., Fung, S. C., and Garten, R. L., "Strong metal-support interactions. Group 8 noble metals supported on TiO₂", *J. Am. Chem. Soc.* 100, 170-175 (1978).

Tauster, S. J., and Fung, S. C., "Strong metal support interactions: Occurrence among binary oxides of groups IIA-VB", *J. Catal.* 55, 29-35 (1978).

Tholen, A. R., "Vibrations and Martensitic transformation in small cobalt particles", *Surf. Sci.* 106, 70-78 (1981).

Teo, B. K., and Keating, K., "Novel triicosahedral structure of largest metal alloy clusters: [(Ph₃P)₁₂Au₁₃Ag₁₂Cl₆]³⁺", *J. Am. Chem. Soc.* 106, 2224-2226 (1984).

Timoshenko, S. P., and Goodier, J. N., *Theory of elasticity*, McGraw-Hill, New York, (1970).

Vermaak, J. S., Mays, C. W., and Kulhmann-Wilsdorf, D., "On surface stress and surface tension-I", *Surf. Sci.* 12, 128-133

(1968).

Vicsek, T., "Pattern formation in diffusion limited aggregation", *Phys. Rev. Lett.* 53, 2281-2284 (1984).

Vieira, J. M., and Brook, R. J., "Lattice, grain-boundary, surface, and gas diffusion constants in magnesium oxide", *Structure and properties of MgO & Al₂O₃ ceramics, Advances in ceramics* (ed. Kingery, W. D.), Vol.10, American Ceramic Society, 438-462 (1984).

Waite, T. R., "Diffusion limited annealing of radiation damage in germanium", *Phys. Rev.* 107, 471-478 (1957).

Wallenberg, L. R., Bovin, J. O., Petford-Long, A. K., and Smith, D. J., "Atomic-resolution study of structural rearrangements in small platinum crystals", *Ultramicroscopy* 20, 71-76 (1986).

Wallenberg, L. R., "Atomic imaging in real time of small metal clusters: a high resolution electron microscopy study", PHD thesis, LUND University, Lund, Sweden (1987).

Wang, L., Qiao, G. W., Ye, H. Q., Kuo, K. H., Chen, Y. X., "High resolution electron microscopic investigation of supported platinum particles reduced at high temperatures", *J. Electron Microscopy Technique* 10, 7-14 (1988).

Wang, S. W., Falicov, L. M., and Searcy, A. W., "The equilibrium shapes of small particles", *Surf. Sci.* 143, 609-625 (1984).

Wautelet, M., Laude, L. D., and Antoniadis, C., "Phase diagrams of thin films and wires", *Mat. Chem. and Phys.*, 14, 57-61 (1986).

Werfelmeier, W., "Ein geometrisches modell des atomkerns", *Z. Physik* 107, 332-346 (1937).

Williams, E. D., and Bartelt, N. C., "Surface faceting and the equilibrium crystal shape", *Ultramicroscopy* 31, 36-48 (1989).

Williams, P., "Motion of small gold clusters in the electron microscope". *Appl. Phys. Lett.* 50, 1760-1762 (1987).

Winterbottom, W. L., "Equilibrium shape of a small particle in contact with a foreign substrate", *Acta Met.* 15, 303-310 (1967).

Witten, T. A., and Sander, L. M., "Diffusion-limited aggregation, a kinetic critical phenomenon", *Phys. Rev. Lett.* 47, 1400-1403 (1981).

Woltersdorf, J., Nepijko, A. S., and Pippel, E., "Dependence of the lattice parameters of small particles on the size of the nuclei", *Surf. Sci.* 106, 64-69 (1981).

Yacaman, M. J., Fuentes, S., and Dominguez, J. M., "The effect of shape and crystal structure of small particles on their catalytic activity", *Surf. Sci.* 106, 472-477 (1981).

Yacaman, M. J., Heinemann, K., Yang, C. Y., and Poppa, H., "The structure of small vapor deposited particles, II. experimental study of particles with hexagonal profile", *J. Cryst. Growth* 47, 187-195 (1979).

Yagi, K., Takayanagi, K., Kobayashi, K., and Honjo, G., "In situ observation of growth processes of multiply twinned particles", *J. Crystal Growth* 28, 117-124 (1975).

Yang, C. Y., "Crystallography of decahedral and Icosahedral particles", *J. Crystal Growth* 47, 274-282 (1979).

Appendix.2.A

2.A.1 Equilibrium Particle Shapes and the Wulff Construction

One of the most interesting problems in surface thermodynamics is that of the equilibrium shape of a small particle; the derivation here is based on the treatment of Herring (1962): the problem can be analytically stated as this: for a given amount of matter in a particle, what shape minimizes the quantity

$$\int \gamma dA$$

where γ is the excess free energy per unit area of the surface (strain free term) and A the area on the surface, the integral taken over the entire surface of the particle. This is strictly valid only in situations where the kinetic effects (like a small change in shape) occur sufficiently fast for equilibration to occur but all such questions shall be neglected and it shall be assumed that the particle is under thermodynamic equilibrium. The formulation of the problem was proposed as far back as 1878 by Gibbs and solutions given by

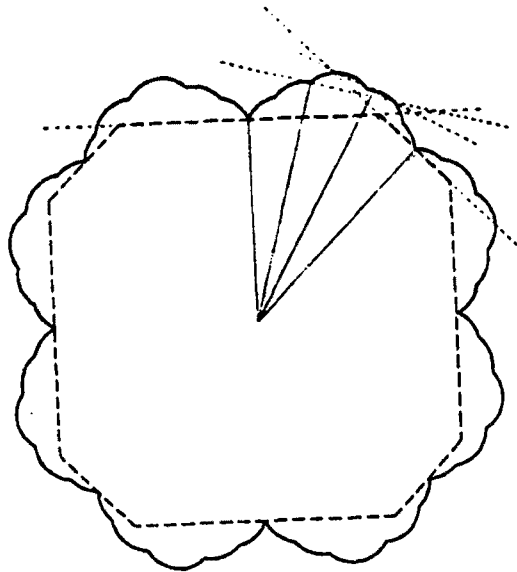


Fig.2.A.1 Schematic showing the polar plot (solid line) for surface free energy and the Curie-Wulff construction giving the equilibrium shape (dotted line) for a polyhedral particle.

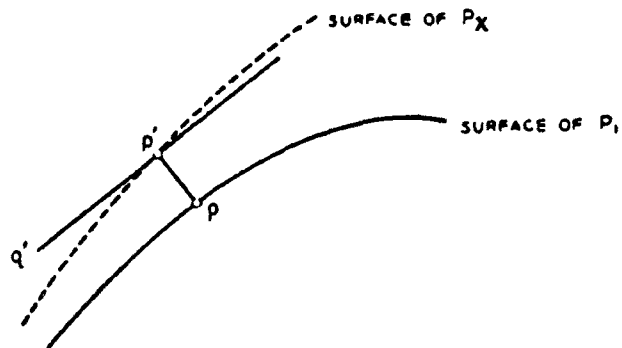


Fig.2.A.2 Schematic showing the geometrical construction used in the proof of Wulff construction (from Herring, 1953).

many authors starting with Wulff (1901) and Dinghas (1944). It should be noted that if γ were a constant then the problem would be reduced to finding a body with the minimum surface area for a given volume, rigorous mathematical proof of which was given by Minkowski in 1901. The solution of Wulff can be stated by the following steps:

1. Consider the γ plot (surface energy plotted in three dimensions as a function of the crystallographic direction in a solid) as a closed surface whose radius vector in the direction of any unit vector n has a length proportional to the surface energy $\gamma(n)$ of a plane normal to n .
2. Draw planes perpendicular to the radius vector at points where the radius vector meets the surface.
3. Then, the body formed by all points reachable from the origin without crossing any of these planes will be geometrically similar to the equilibrium shape of the object. Figure 2.A.1 gives the schematic of this construction which gives for the equilibrium shape, a polyhedron.

The most general and rigorous mathematical proof for this is due to Dinghas based on the Brunn-Minkowski inequality which is defined as follows:

Let P_1 and P_2 be any two bodies and p be a point in the

interior of P_2 called its center. Let $P_2(p)$ be the set of points covered by P_2 when its center is placed at the point p . Let P' be defined as the set of all points included in any $P_2(p)$ when p is allowed to range over P_1 . Then if V_1 , V_2 and V' are volumes corresponding to P_1 , P_2 and P'

$$V' \geq (V_1^{1/3} + V_2^{1/3})^3 \quad (2.A.1)$$

The proof for the Wulff construction is as follows (see Fig.2.A.2):

Let P_1 be any hypothetical shape of the particle that is investigated. Construct the body P_x from P_1 by displacing each point on the surface along the normal n by a distance $x\gamma(n)$. Then if V_x is the volume of P_x

$$\int \gamma dA = [\lim_{x \rightarrow 0} (V_x - V_1)] / x \quad (2.A.2)$$

If p' on P_x $c \int \gamma dA = [\lim_{x \rightarrow 0} (V_x - V_1)] / x$ on P_1 then $pp' = x\gamma(n)$. If the body formed by the Wulff construction with scale factor x is centered on p it will contain no points outside $p'q'$ normal to n through p' . Similar to V' considered above, let V'_x be the volume of P'_x and P_2 the Wulff construction with scale factor x ; then if γ varies smoothly and continuously over the surface

$$[\lim_{x \rightarrow 0} (V'_x - V_1)] / x \leq [\lim_{x \rightarrow 0} (V_x - V_1)] / x \quad (2.A.3)$$

From (Eq.2.A.2) and (Eq.2.A.3) one obtains

$$\begin{aligned} \int \gamma dA &\geq [\lim_{x \rightarrow 0}] \{ (V_1^{1/3} + xV_w^{1/3})^3 - V_1 \} / x \\ &= 3V_1^{2/3}V_w^{1/3} \end{aligned} \quad (2.A.4)$$

Where V_w is the volume of the Wulff construction. This equality can hold only if P_1 and the Wulff construction are geometrically similar and this proves that the Wulff shape is an absolute minimum of $\int \gamma dA$.

2.A.2 Modified Wulff Construction for an MTP

A typical $\langle 110 \rangle$ section of the plot as well as the shape of a single crystal tetrahedra for a fcc material and for a strongly faceted model is shown in Fig.2.A.3. The segments used to construct a multiply twinned particle (Dh or Ic) can be extracted from this shape by incorporating twin boundaries. This introduces changes in the overall shape of the segments and modifications have to be done to the Wulff construction to account for the twin boundaries [see Marks 1980 for details].

It is assumed from the symmetry of the segments that each of the facets which combine to produce (five such units in a Dh) the twin boundaries have energy per unit area which is

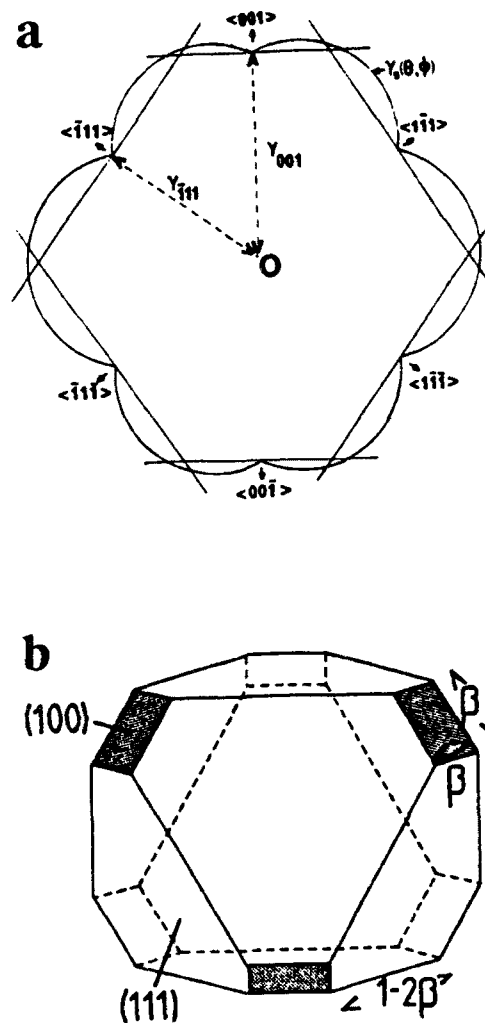


Fig.2.A.3 A typical $\langle 110 \rangle$ section of the γ plot (a) and the shape of a single crystal tetrahedra derived from it (b) for fcc material in a strongly faceted model. The value of β corresponds to $1 - \gamma_{100} / \sqrt{3} \gamma_{111}$ (from Marks, 1980).

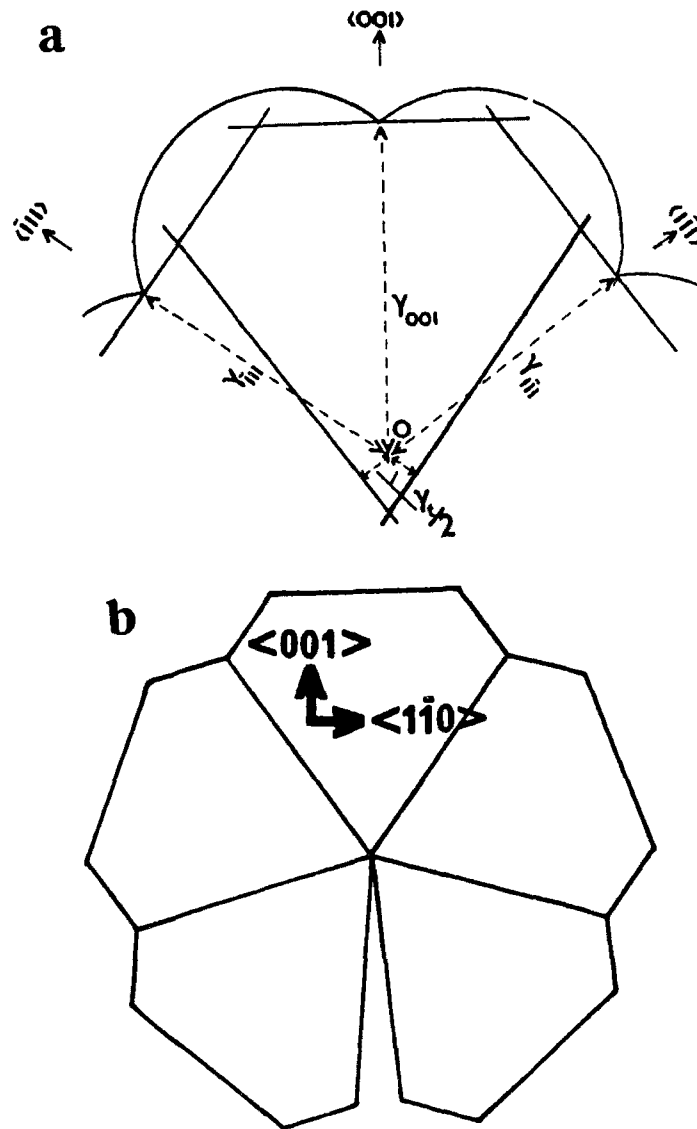


Fig.2.A.4 The shape of the single crystal segment derived from the modified Wulff construction (a) from which the complete D_h particle (schematic is shown in b) is constructed (from Marks, 1980).

half that of a twin boundary. Then incorporating point values of $\gamma_e/2$ in the Wulff construction gives the actual shape of the segments from which a complete Dh particle can be constructed (see Fig.2.A.4). Once the shape of the individual segment is decided (for example in our analysis a more general shape was considered, with lengths of segments made to vary) the problem reduces to working out the surface area and volume of the segments and minimizing the surface energy for constant volume of the material or minimizing the dimensional energy parameter (which depends only on the shape and not the volume of the particle)

$$E_w = \int \gamma dA / \gamma_{111} [dV]^{2/3}$$

In the theoretical analysis different volume fractions were considered for each segments and the analysis done for fixed volume fractions, the value of minimum E_w , using a constrained optimization algorithm with the constraint that the magnitude of the corresponding edges on the adjoining facets have to match.

For a semi-quantitative proof, using Lagrangian variables, of the modified Wulff construction being a stationary value of the total surface energy at constant volume the reader is referred to Marks (1980). It should be

noted that the modified Wulff construction is only one (for a symmetric partition of the boundary) of the several solutions that exist for the problem, but nevertheless gives a stationary value in energy. A similar analysis will be given at the end of the fourth chapter in Appendix 4.B, where the equilibrium shape of a sinking particle will be considered as a modified Wulff construction being a true minimum in energy but subject to certain surface free energy criteria.

Appendix 2.B

2.B.1. Disclinations in Twinned Crystals

Disclinations are defects involving an angular rotation, unlike dislocations which involve only a positional displacement. These defects have been observed in a variety of materials, for example, biological materials [Bouligand 1980], liquid crystals [Kleman 1983], polymers [Li and Gilman 1970], Buckminster Fuller's geodesic domes and in multiply twinned crystals [see deWit 1971, Harris and Scriven 1971]. The last of the examples, multiply twinned crystals or MTPs which form the main topic of this thesis, would have an angular gap of $7^{\circ}20'$ without internal strains. Since this gap is taken up by the crystal, this implies that such a crystal contains a wedge disclination. The importance of these intrinsic disclinations, apart from explaining the internal strains that are so often seen experimentally in these crystals, is that they can act as sources or sinks for dislocations in a plastically deforming crystal which is so characteristic of the behavior seen in MTPs at small sizes.

Since the analysis in the text of strains in small

particles was essentially an analysis based on the disclination strain fields, it will be demonstrated here how the Airy stress function of the disclination is derived using two-dimensional elasticity [Dundurs 1987]. Figure 2.B.1 shows how the operation in forming a wedge disclination is carried out. A sector is cut out of the material and the bottom face is rotated through an angle Ω , and the cut welded shut, keeping the upper face of the cut fixed. This results in a displacement discontinuity in the range $0 < \theta < 2\pi$ of

$$U_0(r, 2\pi) - U_0(r, 0) = \Omega_r r \quad (2.B.1)$$

The Airy stress function (ϕ) in 2-D elasticity, introduced by G. B. Airy in 1862, is a biharmonic function which can be used to set up a problem from which solutions can be easily derived for different boundary conditions. The stresses are related to this function through second degree partial differentials as:

$$\begin{aligned} \sigma_{xx} &= \partial^2 \phi / \partial y^2, \quad \sigma_{yy} = \partial^2 \phi / \partial x^2, \\ \sigma_{xy} &= -\partial^2 \phi / \partial x \partial y \end{aligned} \quad (2.B.2)$$

The function is formed by a linear combination of biharmonic functions that satisfy the equilibrium and compatibility conditions in elasticity. The stresses and displacements for each of these functions have been worked out using Hooke's law

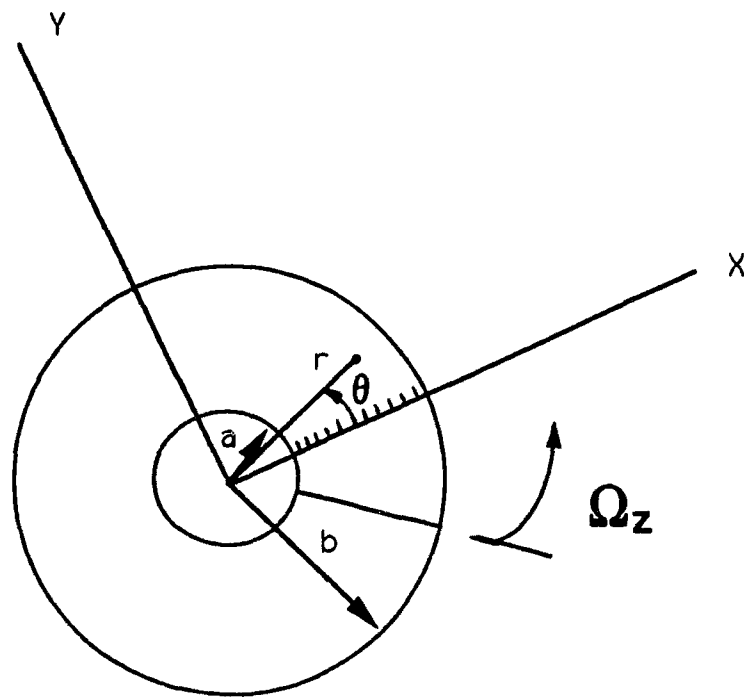


Fig.2.B.1 Schematic showing the operation in forming a wedge disclination; a wedge of material is cut out and the cut weld shut either by closing the gap (positive sign for the disclination) or inserting an extra wedge of material (negative). Also shown in the figure is the coordinate system used in evaluating the Airy stress function.

$\kappa = 3 - 4\nu$ for plane strain,
 $\kappa = (3 - \nu)/(1 + \nu)$ for plane stress

Rigid body displacements:
 $u_r = C_1 \cos\theta + C_2 \sin\theta$
 $u_\theta = -C_1 \sin\theta + C_2 \cos\theta + C_3 r$

U	σ_{rr}	$\sigma_{r\theta}$	$\sigma_{\theta\theta}$	$2Gu_r$	$2Gu_\theta$
r^2	2	0	2	$(\kappa-1)r$	0
$\log r$	$1/r^2$	0	$-1/r^2$	$-1/r$	0
θ	0	$1/r^2$	0	0	$-1/r$
$r^2 \log r$	$2 \log r + 1$	0	$2 \log r + 3$	$(\kappa-1)r \log r - r$	$(\kappa+1)r\theta$
$r^2 \theta$	2θ	-1	2θ	$(\kappa-1)r\theta$	$-(\kappa+1)r \log r$
$r^3 \cos\theta$	$2r \cos\theta$	$2r \sin\theta$	$6r \cos\theta$	$(\kappa-2)r^2 \cos\theta$	$(\kappa+2)r^2 \sin\theta$
$r^3 \sin\theta$	$2r \sin\theta$	$-2r \cos\theta$	$6r \sin\theta$	$(\kappa-2)r^2 \sin\theta$	$-(\kappa+2)r^2 \cos\theta$
$r\theta \sin\theta$	$2 \cos\theta/r$	0	0	$\frac{1}{2}[(\kappa-1)\theta \sin\theta + (\kappa+1) \log r \cos\theta - \cos\theta]$	$\frac{1}{2}[(\kappa-1)\theta \cos\theta - (\kappa+1) \log r \sin\theta - \sin\theta]$
$r\theta \cos\theta$	$-2 \sin\theta/r$	0	0	$\frac{1}{2}[(\kappa-1)\theta \cos\theta - (\kappa+1) \log r \sin\theta + \sin\theta]$	$\frac{1}{2}[-(\kappa-1)\theta \sin\theta - (\kappa+1) \log r \cos\theta - \cos\theta]$
$r \log r \cos\theta$	$\cos\theta/r$	$\sin\theta/r$	$\cos\theta/r$	$\frac{1}{2}[(\kappa+1)\theta \sin\theta + (\kappa-1) \log r \cos\theta - \cos\theta]$	$\frac{1}{2}[(\kappa+1)\theta \cos\theta - (\kappa-1) \log r \sin\theta - \sin\theta]$
$r \log r \sin\theta$	$\sin\theta/r$	$-\cos\theta/r$	$\sin\theta/r$	$\frac{1}{2}[-(\kappa+1)\theta \cos\theta + (\kappa-1) \log r \sin\theta - \sin\theta]$	$\frac{1}{2}[(\kappa+1)\theta \sin\theta + (\kappa-1) \log r \cos\theta + \cos\theta]$
$\cos\theta/r$	$-2 \cos\theta/r^3$	$-2 \sin\theta/r^3$	$2 \cos\theta/r^3$	$\cos\theta/r^2$	$\sin\theta/r^2$
$\sin\theta/r$	$-2 \sin\theta/r^3$	$2 \cos\theta/r^3$	$2 \sin\theta/r^3$	$\sin\theta/r^2$	$-\cos\theta/r^2$

Table 2.B.1 Show the relationship between the bi-harmonic functions that form the Airy stress functions, corresponding stresses and displacements in Cartesian as well as cylindrical coordinates (from Dundurs, 1987).

x	$2G u_x$	$2G u_y$	σ_{xx}	σ_{yy}	σ_{xy}
$r \log r \cos \theta$	$\frac{1}{2}(\kappa - 1) \log r - \frac{x^2}{r^2}$	$\frac{1}{2}(\kappa + 1) \theta - \frac{xy}{r^2}$	$-\frac{x}{r^2} + \frac{2x^2}{r^4}$	$-\frac{y}{r^2} + \frac{2x^2 y}{r^4}$	$\frac{2x}{r^2} - \frac{2x^2 y}{r^4}$
$r \theta \sin \theta$	$\frac{1}{2}(\kappa + 1) \log r - \frac{x^2}{r^2}$	$\frac{1}{2}(\kappa - 1) \theta - \frac{xy}{r^2}$	$\frac{2x^2}{r^2}$	$\frac{2x^2 y}{r^4}$	$\frac{2x}{r^2} - \frac{2x^2 y}{r^4}$
$\log r$	$-\frac{x}{r^2}$	$-\frac{y}{r^2}$	$-\frac{1}{r^2} + \frac{2x^2}{r^4}$	$\frac{2xy}{r^4}$	$\frac{1}{r^2} - \frac{2x^2}{r^4}$
$\cos 2\theta$	$-(\kappa - \kappa) \frac{x}{r^2} + \frac{4x^2}{r^4}$	$-(\kappa + 1) \frac{y}{r^2} + \frac{4x^2 y}{r^4}$	$\frac{12x^2}{r^4} - \frac{16x^4}{r^6}$	$\frac{8xy}{r^4} - \frac{16x^2 y}{r^6}$	$\frac{4}{r^2} - \frac{20x^2}{r^4} + \frac{16x^4}{r^6}$
$\frac{\cos \theta}{r}$	$-\frac{1}{r^2} + \frac{2x^2}{r^4}$	$\frac{2xy}{r^4}$	$\frac{2x}{r^2} - \frac{8x^2}{r^4}$	$\frac{2y}{r^2} - \frac{8x^2 y}{r^4}$	$-\frac{6x}{r^2} + \frac{8x^2}{r^4}$
$r \log r \sin \theta$	$-\frac{1}{2}(\kappa + 1) \theta - \frac{xy}{r^2}$	$\frac{1}{2}(\kappa - 1) \log r + \frac{x^2}{r^2}$	$\frac{y}{r^2} + \frac{2x^2 y}{r^4}$	$\frac{x}{r^2} - \frac{2x^2}{r^4}$	$\frac{y}{r^2} - \frac{2x^2 y}{r^4}$
$r \theta \cos \theta$	$\frac{1}{2}(\kappa - 1) \theta + \frac{xy}{r^2}$	$-\frac{1}{2}(\kappa + 1) \log r - \frac{x^2}{r^2}$	$-\frac{2x^2 y}{r^4}$	$-\frac{2x}{r^2} + \frac{2x^2}{r^4}$	$-\frac{2y}{r^2} + \frac{2x^2 y}{r^4}$
θ	$\frac{y}{r^2}$	$-\frac{x}{r^2}$	$-\frac{2xy}{r^4}$	$-\frac{1}{r^2} + \frac{2x^2}{r^4}$	$\frac{2xy}{r^4}$
$\sin 2\theta$	$(\kappa - 1) \frac{y}{r^2} + \frac{4x^2 y}{r^4}$	$(\kappa + 1) \frac{x}{r^2} - \frac{4x^2}{r^4}$	$\frac{4xy}{r^4} - \frac{16x^2 y}{r^6}$	$\frac{2}{r^2} - \frac{10x^2}{r^4} + \frac{16x^4}{r^6}$	$\frac{12xy}{r^4} + \frac{16x^2 y}{r^6}$
$\frac{\sin \theta}{r}$	$\frac{2xy}{r^4}$	$\frac{1}{r^2} - \frac{2x^2}{r^4}$	$\frac{2y}{r^2} - \frac{8x^2 y}{r^4}$	$-\frac{6x}{r^2} + \frac{8x^2}{r^4}$	$-\frac{2y}{r^2} + \frac{8x^2 y}{r^4}$

Table 2.B.1 Show the relationship between the bi-harmonic functions that form the Airy stress functions, corresponding stresses and displacements in Cartesian as well as cylindrical coordinates. (continued from last page)

and the relationship in (Eq.2.B.2) and tabulated in Table 2.B.1 [from Dundurs 1987]. The functions that satisfy the disclination problem in Fig.2.B.1 are r^2 , $r^2 \log r$ and $\log r$.

The Airy stress function can then be written as:

$$\phi = A (r^2 \log r + Br^2 + C \log r) \quad (2.B.3)$$

Using Table.2.B.1 to calculate the displacements and using (Eq.2.B.1) the value of A is readily obtained as

$A = \Omega_{\mu} / \pi(\kappa+1)$ where μ and κ are as given before in the text.

Now using the condition that there are no tractions on both the free surfaces, ie.

$$\sigma_{rr}(a, \theta) = \sigma_{rr}(b, \theta) = 0 \quad (2.B.4)$$

one gets the complete Airy stress function for the disclination as:

$$\begin{aligned} \phi = \Omega_{\mu} / \pi(\kappa+1) \{ & r^2 \log r \\ & - [(b^2 \log b - a^2 \log a) / (b^2 - a^2) + 1/2] r^2 \\ & + [2a^2 b^2 \log(b/a) / (b^2 - a^2)] \log r \} \end{aligned} \quad (2.B.5)$$

In the limit of a tending to 0, this reduces to

$$\phi = \Omega_{\mu} / \pi(\kappa+1) \{ r^2 \log r - (\log b + 1/2) r^2 \} \quad (2.B.6)$$

The stresses and displacements can be calculated from this using Table.2.B.1 and it turns out that for the disclination the stresses are logarithmically singular at the origin.

Appendix 4.A

4.A.1 Evaluation of Interfacial Free Energy & Surface Anisotropy from Wulff Construction

This section will deal with the calculation of the gold-magnesium oxide interfacial free energy and surface anisotropy ratios of gold small particles from the geometrical shape of gold particles sitting on magnesium oxide support. A major assumption here will be that the shapes of the particles will be thermodynamic equilibrium shapes at room temperature and that the application of Wulff construction is valid. To some extent this assumption is valid because the specimens were annealed over a light bulb and equilibrated for long periods of time, although not high temperature annealed. The results from many particles were consistent within reasonable limits.

Figure 4.A.1 shows two different shapes of gold particles, one polyhedral (Fig.4.A.1.a) and the other almost hemispherical (Fig.4.A.1.c), sitting on MgO. The corresponding schematic of these are reproduced in Fig.4.A.1.b and Fig.4.A.1.d and their Wulff centers located by circumscribing the appropriate polygon or circle around them. The Wulff

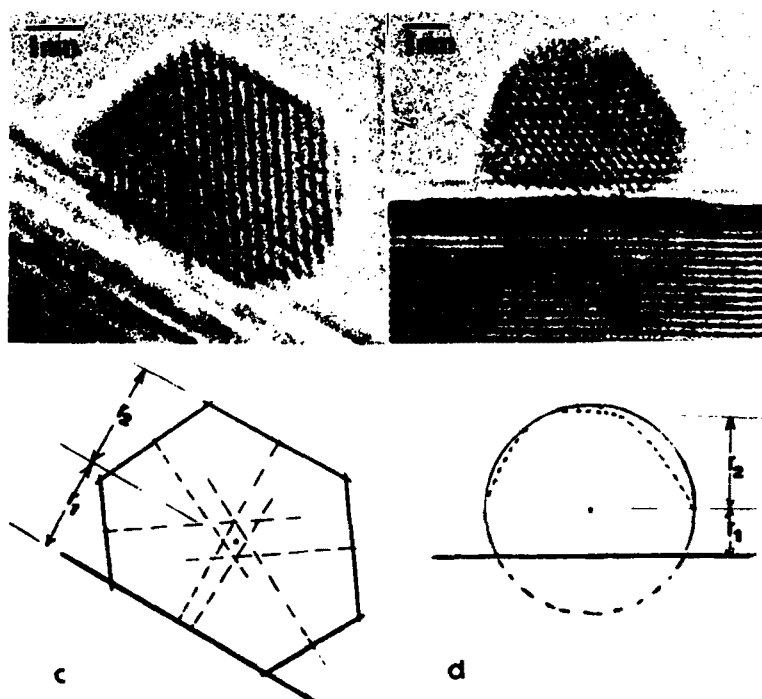


Fig.4.A.1 Experimental images and corresponding schematics for Wulff construction shapes used in the evaluation of interfacial energies of small gold particles on MgO substrates.

centers have been located by drawing the perpendicular bisectors of surface facets in the case of the polyhedral particle and locating the center of the circle for the hemispherical particle. In the case of the former, the surface facets can easily be indexed from the angular relations between various low index faces in fcc materials and the lattice of atoms on these faces. For the hemispherical particle the surface energy is assumed to be an average value of the (111) and (100) facets. The surface anisotropy is only determined for the polyhedral shape since the surface facets are defined only on this.

From chapter 4, Eq.4.3, the energy of the interface can be written as:

$$\gamma_{\text{int}} = \gamma_{\text{sub}} + (r_1/r_2) \gamma_p^{(hkl)} \quad (4.A.1)$$

where r_1 and r_2 are the distances of the interface and the particle (hkl) facet from the Wulff center. For the Au-MgO system the equation can be rewritten as:

$$\gamma_{\text{int}} = \gamma_{\text{MgO}}^{(100)} + (r_1/r_2) \gamma_{\text{gold}}^{(hkl)} \quad (4.A.2)$$

From the values of r_1 and r_2 in both cases and the surface free energies of (100) MgO as 1200 ergs/cm² and (hkl) gold as 1400 ergs/cm², the interfacial energy of Au-MgO is obtained as 2400 ergs/cm² for the polyhedral shape and 1900 ergs/cm² for

the spherical shape. From many different particles the average value of the interfacial energy for Au/MgO system falls around ~ 2000 ergs/cm², which is consistent with interfacial energies in many metal-oxide systems [Winterbottom 1967].

The value of surface anisotropy ratio is determined by finding the ratio of the distance from the Wulff center to the corresponding (hkl) faces. The value of this ratio for the (100) to the (111) face is found (from many particles) to be approximately 1.03-1.1, ie. the difference in surface energies of the two faces being of the order of 3-10%. This value is again consistent with other experimental observations [see for example, Flueli and Borel 1988]. It should be noted that the errors involved in the determination of the values of interfacial energies or anisotropy values using a Wulff construction is quite large and quite sensitive to the defocus value used in imaging due to the shift of contrast for the cut-off surface layer. For example, a shift of one atomic layer for the cut off surface in a 30 Å particle (which contains about 20 atomic layers), would introduce an error of 5%. This error will increase with decreasing particle size. Also, the determination of the Wulff center is only approximate since the perpendicular bisectors of the surface

facets do not always converge to one unique center since the shape of the polyhedron shapes are often asymmetric. Nevertheless these calculations give order of magnitude values and can be compared with theoretical values or existing experimental results for other systems.

Appendix 4.B

4.B.1 Equilibrium Shape of the Sinking Particle

The problem here is that of the equilibrium shape of a small particle when it is specifically included, the possibility that the particle can partially sink into the substrate. Most of the previous work [Winterbottom 1967; Pillar and Nuttig 1967; Heyraud and Metois 1980; Williams and Bartelt 1989; Metois and Heyraud 1989] on particles on a substrate have focussed on evaluating the equilibrium shape particle (ESP) by replacing one of the vacuum-solid interface with a solid-solid interface. This approach readily leads to a variant of the Wulff or the Herring construction, what is called a Winterbottom shape. Here, attempt will be made to address the ESP of a particle that is partially immersed in the substrate and to prove that the ESP corresponds to a Wulff construction (modified to account for the interfacial energies) which is a local minimum always and a true minimum when certain surface free energy criterion is satisfied.

The purpose of this section is to improve upon the theoretical model that we earlier proposed in chapter 4 for

the sinking particle, and consider explicitly the equilibrium shape of a particle that is sinking into the substrate. In general the problem does not appear to have any analytical solution, but with some assumptions about the directional dependence of the surface free energies it can be solved in a closed form by using the approach mentioned previously for the twinned particle as developed by Marks (1985a). The kinetics of the problem will not be considered here, which could lead to quite different results.

4.B.2 Analysis of the Sinking Problem

The model will employ two basic approximations:

- a) That the substrate is large compared to the size of the particle. With this approximation one can readily show that the change in surface energy due to redistribution of the volume displaced by the particle of the substrate material is of the order of $\Gamma V_p/V^{1/3}$ where Γ and V_p are the specific free energy of the substrate and volume displaced by the particle of the substrate material and V the total substrate volume; this is small and hence can be neglected.
- b) That the interfacial energy is always proportional to the surface free energy of the particle facet in contact with the

substrate, independent of facet orientation. This is a relatively severe approximation, but without it no simple analytical solution appears to exist.

The minimization of the free energy functional in the sinking problem can be done using the method of Lagrange and as stated by Von Laue (1943) and Dinghas (1944). It is important to define the notation used for the free energy terms:

Γ : free energy per unit area of the substrate

γ : free energy per unit area of the particle, implicitly a function of the facet normal

ξ : free energy of creating an interface by joining unit area of the free particle and free substrate surface, again implicitly a function of the facet normal for a given epitaxial orientation

h_j : normal distance to the 'j' facet

h_s : normal distance to the substrate surface

A_j : area of the 'j' facet

A_s : cross-sectional area of the particle in the substrate surface plane

We can write the problem to be solved as minimizing:

$$F = \sum \gamma_j A_j - \Gamma A_s - 2\lambda \sum h_j A_j \quad (4.B.1)$$

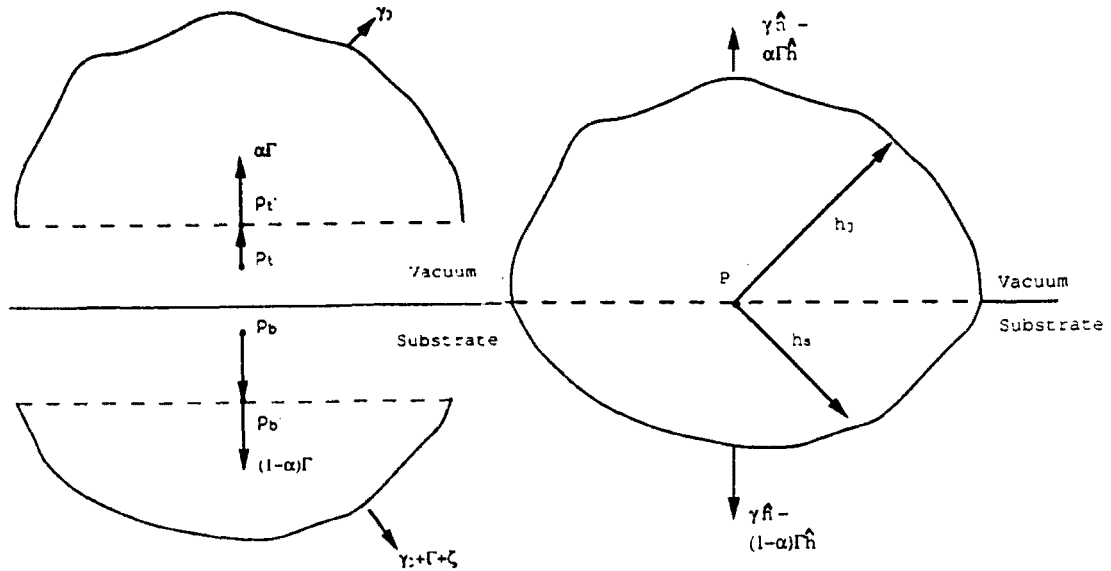


Fig.4.B.1 Schematic showing the geometry of the equilibrium particle shape which is cut along the plane of the interface. P_t and P_b shows the individual Wulff centers for top and bottom parts which have been rescaled to P'_t and P'_b . P is the equivalent center for the combined particle.

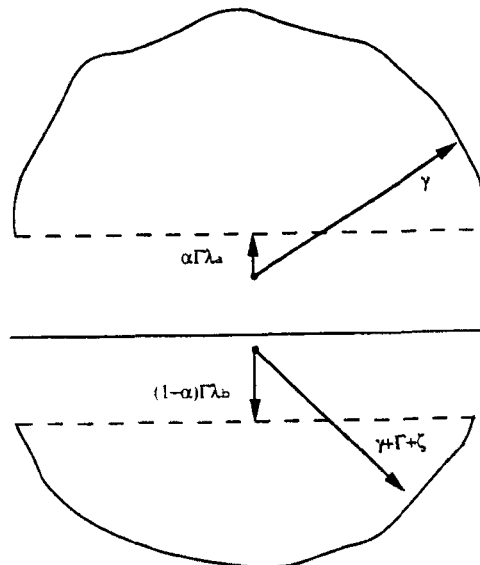


Fig.4.B.2 Schematic showing the Wulff construction of the top and bottom parts of the equilibrium shape with different scaling.

(also see Fig.4.B.1). An approach similar in spirit to that used for the modified Wulff construction for a twinned particle [Marks 1985a] will be used now, namely using a mathematical cut on the particle in the plane of the surface and partitioning the term involving Γ into two terms $\alpha\Gamma$ for below the substrate and $(1-\alpha)\Gamma$ for above. The minimization problem can then be rewritten as:

$$F = F_a + F_b \quad (4.B.2)$$

Where F_a is for the region above the surface, where

$$F_a = \sum \gamma_j^p A_j - (1-\alpha)\Gamma A_s - 2\lambda_a \{ \sum h_j A_j - h_s A_s \} \quad (4.B.3)$$

and F_b is for the region below the surface:

$$F_b = \sum (\gamma_j^p + \xi_j + \Gamma) A_j - \alpha\Gamma A_s - 2\lambda_b \{ \sum h_j A_j + h_s A_s \} \quad (4.B.4)$$

There are two possible types of solutions; either both F_a and F_b are independently minimized or the sum of the two. The first is simple since (Eq.4.B.3) and (Eq.4.B.4) are Wulff problems for which the solutions are given by

$$\gamma_j = \lambda_a h_j \quad (4.B.5)$$

$$\gamma_j + \xi_j + \Gamma = \lambda_b h_j \quad (4.B.6)$$

$$(1-\alpha)\Gamma = -\lambda_a h_s^a \quad (4.B.7)$$

$$\alpha\Gamma = -\lambda_b h_s^b \quad (4.B.8)$$

Equations (4.B.5-4.B.8) indicate that we have Wulff constructions for the top and bottom parts independently, but

the scale of the two Wulff constructions can be different. To determine the relative scales, which is determined by the ratio of λ_a and λ_b , we require that the length of any facet which is common to both the top and bottom parts is the same, and that the two parts fit together. In general, the only way that the two parts can fit together is if the Wulff centers (after scaling by λ_a , λ_b) are the same, in which case:

$$\lambda_b/\lambda_a = \gamma/(\gamma + \xi + \Gamma) \quad (4.B.9)$$

and

$$h_b^* = -h_a^* \quad (4.B.10)$$

$$\alpha = -\gamma/(\xi + \Gamma) \quad (4.B.11)$$

The shape that we have generated is in fact very simple; it is a Wulff construction for an isolated particle of unit scale ($\lambda_a=1$) with the interface located a distance $\Gamma(\xi+\gamma+\Gamma)/(\xi+\Gamma)$ above the Wulff center, see Fig.4.B.2.

A stationary value of F is thus obtained but the question now is whether this is a true minimum, a saddle point or a point of inflexion. The minimization problem can also be written as minimizing $S/V^{2/3}$ where S and V are respectively the total surface free energy including the substrate term and the volume for the top and bottom parts. For a true minimum, for any perturbation of the shape we require that

$$\delta S_a + \delta S_b > (\delta V_a + \delta V_b) / (V_a + V_b) . \quad (4.B.12)$$

We can demonstrate that we have a true minimum by considering different types of deformations of the shape, and showing that they all obey (Eq.4.B.12). There are three different types of deformations:

1) A deformation of top or bottom only which does not alter the substrate cross-sectional area. This is equivalent to a deformation of the vacuum Wulff construction and is therefore towards higher energy, see for instance Fig.4.B.3.

2) A deformation which changes the substrate intersection cross-sectional area and does not transfer volume between the top and bottom. This can always be treated (by rescaling) as a deformation which increases the volume V , see for instance Fig.4.B.4. Independently, the top and bottom can both be considered as Winterbottom constructions which independently satisfy for a given value of the cut α

$$\delta S > \delta V/V \quad (4.B.13)$$

(the above inequality results since the change in $S/V^{2/3}$ with respect to V should be larger than zero since the shape is at least a local minimum in energy) so that for this type of deformation the change in surface free energy is unconditionally positive and therefore,

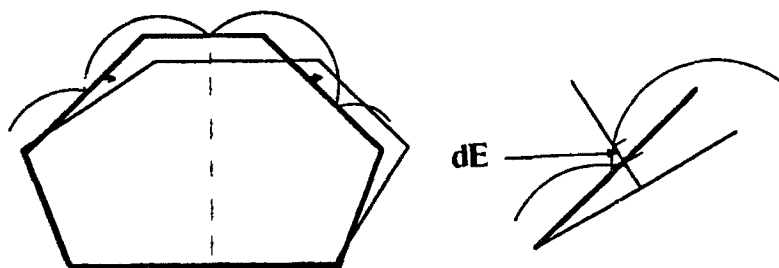


Fig.4.B.3 Schematic showing the deformation where top and bottom Wulff constructions are independently deformed with out changing the substrate cross-section, resulting in higher energy.



Fig.4.B.4 Deformation which changes the substrate intersection cross-sectional area but does not transfer volume between the top and bottom which increases net volume of the shape.

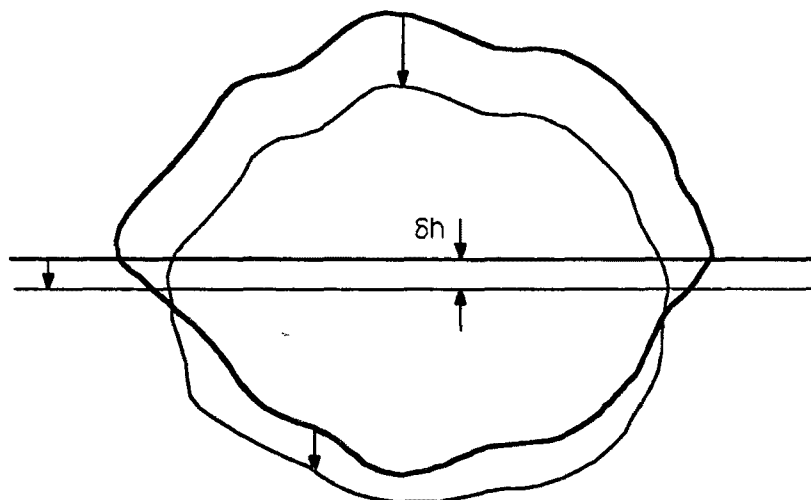


Fig.4.B.5 Deformation of the third kind which involves volume transport between the top and bottom parts.

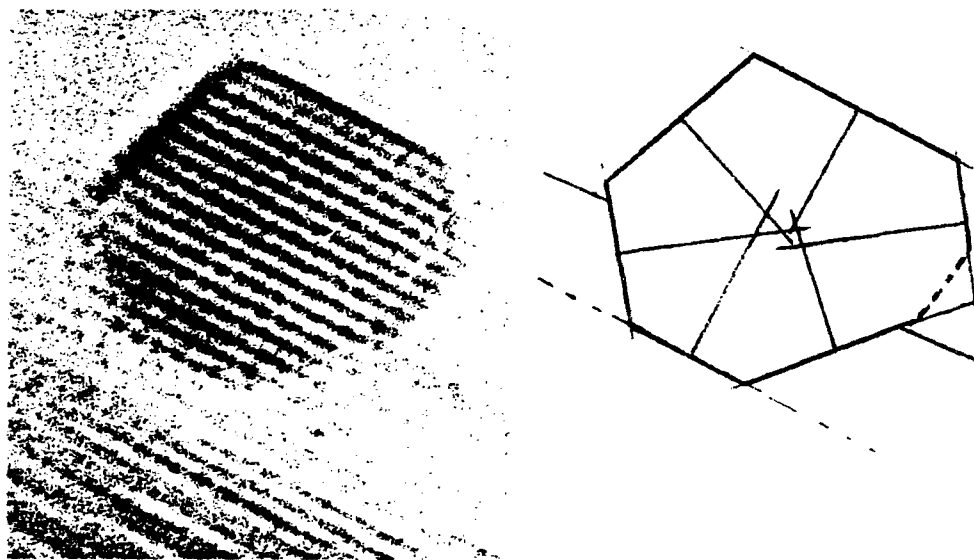


Fig.4.B.6 The image of a partially sunken particle and its tracing to show the position of the Wulff center inside the particle volume.

$$\begin{aligned} \delta S_a + \delta S_b &> (V_a \delta S_a + V_b \delta S_b) / (V_a + V_b) \\ &> (\delta V_a + \delta V_b) / (V_a + V_b) \end{aligned} \quad (4.B.14)$$

which is towards higher energy.

3) The only possible remaining deformation is one which involves movement of the effective substrate height (Fig.4.B.5); in other words transfers volume from the top to the bottom or vica-versa. For the modified Wulff construction it was argued that for the analogous case where the substrate plane is replaced by a twin boundary, the fact that the twin boundary energy was small relative to the external facet free energy introduced a constraint which eliminated this mode of deformation. This constraint effect was proved by more detailed numerical calculations. Here the existence of a minimum can be seen more strongly. This type of deformation is equivalent to moving the substrate height with respect to the Wulff center, plus some changes to the outer surface. All components of the deformation in addition to moving the substrate height are towards higher energy since they can be considered as deformation types a) or b) above. Therefore the only possible mode of this deformation which could reduce the surface free energy is moving the substrate height without any other shape changes, which is a deformation at constant

volume. Considering a motion of the substrate plane upwards by δh , the change in the surface free energy due to the outer surface can be written as

$$\begin{aligned} dS/dh &= \Sigma(\gamma + \xi + \Gamma) dA_i/dh \\ &+ \Sigma\gamma dA_1/dh - \Gamma dA_s/dh \end{aligned} \quad (4.B.15)$$

using $\Sigma h_i dA_i/dh_k = A_k$

$$\begin{aligned} dS/dh &= \{(\xi + \Gamma)/\gamma\} A_s \\ &- (\Gamma+h[(\xi + \Gamma)/\gamma]) dA_s/dh \end{aligned} \quad (4.B.16)$$

so that

$$d^2S/dh^2 = -(\Gamma+h[(\xi + \Gamma)/\gamma]) d^2A_s/dh^2 \quad (4.B.17)$$

or at the stationary modified-Wulff value

$$d^2S/dh^2 = -\Gamma(1+[(\xi + \Gamma + \gamma)/\gamma]) d^2A_s/dh^2$$

Since A_s is positive, and for a convex Wulff construction the second derivative is always negative, then if $(\xi + \Gamma + 2\gamma) > 0$ the solution is always a minimum - note that the condition is equivalent to substrate intersection lying within particle.

Since all possible deformations of the shape are towards higher energy, the shape generated previously is a minimum.

4.B.3 Discussion

With the above analysis it is seen, albeit for a restricted set of surface free energy conditions, the

equilibrium shape of a buoyant small particle. In between the conditions for particle wetting the substrate and the substrate wetting the particle, the real shape of a particle in equilibrium is partially submerged into the substrate. It is very important to stress the equilibrium shape of a particle, and there are numerous physical constraints on achieving equilibrium; the particle must be in equilibrium with its vapor and the single atom population on the substrate and the substrate must be in equilibrium with its vapor. As perhaps most clearly demonstrated by Metois and Heyraud (1989) equilibrium is only occasionally reached. The same conclusion can be drawn from our own experiments, see for instance figures 4.4-4.6. Thermodynamically, the results in these figures do not correspond to minimizing the MgO surface free energy, but the kinetics of the process are dominating the process. Despite this, the results shown are in fact in reasonable agreement with the theoretical predictions. For instance, shown in Fig.4.B.6 is the image and a tracing of the particle in Figure 4.5.c which indicates that there is close to a true Wulff center for the particle.

What about the situation when the conditions for the surface free energies are relaxed? This can be seen from the

arguments used for the Modified Wulff construction. The energy can be represented as a function of shape in a potential energy surface with a constraint that the top and bottom segments fit together. Rather than one simple minimum without the constraint, one can have a whole family of minima in the presence of the constraint. In fact, it does not follow that there exists one simple minimum at all; there may very well be many. This is clear from the experience to date in calculating parts of this potential energy surface (see earlier chapters), which clearly demonstrated that this is the case. In addition, the experimental results also support this conclusion; in figure 4.5 the development of a twin in c and d can be clearly seen.

In conclusion, predictably, changes in the substrate should be taken into account when considering the equilibrium shape of a small particle. However, application of equilibrium theories to small particles should be done with substantial care since the correct approach to small particles is via a potential energy surfaces.

VITA

Name: Ajayan P. M.
Place of Birth: Kodungallur, Kerala, India
Date of Birth: July 15, 1962

Education: Northwestern University, Evanston, IL
Ph.D. Materials Science & Engg.
Banaras Hindu University, Varanasi, India
B.Tech. Metallurgical Engineering

Publications:

Marks, L. D., Ajayan, P. M., and Dundurs, J., Ultramicroscopy, 20, 77 (1986).
Ajayan, P. M., Marks, L. D., and Dundurs, J., Mat. Res. Symp. Proc., 82, 469 (1987).
Dundurs, J., Marks, L. D., and Ajayan, P. M., Phil. Mag., 57, 605 (1988).
Ajayan, P. M., and Marks, L. D., Mat. Res. Symp. Proc., 111, 53 (1988).
Ajayan, P. M., and Marks, L. D., Phys. Rev. Lett., 60, 585 (1988).
Ajayan, P. M., and Marks, L. D., J. Phase Transitions, in press (invited review).
Ajayan, P. M., and Marks, L. D., Nature, 338, 139 (1989).
Ajayan, P. M., and Marks, L. D., Phys. Rev. Lett., 63, 279 (1989).
Ajayan, P. M., and Marks, L. D., Mat. Res. Soc. Symp. Proc., 139, 333 (1989).
Ajayan, P. M., Proc. 47th annual meeting of EMSA, 254 (1989).
Ajayan, P. M., and Marks, L. D., Appl. Phys. Lett., submitted.
Marks, L. D., and Ajayan P. M., Chemtech, submitted (invited).

Future Adress:

NEC Corporation, Fundamental Research Labs
34 Miyukigaoka, Tsukuba-shi
Ibaraki-305, Japan

